DESIGN OF A PASSIVE HYDRAULIC SIMULATOR FOR ABNORMAL MUSCLE BEHAVIOR REPLICATION

BY

JIAHUI LIANG

THESIS

Submitted in partial fulfillment of the requirements
for the degree of Master of Science in Mechanical Engineering
in the Graduate College of the
University of Illinois at Urbana-Champaign, 2016

Urbana, Illinois

Advisors:

Professor Elizabeth T. Hsiao-Wecksler
Professor Randy H. Ewoldt

ABSTRACT

Spasticity and rigidity are two abnormal hypertonic muscle behaviors commonly observed in passive joint flexion and extension evaluation. Clinical evaluation for spasticity and rigidity is done through in-person assessment using qualitative scales. Due to the subjective nature of this evaluation method, diagnostic results produced from these clinical assessments can have poor reliability and inconsistency. Incorrect diagnosis and treatment often result in worsening of the abnormal muscle behaviors, reducing the quality of life and leading to an increased cost of healthcare. Several programmable, robotic simulators had been developed to improve the accuracy of clinical evaluation by providing clinician practical training opportunities; however none of these training devices are commercially available due to technical and manufacturing limitations. For this reason, a novel, purely mechanical, hydraulic-based simulator design was proposed as an alternative approach to abnormal muscle behavior simulation. The original goal of the project presented in this thesis was to address both spasticity and rigidity in the elbow joint during flexion; however due to time constraints, the initial prototype can only mimic spasticity. The hydraulic-based simulator utilized a novel damper design using viscous fluid in combination with creative flow channel configurations to replicate different levels of spasticity behaviors depicted on a qualitative scale. The simulator was capable of generating a wide range of speed-dependent force feedbacks without need for any computational controls. Preliminary results obtained from evaluating the simulator suggested the possibility of using this novel design in replicating the speed-dependent characteristics of spasticity. The framework and method implemented in the current simulator prototype could be further developed and expanded to replicate spasticity or other types of abnormal behaviors, such as rigidity, in various human joints (not limiting the design to just the elbow joint).

ACKNOWLEDGMENTS

First I would like to thank my advisor, Prof. Elizabeth T. Hsiao-Wecksler, for giving me the opportunity to work in the Human Dynamics and Controls Lab (HDCL) the past two years. I have learned a tremendous amount of knowledge here and I am constantly inspired by her energy and enthusiasm for design and research. Prof. Hsiao-Wecksler's tireless guidance and support had been a crucial part to the completion of this thesis.

I would like to thank my co-advisor, Prof. Randy H. Ewoldt, for his mentorship and assistance throughout different stages of this research. His brilliant thoughts and ideas had always pointed me towards key insights and guided me through the development process of the simulator presented in this work.

I would like to thank fellow HDCL members – Yinan, Leo, Jason, and Rohita – for their work on the abnormal muscle tone quantification device. Their hard work and dedication made it possible to deliver the first couple functional prototypes to our clinical partners for feedback and evaluation.

I would also like to thank other past and present members of HDCL. Alan, Austin, Chen-Zhang, Deen, Matt, Mazhar, Morgan, and Ziming, it was a pleasure getting to know you all. Alan, I had a great time working with you on the wheelchair project and thank you for your support throughout the writing of this thesis. Matt and Mazhar, thank you for giving me so many life and career advices and pointing me to the right direction when I was confused. Ziming and Chen-Zhang, thank you for all those valuable design and machining suggestions for my class and research projects.

In addition to expressing my gratitude towards the people I have met at UIUC, I would also like to acknowledge my friends from MIT. Qian, Rui, Emily, Kelly, Jennifer, Sharon, and Stephen, thank you for your friendship and continual support in the past six years. This paragraph is for all of you.

Lastly, I would like to thank my Mom, Dad, Brother, and Sister-In-Law for their unconditional love and encouragement. Thank you for believing in what I do and always being there for me. Mom and Dad, thank you for all the sacrifices you have made in giving me the best possible future.

This project was funded by the Jump Applied Research for Community Health through Engineering and Simulation (ARCHES) program.

TABLE OF CONTENTS

1 INTRODUCTION

1.1 ABNORMAL HYPERTONIC MUSCLE BEHAVIORS

Abnormal hypertonic muscle behaviors are often found in patients affected by traumatic brain or spinal cord injuries. These behaviors are features of altered performance of the skeletal muscles, resulting in a substantial increase in muscle tone (hypertonicity) that is speed or position dependent. Individuals suffering from any abnormal muscle behaviors may experience discomfort or pain and have difficulties performing many activities of daily living.

1.1.1 SKELETAL MUSCLE

A skeletal muscle group (e.g., triceps and biceps) is composed of much smaller units – skeletal muscle fibers – enclosed in multiple layers of connective tissue structures such as the epimysium, perimysium, and endomysium. A skeletal muscle fiber is a multinucleated cell filled with many structures called myofibrils; each myofibril is composed of subunits called sarcomeres that are arranged from end to end along its structure [1]. Two types of protein filaments are found in a sarcomere: the thicker filament of myosin protein molecules and the thinner filament of actin protein molecules [1]. Contraction within a skeletal muscle fiber is initiated by an electrical stimulus from the associated motor neuron. Once this electrical impulse is received by the muscle fiber, the actin filaments slide inwards between the myosin filaments; this relative sliding of the actin-myosin filaments leads to a shortening of the sarcomeres, which in turn causes the muscle fiber to contract [1, 2]. Depending on the number of muscle fibers that are stimulated during the process, this can result in contraction of the whole muscle [1, 2].

Typically, there are two ways in which the whole muscle structure can generate a force: active and passive [1-3]. Active force is produced by the sliding action of the actin-myosin filaments, while passive force is produced by the tendons and the connective tissue structures (e.g., epimysium, perimysium, and endomysium) enclosing each component within the skeletal muscle [1-3]. The total force generated by the muscle is a sum of the active and passive force components. One way to evaluate the passive force of the skeletal muscle is through external stretching. Stretching a muscle involves overcoming the tissue's internal resistance [1]. At low speeds, a muscle develops less viscous force, thereby offering less resistance to the stretch motion; as stretch speed increases, the muscle develops greater viscous force which in turn contributes to a higher overall force production [1].

1.1.2 ABNORMAL MUSCLE BEHAVIORS

Abnormal muscle behaviors are consequences of motor neuron diseases in which the nerve pathways within the brain or spinal cord responsible for muscle movements are damaged [4-7]. A damaged nerve pathway is caused by the loss of motor neuron inhibition [6, 7] which ultimately disrupts electrical signal transmission within the central nervous system. The human body relies heavily on the nervous system to maintain its functions. Cells require electrical cues to allow the transport of nutrients, proteins, and waste products in and out of their membranes [4, 5]. When motor neurons become disrupted, toxic waste can build up in muscle cells as a natural by-product of normal cell activity [4]. This waste accumulation alters the biomechanical properties of the muscle, resulting in immobilization of the muscle at short length [8]. When shortened for a prolonged time, secondary biomechanical changes occur within the muscle and

the surrounding tissues [7, 8], leading to the different types of abnormal muscle behavior observed clinically.

There are many types of abnormal muscle behaviors: contracture, dystonia, rigidity, spasticity, tremor, and several others [9, 10]. Depending on the condition and disease, a patient may exhibit one or more abnormal behaviors [6, 9, 10]. Typical symptoms associated with these behaviors are pain, increased muscle tone, spasms, overactive reflexes, and decreased functional abilities and motor development [9, 11, 12]. These behaviors will sporadically cause involuntary movements in the joints, greatly affecting activities of daily living and quality of life [10-13].

1.1.3 SPASTICITY AND RIGIDITY

This section focuses on two abnormal muscle behaviors – spasticity and rigidity – that are commonly observed during passive joint flexion and extension evaluation.

Spasticity is a common symptom of upper motor neuron (UMN) syndrome [8, 14-16]. UMN syndrome occurs in conditions affecting motor neurons in the brain or spinal cord such as stroke, multiple sclerosis, traumatic brain injury, and cerebral palsy [15-18], and it has two classical distinctions in terms of its clinical signs [8, 14-16, 18]. Voluntary muscle underactivity, or negative signs, include weakness and loss of dexterity [8, 16, 18]. Involuntary muscle overactivity, or positive signs, are characterized by exaggerated tonic and phasic stretch reflexes, resulting in excessive muscle contraction, spasms, or other forms of inappropriate muscle behavior [8, 16, 18].

Spasticity is a positive clinical sign that affects an estimated 12 million people worldwide [19]. This behavior is usually due to a lesion (or lesions) involving the neural pathways at the

cerebral cortex or spinal cord [7, 14-16, 18, 19]. There is no precise definition for spasticity to this day. The clinical characteristics of spasticity have been described for operational purposes by Lance [20] as a form of hypertonia due to a speed dependent increase in tonic stretch reflexes (muscle tone). Spasticity is dependent on input stretch speed, and it is only elicited when a certain speed threshold is reached [8, 14]. This speed threshold differs by individual and can vary widely. Although spasticity typically triggers at a high stretch speed, studies have demonstrated that low stretch speed may also induce the behavior [14, 21, 22]. As stretch speed increases, muscle resistance intensifies and higher reflex activity is observed [8, 14].

Spasticity, in conjunction with excessive muscle tone, frequently interferes with voluntary motor function in patients, affecting their ability to perform daily living activities [11-13, 17]. Muscle pain or discomfort, reduction in joint range of motion (ROM), and contracture may also occur at the joint crossed by spastic muscles [14, 17], further reducing a patient's independence. The treatment of spasticity has been central to the clinical management of patients with UMN syndrome [14, 16, 18]. Current trends in research and clinical practice have shown that considerable resources are still being invested in both developing and optimizing anti-spasticity treatment protocols [14].

Rigidity is one of the major manifestations of Parkinson's disease (PD) [13, 23]. PD is a chronic and progressive neurodegenerative disorder [13, 23, 24] that involves the malfunction and death of neurons in the brain, mainly in an area called the substantia nigra [24]. The only symptom unequivocally produced by rigidity is a feeling of stiffness [13, 23, 24] and it affects an estimated number of 10 million people worldwide [25]. As a clinical sign, rigidity is described as the behavior of increased resistance to the passive movement of a limb throughout its ROM [23, 26, 27]. Both spasticity and rigidity are neurological impairments associated with an abnormal

increase in muscle tone. However, rigidity is known to be less sensitive to stretch speed [23, 26-29], and this characteristic plays an indispensable role in differentiating rigidity from spasticity during clinical evaluations [29]. In rigidity, the resistance encountered is sustained throughout the whole range of passive movement [26, 27]. As muscle elongates or joint angle increases due to stretch, a uniform increase in resistance is observed [27].

Similar to spasticity, rigidity hinders functional movement and may induce pain and various forms of physical discomfort. Patients with rigidity experience stiffness, slowness of movement, and poor mobility [24], leading to activity limitations and participation restrictions. Spasm and contracture may occur, though uncommon, at affected limbs, and full joint ROM can typically be achieved [12, 13, 24]. As treatment of spasticity is essential to UMN syndrome, treatment of rigidity also forms an integral part of clinical diagnosis and therapeutic evaluation of PD [27].

1.1.4 CURRENT EVALUATION METHODS AND PROBLEMS

A number of studies and surveys have shown that spasticity and rigidity interfere with many activities of daily living, greatly affecting the quality of life in patients and causing anxiety, depression, and social isolation [11-13]. Therefore, proper treatment of these abnormal muscle symptoms is crucial in helping patients to regain their confidence and independence.

Treatment plans of spasticity and rigidity are reliant on correct patient assessment. Clinical evaluation involves performing passive stretch tests at multiple limb joints and characterizing the muscle behavior using qualitative scales [16, 18, 27, 29]. During a typical assessment, a clinician will provide support at the joint and then passively flex or extend the

patient's limb segment at one or more speeds while the patient is instructed to relax (Figure 1.1). Abnormalities in muscle tone, range of motion, and symmetry are noted and a score (from a clinical scale) is assigned to describe the overall condition of the patient. Clinical scales used to describe spasticity and rigidity address multiple degrees of severity and each degree is accompanied by a short qualitative description. In general, the Modified Ashworth Scale (MAS) (Table 1.1) [30] and the Modified Tardieu Scale (MTS) (Table 1.2) [31] are used to assess spasticity, while the Motor Section of the Unified Parkinson's Disease Rating System (UPDRS) (Table 1.3) [32] is used to assess rigidity (see Appendix A for more details regarding qualitative scales used in clinical assessment). However, these qualitative scales are susceptible to problems of sensitivity and reliability. In fact, several studies [33-40] have reported poor reliability and inconsistency on the diagnostic results produced from these clinical scales, demonstrating the need for improving the current evaluation method.

Qualitative scales adopted in a clinical setting are subjective in nature (clinician-dependent) which decreases the inter-rater and intra-rater reliability [33-35, 37, 39]. Inconsistent results are usually due to clinician and subject variability. The same patient may respond differently to a passive stretch test performed by different clinicians due to variations in speeds and stretch techniques [41]. Further, patient factors such as acute sickness, injuries, fatigue level, body posture and position, ability to relax, and level of anxiety may influence the diagnostic results [10, 41]. Another reason for the poor reliability of these assessments is likely to be the qualitative descriptions of these clinical scales which make them open to clinician interpretation [41, 42]. Inexplicit terms such as "slight increase" (MAS 1, MAS 2), "more marked increase" (MAS 3), and "considerable increase" are used to describe different degrees of muscle tone in the MAS, and "slight" (UPDRS 1), "mild to moderate" (UPDRS 2), "marked" (UPDRS 3), and

"severe" (UPDRS 4) are used in the UPDRS. Depending how the clinicians perceive each term, the same feeling of muscle tone may be assigned different scores.

Accuracy and precision of assessment results are critical for designing optimal treatment plans, properly evaluating potential effects of treatment interventions, and monitoring progression of recovery [14, 16, 41]. However, the current evaluation method makes it difficult to obtain accurate, reliable results, thereby posing great challenges for assigning the correct treatment plan to patients. Incorrect diagnosis and treatment often result in worsening of the abnormal muscle symptoms, which can lead to an increased cost of healthcare [10].

Figure 1.1: Demonstration of passive stretch test for the elbow extensor.

Table 1.1: Modified Ashworth Scale for assessing spasticity, adapted from [30].

Score	Description
0	No increase in muscle tone
1	Slight increase in muscle tone, manifested by a catch and release or by minimal resistance at the end of the range of motion when the affected part(s) is moved in flexion or extension
2	Slight increase in muscle tone, manifested by a catch, followed by minimal resistance throughout the reminder (less than half) of the range of motion
3	More marked increase in muscle tone through most of the range of motion, but affected part is easily moved
4	Considerable increase in muscle tone, passive movement difficult
5	Affected part is rigid in flexion or extension

Table 1.2: Modified Tardieu Scale for assessing spasticity, adapted from [31].

Score	Description
0	No resistance throughout passive movement
1	Slight resistance throughout, with no clear catch at a precise angle
2	Clear catch at a precise angle followed by release
3	Fatigable clonus (<10 secs) occurring at a precise angle
4	Un-fatigable clonus (>10 secs) occurring at a precise angle
5	Joint immobile

Table 1.3: Unified Parkinson's Disease Rating System for assessing rigidity, adapted from [43].

Score	Description
0	Rigidity absent
1	Rigidity slight or detectable only when activated by mirror or other movements
2	Rigidity mild to moderate
3	Rigidity marked, but full range of motion easily achieved
4	Rigidity severe; range of motion achieved with difficulty

1.1.5 EXISTING QUANTITATIVE DATA

Clinical assessments of spasticity and rigidity are mainly qualitative. The validity of the assessment results is sometimes in doubt due to poor inter-rater and intra-rater reliability [30, 33-37, 39]. Several methods involving the use of custom-fabricated instrumentation [17, 26, 27, 29, 42, 44-54] have been introduced to measure these abnormal muscle behaviors, but none have been adopted outside of a research laboratory setting. A possible reason is that these methods are too different from the crucial aspects of a clinical exam, hence it is hard to incorporate them into the actual evaluation procedure. Quantifying spasticity and rigidity has always been a challenging task. Although the current quantitative methods were all deemed to be unfeasible in general clinical practice, data collected from pilot studies using these methods have provided important information in understanding and differentiating the clinical features of spasticity and rigidity.

The feel of spasticity and rigidity varies depending on the limb joint. For instance, the magnitude of muscle resistance at the elbow joint is greater than that at the wrist joint for the same qualitative rating, hence different methods have been developed to obtain quantitative data from each joint. This section mainly reviews methods used to quantify elbow spasticity and rigidity and quantitative data from literature that correlate with existing clinical scales (e.g. MAS, MTS and UPDRS).

Attempts made to quantify spasticity and rigidity in the upper extremity can be tracked back to the 1980s. Earlier studies on spastic and rigid muscle focused on relating the associated clonus behavior in the affected limb joint to different clinical diagnosis (e.g. stroke, multiple sclerosis, and Parkinson's disease) by using electromyography (EMG) sensors [52, 53]. The affected limb of the patient was subjected to passive stretch test and patterns of the repeated

bursts of EMG during clonus were identified, analyzed, and correlated to a frequency range. In the late 1980s, Watts et al. developed a manual device consisting of a rotary potentiometer and a torque motor to measure muscle stiffness (output torque due to position) of PD patients and healthy normal controls at the elbow joint [45, 46]. Their findings revealed that PD patients, even with relatively mild symptoms, had higher joint stiffness than normal controls.

Several studies have been conducted with manual instrumentation consisting of EMG sensors, position sensors and torque or force transducers in the 1990s [26, 48, 50, 54, 55]. Most of these studies, however, were done on a small patient population (e.g., $n < 10$) with unidentified clinical scores. The main focus had been on developing generalized mathematical models, such as a linear spring-damper model [55], a nonlinear activation model [54], and a impedance model [48], to explain the torque response of affected muscles with respect to either passive stretch speed or stretch position rather than correlating quantitative data to the clinical scales.

There was an increase in the number of quantification studies designed to characterize spasticity and rigidity in relation to their clinical scales in the 2000s [17, 27, 29, 42, 44, 47, 49, 51]. Analysis methods, such as regression analysis, derivative analysis, and analysis of variance, were introduced to better extract the clinical features associated with each degree of abnormal muscle behaviors. Experimental results of joint torque were analyzed and represented in relation to speed, position, clinical score, and other patient factors such as age, gender, and medication.

Efforts in quantifying and analyzing elbow spasticity were mostly made by a group from National Cheng Kung University in Taiwan [29, 49, 51]. This group performed a series of experiments using a portable muscle tone system to quantify the speed dependency of spasticity and how it related to the Modified Ashworth Scale. Their instrument was based on a motor-

driven system consisting of EMG sensors, a rotary encoder, a gyroscope, and a differential pressure sensor to measure the summation of reactive resistance across flexion and extension directions. The device could move the affected limb in a fixed ROM of approximately 60 deg at different speeds. They proposed a viscosity measurement which related the output torque to the input stretch frequency (the rate at which a stretch test was performed) as a means to quantify spasticity. Their analysis results showed that as input stretch speed increased, muscle resistance increased linearly and that for patients with more severe condition, this viscous response would be more noticeable. Their findings provided a correlation between the speed-dependent torque of spasticity in the elbow joint (Table 1.4) to scores on the MAS (Table 1.1). These results were only for MAS scores of 0 – 4, since no patients were evaluated with a MAS score of 5. Refer to Appendix B for details of the derivation of Table 1.4 from data presented in [49, 51].

Table 1.4: Average (±standard deviation) viscosity of elbow muscles during passive stretch (for both flexion and extension) in relation to MAS score (derived from [49, 51]).

MAS Score	Viscosity - *B* [N.m/(cycles/s)]
0	0.045 ± 0.035
1	0.105 ± 0.052
2	0.117 ± 0.064
3	0.172 ± 0.071
4	0.365 ± 0.001
5	NA

Another scale frequently used by clinicians to rate spasticity is the Modified Tardieu Scale. Quantification of the MTS requires precise determination of the catch angle and clonus frequency [17, 44], and there are very few studies on this matter. Wu et al. developed a manual spasticity evaluator consisting of EMG sensors, a rotary potentiometer, and a torque sensor in an attempt to quantify the MTS [17, 44]. Their pilot studies confirmed the feasibility of the manual

evaluator and their derivative analysis method (derivative of torque with respect to time); however the results were insufficient to fully quantify the MTS due to a small sample size (n = 10).

Rigidity is less complex in comparison to spasticity. Multiple research groups have designed studies to quantify and model the rigidity behaviors [27, 29, 42, 47]. Patrick et al. devised a mathematical model relating muscle torque response to UPDRS rating using data collected from a manual quantification device consisting of a flexible position sensor, a 3D motion sensor, and a force transducer [42]. Xia et al. examined the correlation between rigidity and the interaction of stretch reflex and shortening during passive joint movements using a motor-based system consisting of a servomotor, EMG sensors, a rotary encoder, and a torque transducer [27, 56]. Out of these different studies, Sepehri et al. produced one of the most complete data sets for rigidity in relation to the UPDRS using a manual device [47]. Their instrumentation setup consisted of EMG sensors, a rotary potentiometer, and a force transducer. The study involved 117 individuals, of which 100 were PD patients, spanning across all levels of UPDRS. The findings by Sepheri et al. (Table 1.5) revealed that full ROM was generally achieved in rigidity patient; however, joint stiffness (output torque due to position) significantly increased as UPDRS rating increased.

Table 1.5: Rigidity experimental results of elbow muscles in relation to UPDRS scores, adapted from [47]. Mean ± standard deviation.

UPDRS		Range of Motion [deg]	Stiffness [N.m/deg]
Score	# Subjects		
0	17	127.9 ± 17.6	0.042 ± 0.007
1	32	128.9 ± 14.8	0.053 ± 0.009
2	31	122.7 ± 15.8	0.059 ± 0.012
3	32	123.6 ± 10.1	0.067 ± 0.010
4	5	127.3 ± 12.9	0.074 ± 0.009

The aforementioned methods developed to quantify spasticity and rigidity all involved rigid, bulky testing setups that limited the mobility of the patient. Since spasticity and rigidity are multifactorial in nature, any external constraint may alter the muscle behavior, possibly resulting in quantitative data that do not match the qualitative score of the patient. Clinician involvement in evaluation of spasticity and rigidity is necessary in improving the accuracy of diagnosis.

1.2 CLINICAL TRAINING SIMULATORS OF ELBOW SPASTICITY AND RIGIDITY

In a clinical setting, spasticity and rigidity are manually tested using qualitative scales. Rating accuracy and consistency are directly related to clinician experience [30, 33, 35, 39]. During clinical training, an instructor can replicate rigidity through isometric contraction to stiffen the muscle. Spasticity, on the other hand, is difficult to artificially mimic, hence training on patients is necessary. However, recurrent training opportunities are limited due to patient availability. It is difficult to continually recruit patients with diverse degrees of spasticity and rigidity for training purposes. Further, repeated cycles of passive stretching should not be performed within a short timeframe because it is known that muscle tone will change with repeated joint movements [41]. For this reason, even if a patient is successfully brought to the classroom for evaluation training, the muscle tone felt by each trainee will be different.

Clinical training for abnormal muscle tone evaluation lacks a practical tool to enable young clinicians and healthcare professional students to experience and distinguish among various behaviors (e.g. spasticity and rigidity). There is a clear need for simulators in this area to deliver better quality, structured training in the classroom. These clinical training simulator devices will serve as an alternative to real patients, and ultimately help to reduce instructional

and training costs by saving time and money involved in the recruiting, scheduling, testing, and financially compensating patient volunteers. Moreover, when using a simulator, a student can make mistakes and learn from them without the fear of harming the patient [57]. Simulation-based training has the potential to not only allow young medical professionals to gain more practical experience through deliberate practice, but also help in standardizing diagnostic procedures for improved patient treatment and therapy [57, 58].

1.2.1 EXISTING RESEARCH SIMULATORS

To improve the accuracy and reliability of clinical diagnosis, a few medical simulators [41, 59-65] that can replicate different abnormal muscle behaviors have been developed to provide practical training in the classroom. However, no simulators are commercially available. In this section, simulators designed to mimic spasticity and rigidity in the elbow joint are reviewed and discussed.

The Upper Limb Patient Simulator (Figure 1.2a) [59, 65] was developed at the University of Tokyo to simulate spasticity and rigidity. This simulator worked only in the direction of elbow flexion and it used a customized magnetorheological (MR) fluid brake for torque control during simulation. An encoder and strain gauges were used for feedback control and a motor was installed in parallel to the fluid brake to increase the variety and reality of the simulated behavior. MR fluid is a smart material consisting of iron particles (typically 1-20 microns in size) suspended in a liquid. Its viscosity increases (and is typically non-Newtonian shear-thinning) when subjected to a magnetic field due to particle aggregation into chain structures. Taking advantage of this particular property of the MR fluid, this simulator was able to generate passive reaction force even in slow speed and it could mimic human joint compliance. Preliminary

testing results showed that the device could be programmed to replicate different spasticity and rigidity behaviors measured from actual patients; however, no further studies regarding the device were published since 2011.

The Haptic Simulator for Elbow Joint Spasticity (Figure 1.2b) [64] was developed at The Johns Hopkins University. This simulator was made to resemble the arm of a small child and it could work in both flexion and extension. It used an electric brake and motor for replication of spasticity and an encoder for feedback control. This hybrid actuation system was similar to the Tokyo simulator; however the use of the electric brake made it challenging for the device to produce realistic feedback at low input speeds. There were no published testing or validation data for this device; hence its feasibility remains unknown.

The Haptic Elbow Spasticity Simulator (HESS) (Figure 1.2c) [41] was developed at the National Institutes of Health. HESS was one of the most recent simulators developed for training purposes. It had one degree of freedom at the elbow joint and worked in both flexion and extension. The design consisted of an electric motor and a 2-staged cable drive mechanism for torque manipulation, and it used a torque transducer for feedback control and haptic interaction. The control strategy for the simulated spastic response was divided into three stages: pre-catch, catch, and post-catch, and a mathematical model was developed to characterize each stage to ensure accurate representation of the true behavior. Preliminary testing results showed that HESS was able to consistently reproduce the behaviors of five different subjects representing MAS 0 – 4 and the haptic interface allowed users to experience force feedback matched to their input movements.

The Pneumatic Elbow Simulator for Spasticity and Rigidity (Figure 1.2d) [62] was developed at Bradley University. This simulator had one degree of freedom, and it worked only

in flexion. The device consisted of a pneumatic linear cylinder working in a closed fluid system for force generation and a rotary potentiometer for feedback control. The actuator could act as a pneumatic spring or damper during operation, and the inherent compressibility of the working fluid, air, allowed for modest replication of human joint compliance. Similar to the Johns Hopkins simulator, there were no published testing or validation data for the Bradley simulator.

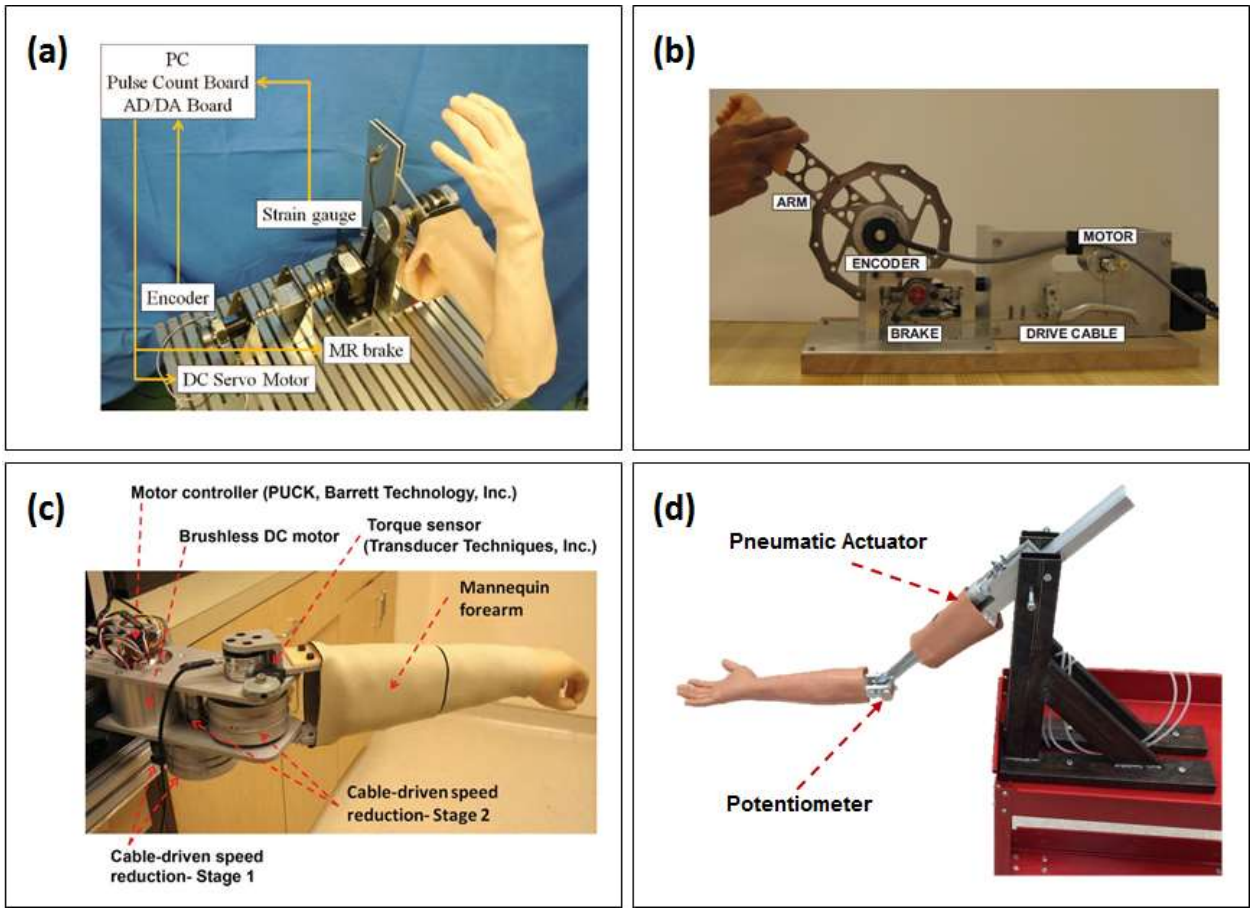

Figure 1.2: (a) The Upper Limb Patient Simulator [59]. (b) The Haptic Simulator for Elbow Joint Spasticity [64]. (c) The Haptic Elbow Spasticity Simulator [41]. (d) The Pneumatic Elbow Simulator for Spasticity and Rigidity [62].

1.2.2 VISCOUS DAMPER DESIGN

Simulators discussed in the previous section all relied on an active actuation system and complex real-time control algorithms to replicate different abnormal muscle behaviors. The main control effort has been to accurately mimic the speed dependency of spasticity over varying degrees of severity. When examining the fundamental properties of spasticity, it is not difficult to realize that this behavior shares many similarities with those of a viscous damper. In fact, when analyzing the clinical features of spasticity, researchers often use the term "viscous" [29, 41, 49, 51, 64] to describe its speed dependency.

Viscous dampers using MR fluid have been implemented in spasticity simulators [59, 63, 65]. The unique composition of this smart material enables active, programmable damping control by varying the input electrical current (which results in a magnetic field of varying strength). Design and development of an active damping system using a MR fluid constitute a new research category that is apart from traditional passive damping system. In this section, the discussion is focused on passive viscous dampers.

Viscous damper technology originated with military and aerospace applications [66], but it is found in many mechanical systems as a means to protect structures from destructive shock and vibration nowadays [66-68]. Viscous dampers are often fluid-based. A fluid viscous damper dissipates the input energy by pushing fluid through an orifice, producing a differential pressure inside its internal chamber which then creates a force [67]. The resulting force is proportional to the relative speed between the ends of the damper [66, 67].

In general, a viscous damper (Figure 1.3) contains the following elements: piston rod, piston head, cylinder, fluid, accumulator and seal. The piston rod is rigidly attached to the piston head to form a single piston that goes through the center of a fluid-filled cylinder. An

accumulator is often found at the end of the cylinder to account for the internal volume change as the piston strokes, and this accumulator can be a block of closed-cell plastic foam, a moveable pressurized piston, or a rubber bladder [66]. Effective sealing plays an important role in the damper design. When correctly designed and fabricated, a viscous damper should have nearly perfect sealing with zero leakage [66]. However, if leakage is inevitable, an external liquid storage device can be used to keep the cylinder full during operation.

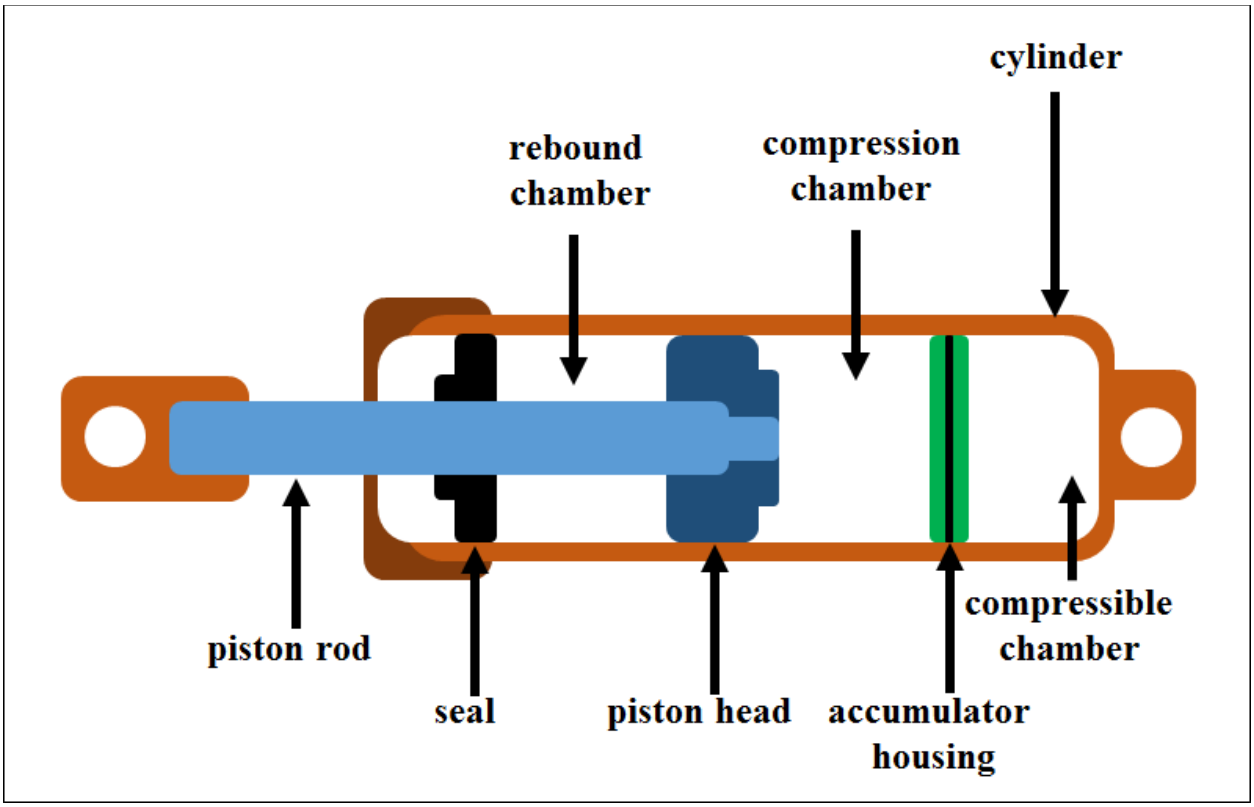

Figure 1.3: Elements of a typical viscous damper.

A viscous damper can generate a wide range of force output depending on the input motion. As the piston moves, it pushes fluid from the compression chamber to the rebound chamber through orifices around and through the piston head [66, 69]. This movement of fluid from a larger area (compression chamber) to a smaller area (orifices) and from a smaller area

(orifices) to a larger area (rebound chamber) results in the dissipation of energy due to head loss, resulting in a pressure difference across the piston head [69]. This differential pressure produces a force that resists the motion of the piston.[69]

Performance of a viscous damper is largely dependent on its working fluid. Depending on the application, the working fluid typically is expected to maintain a similar viscosity over a large temperature range, have excellent thermal stability and not degrade with age. For this reason, silicone oil is often used as completely nontoxic and one of the most thermally stable fluids available [66, 70].

The unique material properties of silicone oil make it a good working fluid in viscous dampers [66, 67]. Silicone oil is clear, odorless and it comes in a wide range of viscosities. The material is a liquid polymerized siloxane with organic side chains [70], and there are no reported harmful effects of such polymers on organisms in the environment.

The backbone of silicone oil is composed of alternating silicon and oxygen atoms [70]. This silicon-oxygen (Si-O) chain is similar to the structure found in many high-temperature materials such as quartz, glass and sand, making silicone oil more resistant to attack by temperature extremes, shear stresses and chemicals [71]. One big advantage of silicone oil is that it can be easily engineered to have a specific viscosity. Viscosity of silicone oil is determined by the length of its Si-O chain, with a longer Si-O chain resulting in a bigger polymer (larger molecular weight) and higher viscosity [70, 72]. While most fluids show some degree of change in viscosity with temperature change, silicone oils exhibit a much smaller degree of change over a wider temperature range [71], making it ideal in applications that require accurate viscosity.

1.3 THESIS ORGANIZATION

In this thesis, a new perspective was taken to explore creative simulator designs through a purely mechanical approach. The original goal of this research was to mimic both spasticity and rigidity by developing passive damper designs using viscous fluids combined with different flow channel configurations. However due to time constraints in the development process, only spasticity is addressed in the final design. The finished prototype is a simple, portable, purely mechanical simulator that can replicate the generalized force due to position representing normal and different levels of abnormal muscle behaviors.

Chapter 1 provided a general background of abnormal muscle behaviors with specific focus on spasticity and rigidity. This chapter also reviewed several methods used to quantify different clinical scales for evaluating these abnormal muscle behaviors at the elbow joint and introduced clinical training simulators for the elbow that have been developed by different research groups.

Chapter 2 focused on the design, modelling and validation of a purely mechanical, fluid-based simulator for replicating spasticity at the elbow joint. An analytical model of the fluid behavior was developed and validated to allow for deterministic, predictive design. By evaluating this simulator prototype, new insights regarding viscous pressure flow in relation to geometry, speed and viscosity are drawn. The findings from this chapter suggest the possibility of using a novel hydraulic-based design to mimic the biomechanical properties of human muscle.

Chapter 3 expanded the simulator design work presented in Chapter 2 to replicate the less speed-sensitive rigidity behavior, summarizes the conclusion, and provides recommendation for the next steps of the fluid-based simulator development process.

This thesis ends with appendices that provided additional information on clinical background (Appendix A), data derivation process (Appendix B), and other materials related to the hydraulic-based simulator design that were not presented in the main text (Appendix C, D, E, and F).

1.4 LIST OF REFERENCES

[1] C. A. Oatis, *The mechanics and pathomechanics of human movement*, 2 ed. Philadelphia, PA: Williams and Wilkins, Lippincott, 2003.

[2] I. Rayment, H. M. Holden, M. Whittaker, C. B. Yohn, M. Lorenz, K. C. Holmes, and R. A. Milligan, "Structure of the actin-myosin complex and its implications for muscle contraction," *Science*, vol. 261, pp. 58-65, Jul 2 1993.

[3] C. J. Zuurbier, A. J. Everard, P. van der Wees, and P. A. Huijing, "Length-force characteristics of the aponeurosis in the passive and active muscle condition and in the isolated condition," *J Biomech*, vol. 27, pp. 445-453, Apr 1994.

[4] National Health Service. (2015). *Motor neurone disease – Causes* [Web]. Available: http://www.nhs.uk/Conditions/Motor-neurone-disease/Pages/Causes.aspx [Accessed: Jul. 2, 2016]

[5] M. Hafezparast, R. Klocke, C. Ruhrberg, A. Marquardt, A. Ahmad-Annuar, S. Bowen, G. Lalli, A. S. Witherden, H. Hummerich, S. Nicholson, P. J. Morgan, R. Oozageer, J. V. Priestley, S. Averill, V. R. King, S. Ball, J. Peters, T. Toda, A. Yamamoto, Y. Hiraoka, M. Augustin, D. Korthaus, S. Wattler, P. Wabnitz, C. Dickneite, S. Lampel, F. Boehme, G. Peraus, A. Popp, M. Rudelius, J. Schlegel, H. Fuchs, M. Hrabe de Angelis, G. Schiavo, D. T. Shima, A. P. Russ, G. Stumm, J. E. Martin, and E. M. Fisher, "Mutations in dynein link motor neuron degeneration to defects in retrograde transport," *Science*, vol. 300, pp. 808-812, May 2 2003.

[6] D. Purves, G. J. Augustine, D. Fitzpatrick, L. C. Katz, A.-S. LaMantia, J. O. McNamara, and S. M. Williams, "Damage to Descending Motor Pathways: The Upper Motor Neuron Syndrome," in *Neuroscience* 2ed Sunderland, MA: Sinauer Associates 2001.

[7] R. L. Lieber, S. Steinman, I. A. Barash, and H. Chambers, "Structural and functional changes in spastic skeletal muscle," *Muscle Nerve,* vol. 29, pp. 615-627, May 2004.

[8] G. Sheean, "The pathophysiology of spasticity," *Eur J Neurol,* vol. 9 Suppl 1, pp. 3-9, 53-61, May 2002.

[9] American Association of Neurological Surgeons. (2013). *Movement Disorders* [Web]. Available:http://www.aans.org/patient%20information/conditions%20and%20treatments/movement%20disorders.aspx [Accessed: Jul. 2, 2016]

[10] E. B. Brokaw, D. A. Heldman, R. J. Plott, E. J. Rapp, E. B. Montgomery, and J. P. Giuffrida, "Development of a clinician worn device for the evaluation of abnormal muscle tone," in *36th Annual International Conference of the IEEE Engineering in Medicine and Biology Society* 2014, pp. 4091-4094

[11] B. G. Vickrey, R. D. Hays, R. Harooni, L. W. Myers, and G. W. Ellison, "A health-related quality of life measure for multiple sclerosis," *Qual Life Res,* vol. 4, pp. 187-206, Jun 1995.

[12] A. Schrag, M. Jahanshahi, and N. Quinn, "What contributes to quality of life in patients with Parkinson's disease?," *J Neurol Neurosurg Psychiatry,* vol. 69, pp. 308-312, 2000.

[13] R. Cano-de-la-Cuerda, L. Vela-Desojo, J. C. Miangolarra-Page, Y. Macias-Macias, and E. Munoz-Hellin, "Axial rigidity and quality of life in patients with Parkinson's disease: a preliminary study," *Qual Life Res,* vol. 20, pp. 817-823, Aug 2011.

[14] A. D. Pandyan, M. Gregoric, M. P. Barnes, D. Wood, F. Van Wijck, J. Burridge, H. Hermens, and G. R. Johnson, "Spasticity: clinical perceptions, neurological realities and meaningful measurement," *Disabil Rehabil,* vol. 27, pp. 2-6, Jan 7-21 2005.

[15] D. Burke, "Spasticity as an adaptation to pyramidal tract injury," *Adv Neurol,* vol. 47, pp. 401-423, 1988.

[16] M. P. Barnes and G. R. Johnson, *Upper motor neurone syndrome and spasticity: clinical management and neurophysiology*: Cambridge University Press, 2008.

[17] Y. N. Wu, H. S. Park, Y. Ren, D. Gaebler-Spira, J. J. Chen, and L. Q. Zhang, "Measurement of elbow spasticity in stroke patients using a manual spasticity evaluator," in *28th Annual International Conference of the IEEE Engineering in Medicine and Biology Society* 2006, pp. 3974-3977

[18] M. P. Barnes, "An overview of the clinical management of spasticity," in *Upper motor neurone syndrome and spasticity: clinical management and neurophysiology*, M. P. Barnes and G. R. Johnson, Eds., ed Cambridge, United Kingdom: Cambridge University Press, 2001, pp. 1-11.

[19] American Association of Neurological Surgeons. (2006). *Spasticity* [Web]. Available: http://www.aans.org/Patient%20Information/Conditions%20and%20Treatments/Spasticity.aspx [Accessed: Jul. 2, 2016]

[20] J. W. Lance, "Symposium synopsis," in *Spasticity: disordered motor control*, ed Chicago, IL: Yearbook Medical 1980, pp. 485-494.

[21] A. Hufschmidt and K. H. Mauritz, "Chronic transformation of muscle in spasticity: a peripheral contribution to increased tone," *J Neurol Neurosurg Psychiatry,* vol. 48, pp. 676-685, Jul 1985.

[22] J. P. A. Dewald and J. D. Given, "Electrical stimulation and spasticity reduction: fact or fiction?," *Phys Med Rehabil,* vol. 8, pp. 507-522, 1994.

[23] A. Berardelli, A. F. Sabra, and M. Hallett, "Physiological mechanisms of rigidity in Parkinson's disease," *J Neurol Neurosurg Psychiatry*, vol. 46, pp. 45-53, Jan 1983.

[24] Parkinson's Disease Foundation. (2016). *What is Parkinson's Disease?* [Web]. Available: http://www.pdf.org/en/about_pd [Accessed: Jul. 2, 2016]

[25] Parkinson's Disease Foundation. (2016). *Statistics on Parkinson's* [Web]. Available: http://www.pdf.org/parkinson_statistics [Accessed: Jul. 2, 2016]

[26] M. P. Caligiuri, "Portable device for quantifying parkinsonian wrist rigidity," *Mov Disord*, vol. 9, pp. 57-63, Jan 1994.

[27] R. Xia, J. Sun, and A. J. Threlkeld, "Analysis of interactive effect of stretch reflex and shortening reaction on rigidity in Parkinson's disease," *Clin Neurophysiol*, vol. 120, pp. 1400-1407, Jul 2009.

[28] M. Bergui, L. Lopiano, G. Paglia, G. Quattrocolo, L. Scarzella, and B. Bergamasco, "Stretch reflex of quadriceps femoris and its relation to rigidity in Parkinson's disease," *Acta Neurol Scand*, vol. 86, pp. 226-229, Sep 1992.

[29] H. M. Lee, Y. Z. Huang, J. J. Chen, and I. S. Hwang, "Quantitative analysis of the velocity related pathophysiology of spasticity and rigidity in the elbow flexors," *J Neurol Neurosurg Psychiatry*, vol. 72, pp. 621-629, May 2002.

[30] R. W. Bohannon and M. B. Smith, "Interrater reliability of a modified Ashworth scale of muscle spasticity," *Phys Ther*, vol. 67, pp. 206-207, Feb 1987.

[31] R. N. Boyd, S. A. Barwood, C. E. Baillieu, and H. K. Graham, "Validity of a clinical measure of spasticity in children with cerebral palsy in a randomized clinical trial," *Dev Med Child Neurol*, vol. 40, p. 7, 1998.

[32] S. Fahn and R. Elton, *Recent Developments in Parkinson's Disease* vol. 2. Florham Park, NJ: Macmillan Health Care Information, 1987.

[33] W. K. Yam and M. S. Leung, "Interrater reliability of Modified Ashworth Scale and Modified Tardieu Scale in children with spastic cerebral palsy," *J Child Neurol,* vol. 21, pp. 1031-1035, Dec 2006.

[34] A. Siderowf, M. McDermott, K. Kieburtz, K. Blindauer, S. Plumb, I. Shoulson, and G. Parkinson Study, "Test-retest reliability of the unified Parkinson's disease rating scale in patients with early Parkinson's disease: results from a multicenter clinical trial," *Mov Disord,* vol. 17, pp. 758-763, Jul 2002.

[35] M. Richards, K. Marder, L. Cote, and R. Mayeux, "Interrater reliability of the Unified Parkinson's Disease Rating Scale motor examination," *Mov Disord,* vol. 9, pp. 89-91, Jan 1994.

[36] L. V. Metman, B. Myre, N. Verwey, S. Hassin-Baer, J. Arzbaecher, D. Sierens, and R. Bakay, "Test-retest reliability of UPDRS-III, dyskinesia scales, and timed motor tests in patients with advanced Parkinson's disease: an argument against multiple baseline assessments," *Mov Disord,* vol. 19, pp. 1079-1084, Sep 2004.

[37] J. Mehrholz, K. Wagner, D. Meissner, K. Grundmann, C. Zange, R. Koch, and M. Pohl, "Reliability of the Modified Tardieu Scale and the Modified Ashworth Scale in adult patients with severe brain injury: a comparison study," *Clin Rehabil,* vol. 19, pp. 751-759, Oct 2005.

[38] J. Mehrholz, Y. Major, D. Meissner, S. Sandi-Gahun, R. Koch, and M. Pohl, "The influence of contractures and variation in measurement stretching velocity on the

reliability of the Modified Ashworth Scale in patients with severe brain injury," *Clin Rehabil,* vol. 19, pp. 63-72, Jan 2005.

[39] T. Kaya, A. G. Karatepe, R. Gunaydin, A. Koc, and U. Altundal Ercan, "Inter-rater reliability of the Modified Ashworth Scale and modified Modified Ashworth Scale in assessing poststroke elbow flexor spasticity," *Int J Rehabil Res,* vol. 34, pp. 59-64, Mar 2011.

[40] J. F. M. Fleuren, G. E. Voerman, C. V. Erren-Wolters, G. J. Snoek, J. S. Rietman, H. J. Hermens, and A. V. Nene, "Stop using the Ashworth Scale for the assessment of spasticity," *J Neurol Neurosurg Psychiatry,* vol. 81, pp. 46-52, Jan 10 2010.

[41] H. S. Park, J. Kim, and D. L. Damiano, "Development of a Haptic Elbow Spasticity Simulator (HESS) for improving accuracy and reliability of clinical assessment of spasticity," *IEEE Trans Neural Syst Rehabil Eng,* vol. 20, pp. 361-370, May 2012.

[42] S. K. Patrick, A. A. Denington, M. J. Gauthier, D. M. Gillard, and A. Prochazka, "Quantification of the UPDRS Rigidity Scale," *IEEE Trans Neural Syst Rehabil Eng,* vol. 9, pp. 31-41, Mar 2001.

[43] A. E. Lang and S. Fahn, *Assessment of Parkinson's disease*. Boston, MA: Butterworth-Heinemann, 1989.

[44] Y. N. Wu, Y. Ren, A. Goldsmith, D. Gaebler, S. Q. Liu, and L. Q. Zhang, "Characterization of spasticity in cerebral palsy: dependence of catch angle on velocity," *Dev Med Child Neurol,* vol. 52, pp. 563-569, Jun 2010.

[45] A. W. Wiegner and R. L. Watts, "Elastic properties of muscles measured at the elbow in man: I. Normal controls," *J Neurol Neurosurg Psychiatry,* vol. 49, pp. 1171-1176 1986.

[46] R. L. Watts, A. W. Wiegner, and R. R. Young, "Elastic properties of muscles measured at the elbow in man: II. Patients with parkinsonian rigidity," *J Neurol Neurosurg Psychiatry,* vol. 49, pp. 1177-1181, 1986.

[47] B. Sepehri, A. Esteki, E. Ebrahimi-Takamjani, G. A. Shahidi, F. Khamseh, and M. Moinodin, "Quantification of rigidity in Parkinson's disease," *Ann Biomed Eng,* vol. 35, pp. 2196-2203, Dec 2007.

[48] A. Prochazka, D. J. Bennett, M. J. Stephens, S. K. Patrick, R. Sears-Duru, T. Roberts, and J. H. Jhamandas, "Measurement of rigidity in Parkinson's disease," *Mov Disord,* vol. 12, pp. 24-32, Jan 1997.

[49] H. M. Lee, J. J. Chen, M. S. Ju, C. C. Lin, and P. P. Poon, "Validation of portable muscle tone measurement device for quantifying velocity-dependent properties in elbow spasticity," *J Electromyogr Kinesiol,* vol. 14, pp. 577-589, Oct 2004.

[50] J. D. Given, J. P. Dewald, and W. Z. Rymer, "Joint dependent passive stiffness in paretic and contralateral limbs of spastic patients with hemiparetic stroke," *J Neurol Neurosurg Psychiatry,* vol. 59, pp. 271-279, Sep 1995.

[51] J. J. Chen, Y. N. Wu, S. C. Huang, H. M. Lee, and Y. L. Wang, "The use of a portable muscle tone measurement device to measure the effects of botulinum toxin type a on elbow flexor spasticity," *Arch Phys Med Rehab,* vol. 86, pp. 1655-1660, Aug 2005.

[52] R. Iansek, "The effects of reflex path length on clonus frequency in spastic muscles," *J Neurol Neurosurg Psychiatry,* vol. 47, pp. 1122-1124, Oct 1984.

[53] L. J. Findley, M. A. Gresty, and G. M. Halmagyi, "Tremor, the cogwheel phenomenon and clonus in Parkinson's disease," *J Neurol Neurosurg Psychiatry,* vol. 44, pp. 534-546, Jun 1981.

[54] B. D. Schmit, Y. Dhaher, J. P. Dewald, and W. Z. Rymer, "Reflex torque response to movement of the spastic elbow: theoretical analyses and implications for quantification of spasticity," *Ann Biomed Eng*, vol. 27, pp. 815-829, Nov-Dec 1999.

[55] P. H. McCrea, J. J. Eng, and A. J. Hodgson, "Linear spring-damper model of the hypertonic elbow: reliability and validity," *J Neurosci Methods*, vol. 128, pp. 121-128, Sep 30 2003.

[56] R. Xia, K. Markopoulou, S. E. Puumala, and W. Z. Rymer, "A comparison of the effects of imposed extension and flexion movements on Parkinsonian rigidity," *Clin Neurophysiol*, vol. 117, pp. 2302-2307, Oct 2006.

[57] A. H. Al-Elq, "Simulation-based medical teaching and learning," *J Family Community Med*, vol. 17, pp. 35-40, Jan 2010.

[58] J. L. Lane, S. Slavin, and A. Ziv, "Simulation in medical education: A review," *S&G*, vol. 32, pp. 297-314, 2001.

[59] Y. Takhashi, T. Komeda, H. Koyama, S. Yamamoto, T. Arimatsu, Y. Kawakami, K. Inoue, and Y. Ito, "Development of an upper limb patient simulator for physical therapy exercise," in *IEEE 12th International Conference on Rehabilitation Robotics*, 2011, pp. 1-4

[60] H.-S. Park, Q. Peng, and L.-Q. Zhang, "Causality-based portable control system design for tele-assessment of elbow joint spasticity," in *IEEE 9th International Conference on Rehabilitation Robotics*, 2005, pp. 303-306

[61] T. Mouri, H. Kawasaki, Y. Nishimoto, T. Aoki, and Y. Ishigure, "Development of robot hand for therapist education/training on rehabilitation," in *IEEE/RSJ International Conference on Intelligent Robots and Systems*, 2007, pp. 2295-2300

[62] M. Heinrich, C. Mattson, M. Ramuta, J. Stock, J. Liang, M. Morris, S. Tippett, E. Hsiao-Wecksler, and J. Henderson, "Pneumatic Elbow Simulator of Spasticity and Rigidity for Training of Healthcare Clinicians," in *2nd Fluid Power Innovation & Research Conference* Chicago, IL, 2015.

[63] T. Kikuchi, K. Oda, and J. Furusho, "Leg-Robot for Demonstration of Spastic Movements of Brain-Injured Patients with Compact Magnetorheological Fluid Clutch," *Adv Robotics,* vol. 24, pp. 671-686, 2010.

[64] D. I. Grow, M. Wu, M. J. Locastro, S. K. Arora, A. J. Bastian, and A. M. Okamura, "Haptic simulation of elbow joint spasticity," in *IEEE Symposium on Haptic Interfaces for Virtual Environment and Teleoperator Systems*, 2008, pp. 475-476

[65] T. Fujisawa, M. Takagi, Y. Takahashi, K. Inoue, T. Terada, Y. Kawakami, and T. Komeda, "Basic research on the upper limb patient simulator," in *IEEE 10th International Conference on Rehabilitation Robotics*, 2007, pp. 48-51

[66] D. Lee and D. P. Taylor, "Viscous damper development and future trends," *Struct Des Tall Buil,* vol. 10, pp. 311-320, Mar 2001.

[67] G. Haskell and D. Lee, "Fluid viscous damping as an alternative to base isolation," *ASME Publications Pvp,* vol. 330, pp. 35-40 1996.

[68] M. D. Symans and M. C. Constantinou, "Passive fluid viscous damping systems for seismic energy dissipation," *ISET J Earthquake Tech,* vol. 35, pp. 185-206, 1998.

[69] W.-F. Chen and L. Duan, *Bridge Engineering Handbook: Construction and Maintenance,* 2 ed. Boca Raton, FL: CRC press, 2014.

[70] H. H. Moretto, M. Schulze, and G. Wagner, "Silicones," in *Ullmann's Encyclopedia of Industrial Chemistry* ed Hoboken, NJ: John Wiley and Sons, 1993.

[71] Clearco Products. (2016). *Introduction to Silicone Fluids*. Available: www.clearcoproducts.com [Accessed: Jul. 2, 2016]

[72] R. H. Doremus, "Viscosity of silica," *J Appl Phys,* vol. 92, pp. 7619-7629, Dec 15 2002.

2 DEVELOPMENT AND EVALUATION OF A PASSIVE HYDRAULIC SIMULATOR FOR ELBOW SPASTICITY REPLICATION

ABSTRACT

Spasticity is a stretch reflex disorder characterized by an abnormal increase in muscle resistance that is dependent on passive stretch speed. Clinical evaluation for spasticity involves performing stretch tests at multiple limb joints and characterizing the muscle behavior using qualitative scales such as the Modified Ashworth Scale (MAS). Due to the subjective nature of this evaluation method, diagnostic results produced from these clinical assessments can have poor reliability and inconsistency, especially for young healthcare professionals. To improve the reliability of the current evaluation method through repeated training, a novel medical training simulator was proposed. This entirely passive, hydraulic simulator utilized an innovative piston-cylinder damper design using viscous fluid in combination with creative flow channel configurations to replicate different levels of spasticity. The simulator was designed to resemble the arm of a 50^{th} percentile Caucasian male with a range of motion of 82 deg at the elbow joint. The speed-dependent feature of spasticity was represented by rotary viscosity, B_R, which related the output torque of the simulator to the input rotary speed. The simulator mimicked five distinct spasticity behaviors with B_R ranging from 0.33 – 3.60 mN.m/(deg/s) representing MAS levels 0 – 4. Two design iterations were prototyped based on results from a predictive mathematical model and experimental data examining the output force of the viscous damper in relation to channel geometry and input speed. Although the target values for $B_{R.}$ were not exactly replicated by the final prototype, the experimental values followed increasing trends in B_R. The overall performance of the simulator correlated with typical torque versus displacement profiles of

spasticity. Preliminary results suggest the potential for the use of hydraulic simulators to replicate spasticity; however, more precise tuning and better quantification of the behavior are needed in order to calibrate the device to better match the corresponding clinical targets in future development.

2.1 INTRODUCTION

Spasticity is an abnormal muscle behavior commonly associated with the upper motor neuron (UMN) syndrome [1-4]. UMN syndrome occurs in conditions affecting motor neurons in the brain or spinal cord such as stroke, multiple sclerosis, traumatic brain injury, and cerebral palsy [3-5]. Spasticity affects an estimated 12 million people worldwide [6]. This behavior is usually due to a lesion (or lesions) involving the neural pathways at the cerebral cortex or spinal cord [2-7]. Spasticity is dependent on input stretch speed and it is only elicited when a certain speed threshold is reached [1, 2]. As stretch speed increases, muscle resistance intensifies and higher reflex activity is observed [1, 2]. Spasticity, in conjunction with excessive muscle tone, frequently interferes with the voluntary motor function in patients, affecting their ability to perform daily living activities [8, 9].

The treatment of spasticity has been central to the clinical management of patients with UMN syndrome [2, 4, 5]. Clinical evaluation of spasticity involves performing stretch tests at multiple limb joints and characterizing the muscle behavior using qualitative scales [4, 5, 10]. Abnormalities in muscle tone, range of motion (ROM), and symmetry are noted and a score is assigned to describe the overall condition of the patient. Qualitative scales used to rate spasticity address multiple degrees of severity and each degree is accompanied by a short description. In general, the Modified Ashworth Scale (MAS) [11] (Table 2.1) and the Modified Tardieu Scale

(MTS) [12] are used. However, these qualitative scales are susceptible to problems of sensitivity and reliability. Several studies [13-20] have reported poor reliability and inconsistency on the diagnostic results produced from these clinical scales.

Table 2.1: Modified Ashworth Scale for assessing spasticity, adapted from [11].

Score	Description
0	No increase in muscle tone
1	Slight increase in muscle tone, manifested by a catch and release or by minimal resistance at the end of the range of motion when the affected part(s) is moved in flexion or extension
2	Slight increase in muscle tone, manifested by a catch, followed by minimal resistance throughout the reminder (less than half) of the range of motion
3	More marked increase in muscle tone through most of the range of motion, but affected part is easily moved
4	Considerable increase in muscle tone, passive movement difficult
5	Affected part is rigid in flexion or extension

Accuracy and precision of assessment results are critical for designing optimal treatment plans. Rating accuracy and consistency using the MAS and the MTS are directly related to clinician experience [11, 13, 15, 19]. However, recurrent training opportunities for young clinicians are limited due to patient availability. Clinical training for spasticity evaluation lacks a practical tool to enable young clinicians to experience and distinguish among various degrees of severity. There is a clear need for medical training simulators in this area to deliver better quality, structured training. Simulator devices can serve as an alternative to real patients and ultimately help to reduce instructional and training costs involved in the recruiting, scheduling, and testing of patient volunteers. Simulation-based training has the potential to not only allow young medical professionals to gain more practical experience through deliberate practice, but also help in standardizing diagnostic procedures for improved patient treatment and therapy [21, 22].

Several programmable robotic simulators [23-30] that can replicate different abnormal muscle behaviors (e.g. spasticity) have been developed to aid in practical training. These simulators typically involve the use of a high-end actuator (e.g. electric motor or active fluid system) and multiple sensors, along with complex real-time control algorithms to produce realistic force feedback. However, due to the high cost in mechanical components and immaturity in algorithm development, it is difficult to realize the intended goal of these simulators in the foreseeable future. For this reason, a novel resistive hydraulic-based unpowered simulator was proposed.

In this chapter, a new perspective was taken to explore alternative simulator design through a purely mechanical approach. It was the goal of this project to look into the design of a portable, low-cost simulator that can replicate spasticity, apart from the traditional electromechanical approach, in order to guide future development of training devices. Through an iterative design process that involved analytical modelling and experimental prototyping, a passive damper using viscous fluid in combination with creative flow channel configurations was developed. This passive damper was able to generate a wide range of speed-dependent resistive feedbacks without need for any computational control. The damper was subsequently implemented into a forearm structure to replicate five distinct spasticity behaviors representing MAS levels 0 – 4 (Table 2.1) in the elbow joint.

2.2 METHODS

This section presents the development of an unpowered hydraulic-based simulator for triceps muscle spasticity replication during passive elbow flexion. The final simulator prototype was designed to mimic five levels of spasticity on the Modified Ashworth Scale (MAS 0 – 4, Table 2.1). To ensure that the simulator performance would be comparable to actual patients, published data on elbow viscosity were used as design targets for tuning the corresponding spasticity behavior. An iterative design process involved both analytical fluid mechanics modelling (with experimental validation) and experimental prototyping was employed to develop a novel, viscous damper that drove the speed-dependent characteristics of the hydraulic simulator. Values of elbow viscosity calculated based on modelling and experimental results of the viscous damper were used to determine the design of target spasticity behaviors.

2.2.1 QUANTITATIVE DATA OF THE MODIFIED ASHWORTH SCALE

There is a paucity of quantitative data that describe the clinical features of spasticity [10, 31, 32]. Studies on quantifying and analyzing the speed dependency of this behavior were mostly conducted by Chen's group from the National Cheng Kung University in Taiwan [10, 33, 34]. The findings from Chen and colleague's experiments (summarized in Table 2.2) correlated the speed-dependent component of spasticity in the elbow joint to MAS levels 0 – 4. (MAS 5 was not implemented due to lack of quantitative data for this level from any published source.) They proposed a viscosity measurement, *B,* which related the output torque [N.m] to the input stretch frequency [Hz or cycles/s] as a means to quantify the behavior. Their experimental results demonstrated that as input stretch frequency increased (increasing input speed), muscle

resistance increased linearly; and that for patients with more severe condition, this speed-dependent "viscous" response was more noticeable.

In developing the hydraulic-based simulator, quantitative data from the Chen group studies were used as design targets for tuning the initial prototype. Since their viscosity value *B* was presented as ratio of output torque over input frequency [N.m/(cycles/s)], a conversion step was needed to convert the original *B* data to one based on the angular speed that the forearm was rotated. We refer to this modified value as rotary viscosity, B_R, that is, the ratio of output torque to average angular speed [mN.m/(deg/s)] (Eq.(1), refer to Appendix B for derivation). The resulting B_R values were used in the device development process.

$$B_R = B * \frac{1\frac{cycle}{s}}{133.2\frac{deg}{s}} * \frac{1000\,mN}{1\,N}, \tag{1}$$

where 133.2 deg/s was the average angular speed based on an input frequency of 1 Hz or 1 cycle/s over a range of motion of 60 deg.

Table 2.2: Viscosity measurement of elbow joint in relation to MAS scores 0 – 4. Column 2: experimental results summarized from work done by Chen's group [33, 34]. Column 3: same experimental results in relation to average angular speed. Mean ± standard deviation.

MAS Score	Viscosity, *B* [N.m/(cycles/s)]	Rotary Viscosity, B_R [mN.m/(deg/s)]
0	0.045 ± 0.035	0.38 ± 0.29
1	0.105 ± 0.052	0.88 ± 0.43
2	0.117 ± 0.064	0.99 ± 0.53
3	0.172 ± 0.071	1.43 ± 0.59
4	0.365 ± 0.001	3.04 ± 0.01
5	NA	NA

2.2.2 SIMULATOR STRUCTURE

The fully assembled portable hydraulic-based simulator is shown in Figure 2.1. The simulator was designed to have a range of motion (ROM) of 82 deg at the elbow joint and weighed about 2.7 kg, not including the weight of the stand. The crucial component driving the simulator performance was the passive viscous damper, and the development of this component is discussed in the later sections. The aluminum structure fabricated to house the damper was designed to resemble the arm of a 50th percentile Caucasian male in terms of length and mass (Table 2.3). A 3D printed cover was secured around the elbow to mimic the width of the elbow to allow for safe placement of the clinician's hand during the stretch test. A prefabricated mannequin hand was attached after the wrist joint. The shoulder and wrist joints were designed to allow flexion and extension. The final design will be covered with a synthetic skin sleeve.

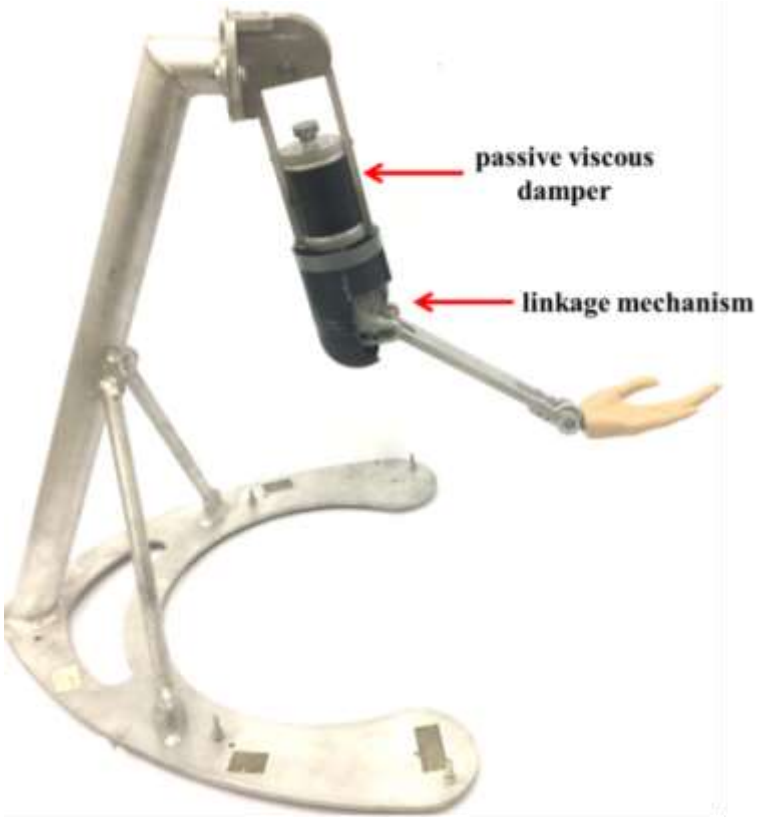

Figure 2.1: Fully assembled hydraulic-based spasticity simulator.

Table 2.3: Body segment parameters of a 50th percentile Caucasian male extracted from [35] and the corresponding parameters of the hydraulic-based simulator.

Segment	Length [mm]		Mass [kg]	
	Average Male	Simulator	Average Male	Simulator
Upper Arm	281.7	280.0	1.98	1.73
Forearm	268.9	270.0	1.18	0.93

A cam-driven transmission mechanism was implemented in the elbow joint to convert the rotary flexing motion of the forearm into the linear pushing motion of the damper piston rod (Figure 2.2). This linkage design dictated the 82 deg ROM for the elbow joint. Geometries associated with the mechanism linkages ensured that the resistive feedback produced by the simulator was comparable to the generalized torque versus angular position profile of spasticity derived from the qualitative descriptions in the MAS [11] and observed behaviors found in the literature [10, 33, 34] (Figure 2.3).

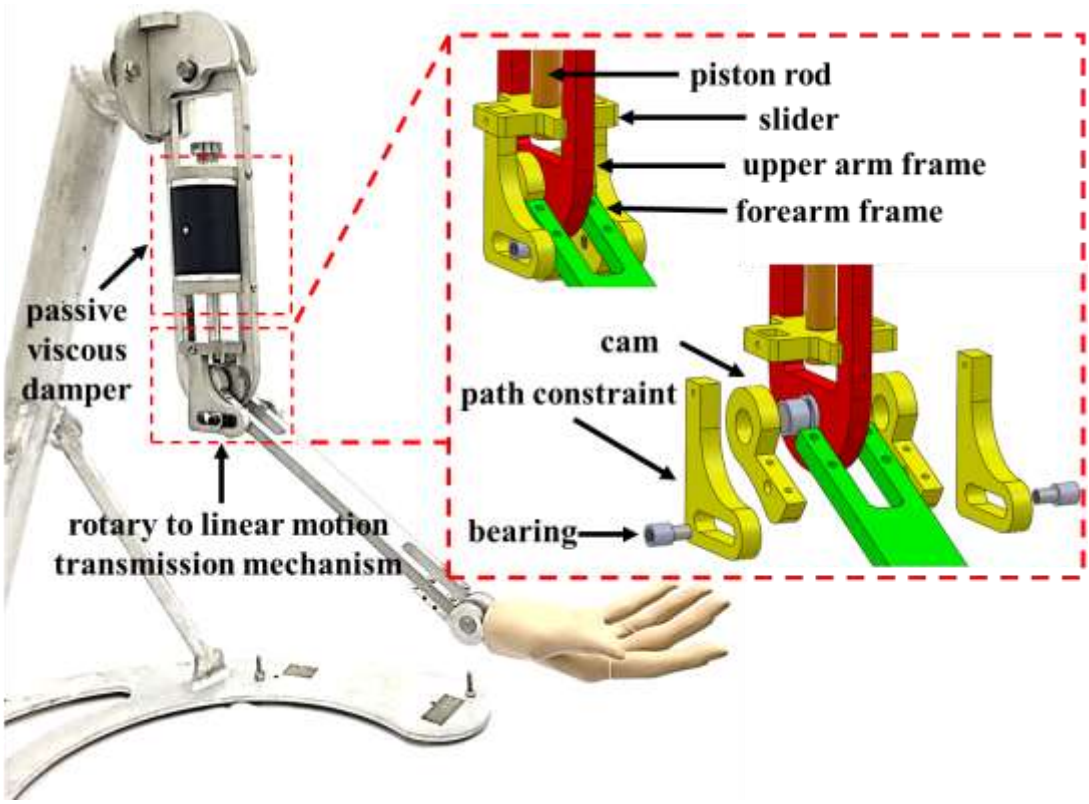

Figure 2.2: Hydraulic-based simulator prototype with exploded view of the linkage mechanism.

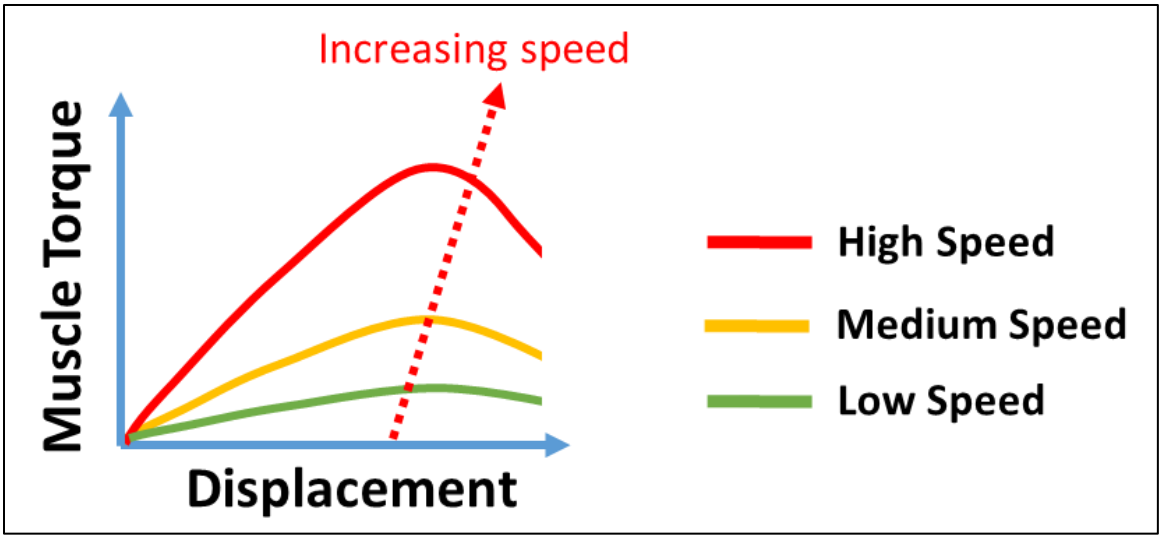

Figure 2.3: Generalized archetypical muscle torque versus displacement profiles for spasticity.

The resistive feedback generated by the hydraulic simulator was ultimately the resistive torque T_R felt or experienced by the clinical user near the wrist joint. The value of resistive torque could be found through relating the output force of the viscous damper to the linkage geometries.

The forces acting on the forearm assembly included: reactions due to the upper arm structure (R_x and R_y), force due to the viscous damper (F_d), force due to gravity (F_g), and force applied by the user ($F_{applied}$) (Figure 2.4). Friction forces at the elbow and wrist joints were neglected to simplify the system. By summing the torque of the system at the elbow joint E, the unknown reactions were eliminated and the following relationship was obtained.

$$\sum \vec{T}_E = \vec{L}_w \times \vec{F}_{applied} - \vec{L}_g \times \vec{F}_g - \vec{L}_d \times \vec{F}_d + I\ddot{\theta} = 0 \qquad (2)$$

In the above equation, $L_{W,}$ $L_{g,}$ and L_d were the segment lengths from the elbow joint to where the corresponding force was located, I was the moment of inertia of the forearm, and $\ddot{\theta}$ was the angular acceleration of the forearm. Assuming a constant rotational speed, the term $I\ddot{\theta}$

was neglected. With other known geometric parameters of the linkage components, Eq.(2) could be rewritten as the following.

$$L_w F_{applied} - L_g F_g \sin(90^o + \theta) - L_d F_d \sin(\beta + \phi + \theta) = 0 \quad (3)$$

In Eq.(3), θ was the angle of the forearm relative to ground, β was the angle of mounting hole on the cam piece relative to forearm, and ϕ was the angle at which F_d was applied relative to ground. The value of $L_w F_{applied}$ was equivalent to the resistive torque T_R felt by the user. Assuming that the force due to gravity was negligible, the relationship between T_R and F_d could be simplified further.

$$T_R = L_d F_d \sin(\beta + \phi + \theta) \quad (4)$$

L_d and β were the design parameters of the linkage mechanism. Desired torque due to position profiles could be generated by choosing the appropriate combinations of L_d and β. For replication of spasticity, the values for these two parameters were chosen such that the resulting simulator behavior resembled that of a typical spasticity curve with maximum output torque always occurred at the mid-range of motion (Figure 2.3). (Refer to Appendix C for different linkage designs.)

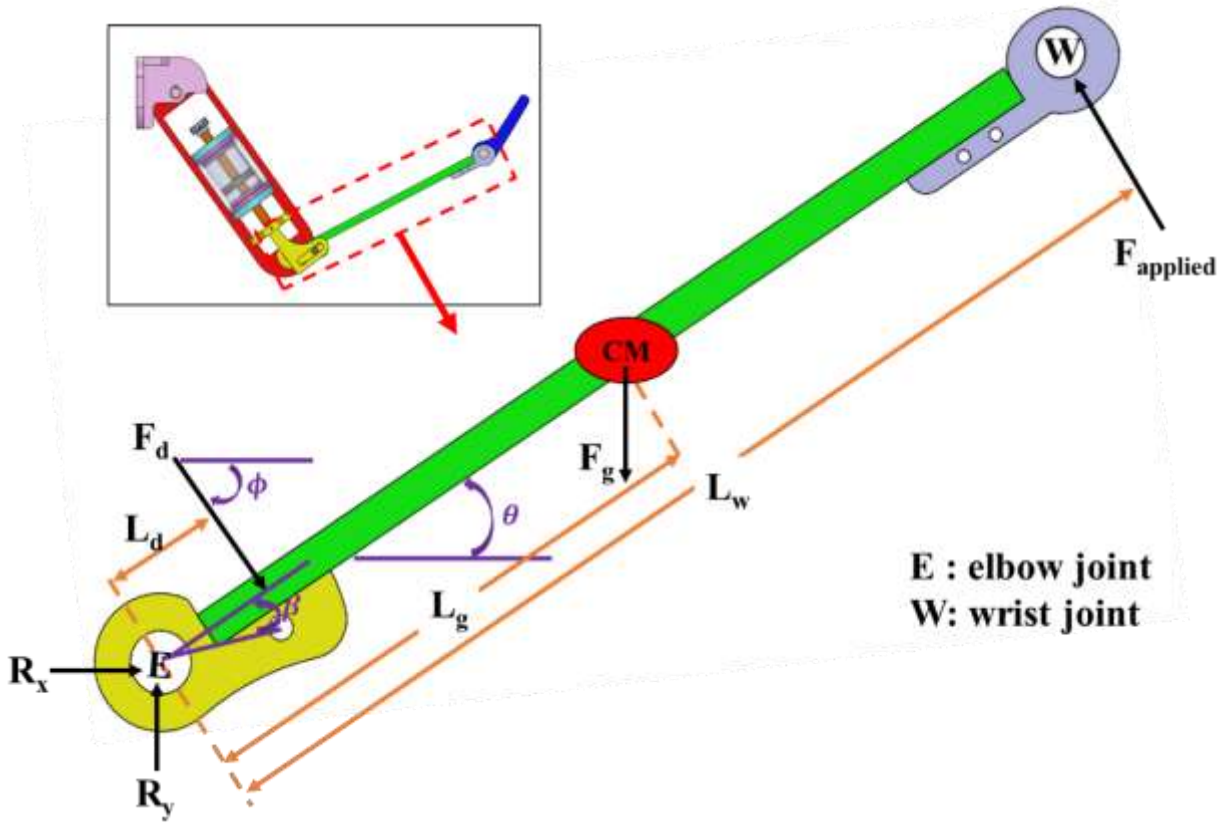

Figure 2.4: Free body diagram of the simulator forearm with relevant geometries during elbow flexion. β and ϕ are fixed during motion and θ determines forearm position.

2.2.3 MODELLING OF FLUID BEHAVIOR

The speed-dependent characteristics of the simulator behavior were driven by the output force (F_d) of the custom-fabricated passive viscous damper. Viscous dampers dissipate input energy by pushing fluid through an orifice, producing a differential pressure which then results in a damping force that is proportional to the input speed [36, 37]. The custom-fabricated damper followed the same operation principal, but the overall design had two unique features: a symmetrical piston structure and a porous piston head (Figure 2.5). A typical viscous damper requires an internal accumulator (e.g. compressed gas or rubber chamber) to account for the volume change due to piston insertion [37]; however, in this custom design, a symmetric piston

structure was used to eliminate the need for an accumulator (eliminating the accumulator removes an elastic aspect of the response, which is not desired). Further, to accommodate the different levels of spasticity, the piston head of the damper contained multiple pairs of orifices of different sizes. During clinical training, an instructor can turn a selection dial to expose the proper pair of orifices and allow students to experience what a certain level of spasticity should feel like.

To ensure that the custom damper design was capable of recreating the speed dependency of spasticity, an analytical modelling approach was used to predict the output damping force F_d in relation to different geometric parameters and input speeds.

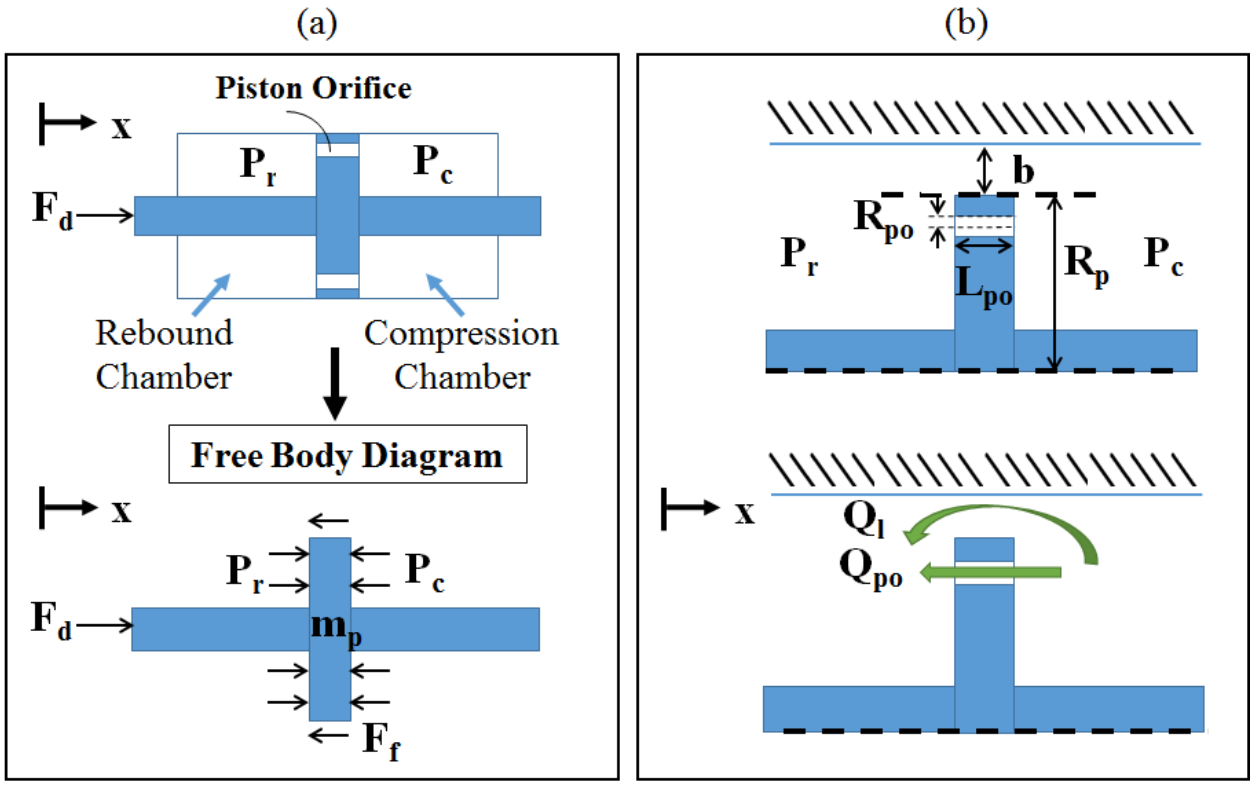

Figure 2.5: (a) Overview of the viscous damper design and forces acting on the piston assembly. (b) Geometry of the piston assembly and flow pathways within the device.

The forces acting on the piston assembly included: the damping force, the force due to pressure differences in the rebound and compression chambers, the friction force on the sealed shaft, and the inertial force (Figure 2.5a). Conservation of momentum is written as

$$F_d + (P_r - P_c)\pi R_p^2 - F_f - m_p\ddot{x} = 0 \quad (5)$$

In the above equation F_d was the damping force, P_r was the pressure in the rebound chamber, P_c was the pressure in the compression chamber, R_p was the radius of the piston head, F_f was the friction force, m_p was the mass of the piston, and $\ddot{x}$ was the acceleration of the piston.

Two flow paths were identified for the working fluid: the flow through the piston orifices (Q_{po}) and the leaking flow through the gap between the piston and cylinder (Q_l) (Figure 2.5b). By conserving the volume of the fluid system, there must be flow from the compression chamber to the rebound chamber which depends on input speed ($\dot{x}$). This total flow through piston orifices and the gap must satisfy

$$\sum Q = Q_{po} + Q_l = \pi R_p^2 \dot{x} \quad (6)$$

The fluid forces and motion were estimated assuming incompressible Newtonian flow. Reynolds number or the ratio of inertial forces to viscous forces was assumed to be small enough (Re < 1000, refer to Appendix D for Reynolds number approximation) such that that viscous, laminar flow dominated. Flow rate through the piston orifice was approximated by Poiseuille's Law for pressure-driven laminar flow through a circular orifice (Eq.(7)) [38]. Flow rate through the gap was determined from both pressure-driven and boundary-driven flow through the narrow gap (Eq. (8)) [39, 40].

$$Q_{po} = \frac{\pi R_{po}^4}{8\mu}\frac{(P_c - P_r)}{L_{po}} \tag{7}$$

$$Q_l = \left(\frac{(P_c - P_r)b^3}{12\mu L_{po}} - \frac{\dot{x}b}{2}\right)2\pi R_p \tag{8}$$

In the above equations, R_{po} was the effective radius of the two piston orifices, L_{po} was the length of the piston orifice, μ was the fluid viscosity, and b was the width of the gap between the cylinder and piston. By substituting the above two flow rate equations into the conservation of volume relationship (Eq.(6)) and rearranging, the differential pressure equation was obtained.

$$\Delta P = P_c - P_r = \frac{24L_{po}R_p\mu\left(R_p + b\right)}{3R_{po}^4 + 4R_p b^3}\dot{x} \tag{9}$$

Assuming a constant speed input, inertial force was ignored and the full dynamics of the system can be expressed by substituting Eq.(9) into Eq.(5), and solving for the damping force,

$$F_d = \frac{(24L_{po}R_p^3\mu\left(R_p + b\right)\pi)/(4R_p b^3)}{(3/4R_p b^3)R_{po}^4 + 1}\dot{x} + F_f \tag{10}$$

Eq.(10) was obtained under the ideal assumptions that flow was always laminar, the damper had zero leakage, and each mechanical component had perfect geometric tolerance. In order to account for any unknown factors arising from the fabrication, assembly, and testing of the actual prototype, three multiplicative correction factors, C_1, C_2 and C_3 were added to the model to make it more robust.

$$F_d = \frac{C_1(24L_{po}R_p^3\mu\left(R_p + b\right)\pi)/(4R_p b^3)}{C_2(3/4R_p b^3)R_{po}^{C_3 4} + 1}\dot{x} + F_f \tag{11}$$

Correction factors were determined by fitting the analytical model to the experimental results. The adjusted model was then used to predict and design the target damping effects or spasticity behaviors.

2.2.4 FABRICATION OF PASSIVE VISCOUS DAMPER

A prototype of the passive viscous damper with the two unique features discussed earlier was designed and fabricated (Figure 2.6 and Figure 2.7). This prototype contained a 4-part piston assembly, a thick-walled cylinder filled with silicone oil, and two endcaps with commercial rubber seals. The piston assembly included two short rods, a piston head containing five pairs of orifices, and a cover plate. The short rods and the cover plate were rigidly connected by a stainless steel screw, and the piston head was fixed to the endcaps through a slender rod that runs down the length of the cylinder. The short rods and cover plate were made from aluminum (6061 aluminum alloy) to ensure structure integrity was maintained when external force was applied to the piston. The piston head and the thick-walled cylinder were made from Delrin® (acetal resin) to minimize friction as the piston stroked. Steel shaft seals (nitrile rubber) and O-Rings (nitrile rubber) were installed in the endcaps to minimize fluid leakage. Silicone oil was selected to be the working fluid since it is nontoxic, thermally stable, and available in a wide range of viscosities [37, 41]. (Supplementary images and CAD renderings of the passive viscous damper are included in Appendix E.)

Volumetric flow rate (and thus speed dependency) of the passive viscous damper was controlled by turning the cover plate to expose the appropriate pair of orifices on the piston head. In the initial design, the radii of the piston orifices were fabricated to have a linearly-varying

geometry change (0.5 mm, 1.0 mm, 1.5 mm, 2.0 mm, and 2.5 mm), allowing for a systematic approach to find the scaling factors shown in the analytical model of fluid behavior (Eq.(11)). Through iterating between analytical modelling and prototyping, the piston radii were later modified (1.5 mm, 1.8 mm, 1.9 mm, 2.0 mm, 2.5 mm) to represent the five levels of spasticity on the Modified Ashworth Scale (MAS 0 – 4).

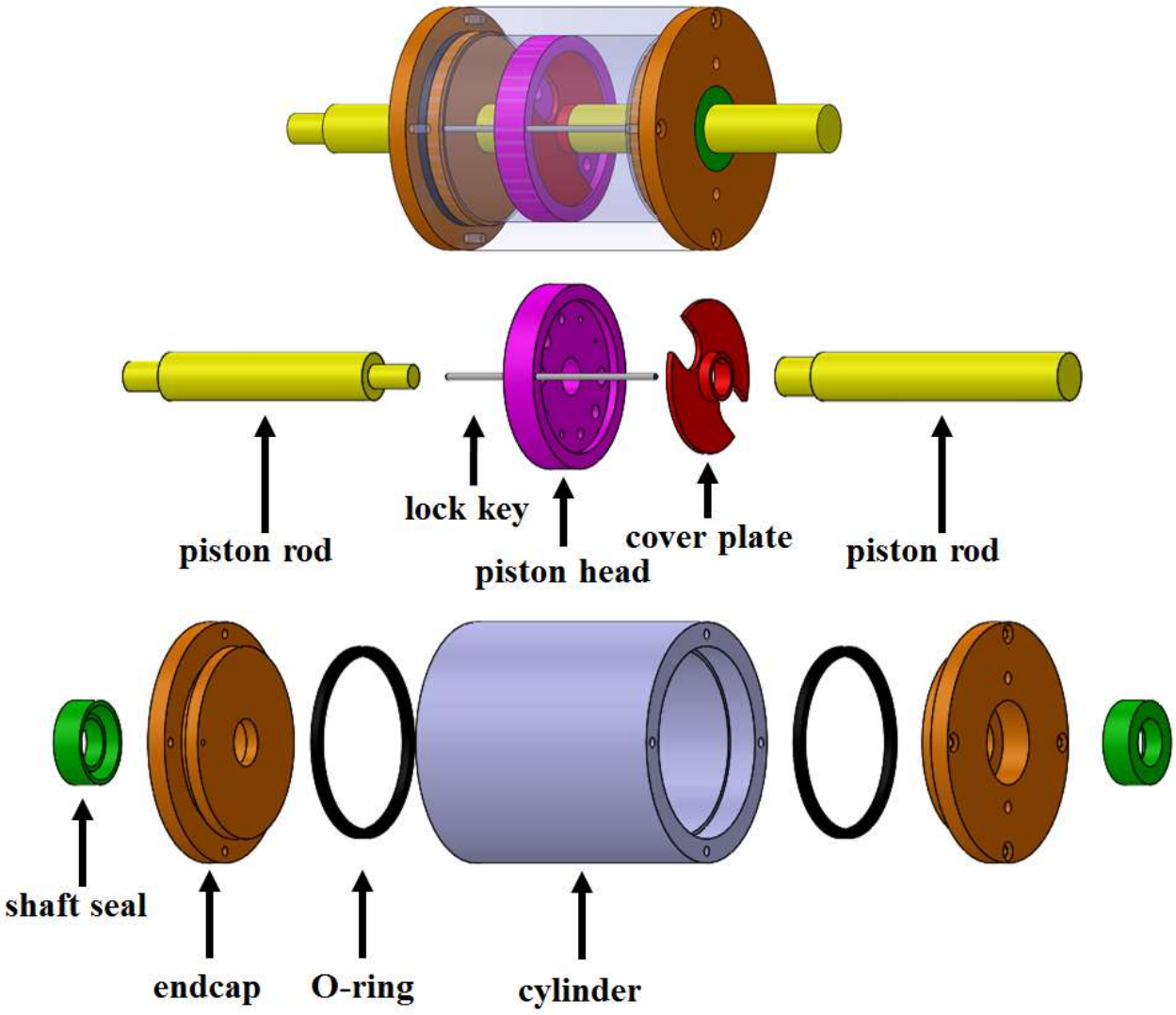

Figure 2.6: Exploded view of the viscous damper 3D solid model.

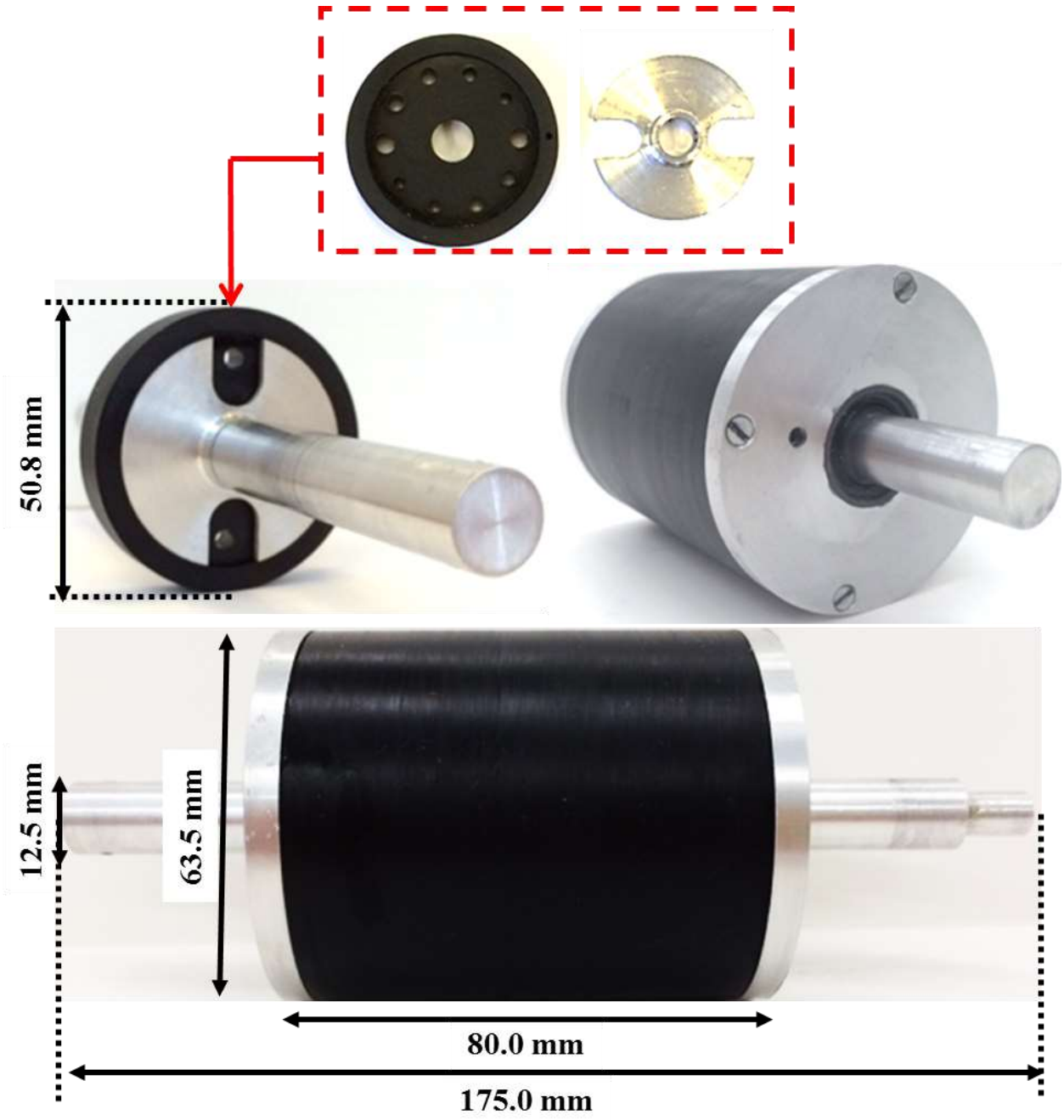

Figure 2.7: Passive viscous damper prototype with piston head for orifice sizes based on the initial design.

2.2.5 EVALUATION OF PASSIVE VISCOUS DAMPER

A commercial material testing system (Instron 5967; High Wycombe, United Kingdom) was used to evaluate the passive viscous damper only (Figure 2.8). Evaluations were performed over four linear speeds (250 mm/min, 500 mm/min, 750 mm/min, and 1000 mm/min) to characterize the speed-dependent or damping effects due to orifice geometry and fluid viscosity. These linear speeds were chosen as multiples of the lowest speed to allow for a more systematic comparison across the experimental results.

Customized mounting brackets (Figure 2.8) were fabricated to attach the passive viscous damper to the material testing system. Weight of the damper and the mounting components were ignored in order to isolate and measure the damping effects. For each test, the machine would travel downward and stop when a preset displacement limit was reached. Only data collected from the moment when the piston touched the force plate until reaching the displacement limit were analyzed (Figure 2.9). Average damping force and the corresponding standard deviation were computed for this region.

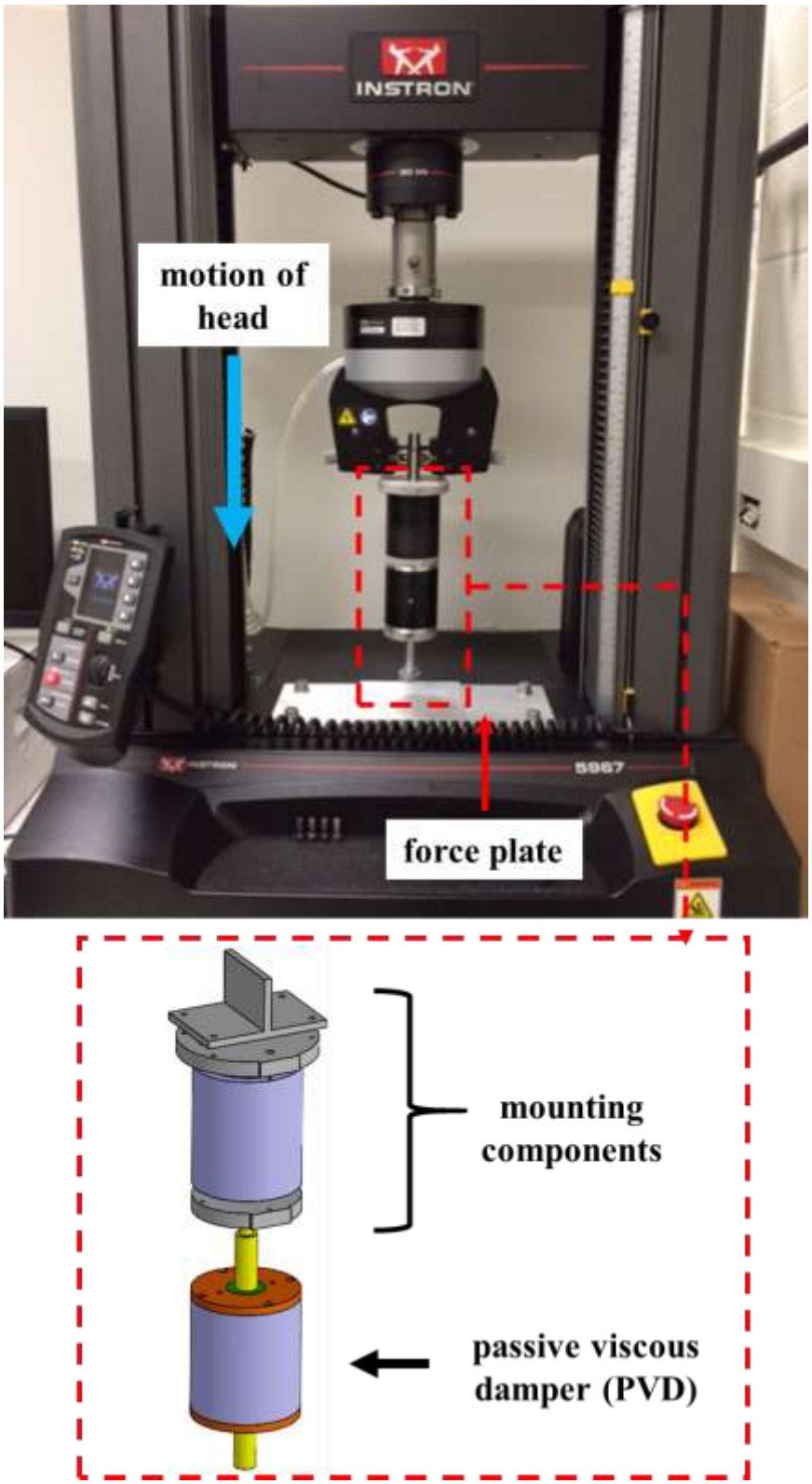

Figure 2.8: Experimental setup of the viscous damper evaluation

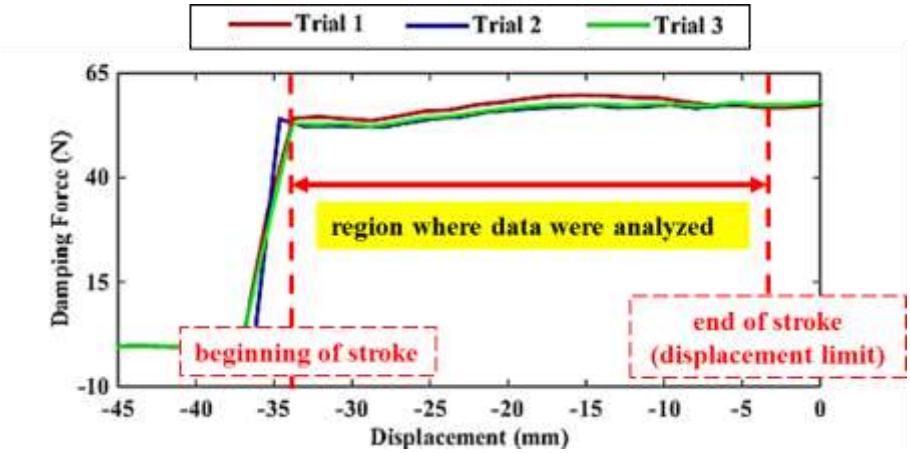

Figure 2.9: Example plot from one set of viscous damper evaluation on the material testing device.

The initial design of the passive viscous damper was tested with two different silicone oils (μ = 100 mPa.s, 150 mPa.s). These particular fluid viscosities were chosen to ensure that the resulting viscous or damping force would be able to replicate the target spasticity behaviors. Evaluation of the initial design involved the testing of 40 unique speed-orifice-viscosity combinations (4 speeds, 5 orifice geometries, and 2 fluid viscosities) and each test was repeated three times, resulting in 120 independent data sets. Experimental results obtained from evaluating the initial design were used to find the scaling factors (C_1, C_2, and C_3) of the analytical model (Eq.(11)) in order to predict the device behavior over a wide range of orifice geometries (R_{po}) and input speeds ($\dot{x}$). The linear viscosity B_L, i.e. the ratio of output damping force (F_d) over linear speed ($\dot{x}$), was calculated for each orifice-viscosity arrangement. The value of B_L was then converted to rotary viscosity B_R or ratio of output torque (T_R) over angular speed ($\dot{\theta}$) (see Appendix B). This conversion step made it possible to compare the experimental results of the viscous damper to quantitative data of the MAS (Table 2.2).

The scaled analytical model determined through initial experimental prototyping was then used to select the proper fluid viscosity and orifice geometries that could simulate spasticity

behaviors representing MAS 0 – 4. Upon adjusting the orifice geometry, the same evaluation was performed on the modified damper design. Only one silicone oil (μ = 150 mPa.s) was tested for the modified design since it was determined to be a better fit for spasticity replication through initial evaluation. Evaluation of the modified design involved the testing of 20 unique speed-orifice-viscosity combinations (4 speeds, 5 orifice geometries, and 1 fluid viscosity) and each test was repeated three times, resulting in 60 independent data sets. Rotary viscosity B_R was calculated for each orifice geometry to ensure the speed-dependent effects resulting from this modified design were comparable to the target spasticity behaviors.

For both evaluations (initial and modified designs), the values of the different parameters (Table 2.4) used in the fluid model and linkage equation were approximated from the physical damper prototype.

Table 2.4: Input parameters for analytical model of fluid behavior (Eq. (11)) and linkage equation (Eq.(4)). The values of C_1, C_2, and C_3 were determined through experiments.

	Symbol	Measured Value
Analytical Model of Fluid Behavior	C_1	0.65
	C_2	1.10
	C_3	1.07
	L_{po}	7.0 mm
	R_p	25.4 mm
	μ	*Varies*
	b	0.3 mm
	R_{po}	*Varies*
	$\dot{x}$	*Varies*
	F_f	12.0 N
Linkage Equation	L_d	35.0 mm
	β	12.5 deg
	ϕ	45 deg
	θ	*Varies*

2.2.6 EVALUATION OF HYDRAULIC SIMULATOR

System-level performance (torque versus position) of the fully assembled hydraulic simulator with the modified viscous damper was measured by two customized sensor modules secured to the upper arm and forearm segments (Figure 2.10). The upper arm module included a 3-axis inertia measurement unit (MPU 6050, Invensense; San Jose, CA) and the forearm module included a miniature load cell (LCM 300, Futek; Irvine, CA) and another 3-axis inertia measurement unit. Applied force, relative angle between segments, and stretch speed data collected during the evaluation were processed by a microcontroller (Teensy 3.2 USB Development Board, PJRC; Portland, OR) in real-time and later transferred to a computer for plotting and analysis.

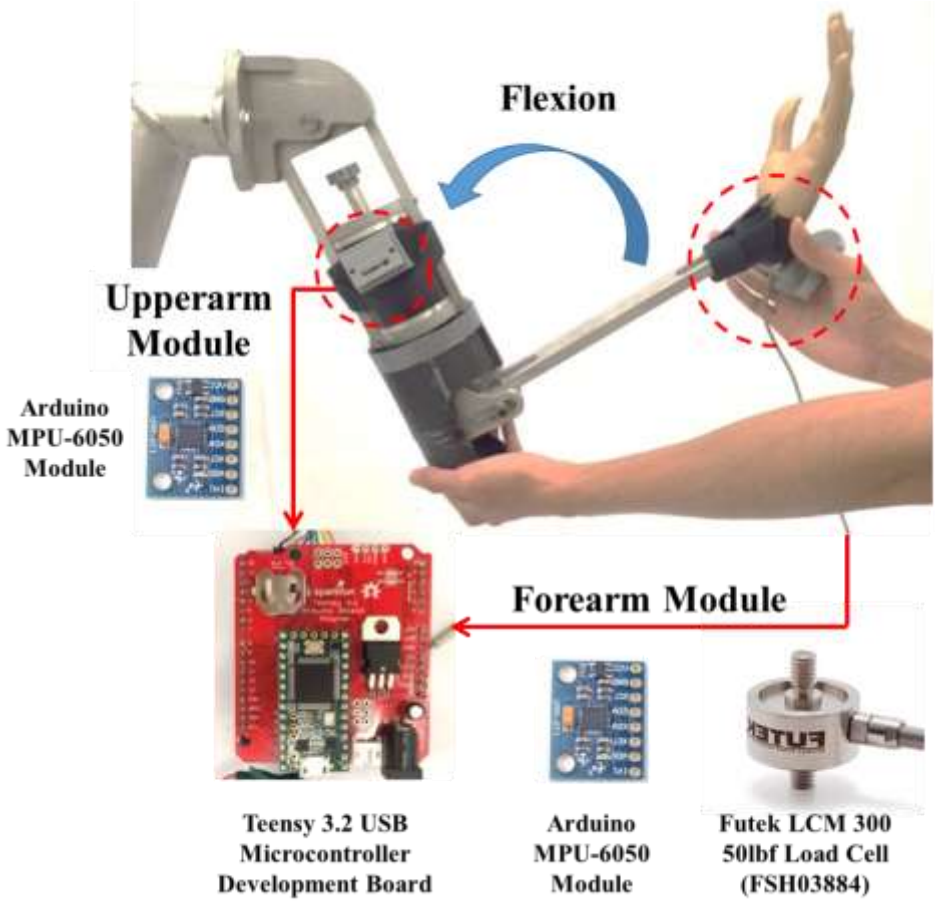

Figure 2.10: Instrumentation setup for the evaluation of the fully assembled hydraulic simulator.

Evaluation was performed for all five orifice radii under different stretch speed conditions. For each test, the user would hold the upper arm segment of the hydraulic simulator at an angle of approximately 30 – 45 deg while moving the distal end of the forearm segment (at the wrist joint) by pressing onto the load cell sensor module in the direction of flexion at various speeds. Slow speeds were defined as anything less than 60 deg/s, fast speeds were defined as anything greater than 150 deg/s, and medium speeds were defined as anything between slow and fast.

2.3 RESULTS

Experimental studies were conducted to assess only the viscous damper designs (initial and modified) and the fully assembled hydraulic-based simulator. (See Appendix F for the full experimental results for the viscous damper analyses.)

2.3.1 RESULTS OF INITIAL DAMPER DESIGN

Experimental results of the initial viscous damper design were displayed in Figure 2.11, Figure 2.12, and Figure 2.13. The correlations of the output damping force (F_d) with respect to orifice geometry (R_{po}), input speed ($\dot{x}$), and fluid viscosity (μ) were obtained. As the size of the orifice decreased, damping force increased exponentially (approximately quartic) and became constant upon reaching a geometric threshold determined by the gap clearance between the piston and outer cylinder (Figure 2.11a and Figure 2.12a). As input speed increased, the output damping force increased linearly and for smaller orifices, this linear increase was more prominent (Figure 2.11b and Figure 2.12b). The viscosity ratio ($\mu_2/\ \mu_1$) of the two silicone oils (μ_1 = 100 mPa.s and μ_2 = 150 mPa.s) is 1.5. At large orifices, the effect of fluid viscosity was

insignificant (output damping force ratio was around 1.0); as orifice radius decreased, damping force ratio increased, indicating that fluid viscosity was influencing the device behavior (Figure 2.13).

The scaling factors C_1, C_2, and C_3 shown in the analytical model of fluid behavior (Eq.(11)) were found through trial and error. These scaling factors were determined to be 0.65, 1.10, and 1.07, respectively, for both working fluids. The scaled analytical model showed good agreeability with experimental and residual values all within ± 5.0 N across all input speeds (Figure 2.11a and Figure 2.12a).

Speed dependency was characterized by the linear viscosity B_L or the slope of the best-fit line between damping force and input speed (Figure 2.11b and Figure 2.12b). The values of B_L for each orifice geometry and silicone oil combination were listed in Table 2.5. B_L was subsequently converted to rotary viscosity B_R such that the experimental results could be compared to the existing quantitative data in the literature [33, 34]. Experimental rotary viscosities for the 150 mPa.s silicone oil with orifice radii of 2.5 mm and 2.0 mm were 0.22 mN.m/(deg/s) and 0.84 mN.m(deg/s), respectively. These B_R values fell in the desired clinical target rotary viscosity range for MAS 0 (0.38 ± 0.29 mN.m/(deg/s)) and MAS 1 (0.88 ± 0.43 mN.m/(deg/s)) (Table 2.2). Therefore, the 150 mPa.s silicone oil was chosen to be used in the modified design.

A plot of the experimental B_R results against the analytical model is shown in Figure 2.14. Numerical values of clinical target rotary viscosity for MAS 0 – 4 shown along the analytical B_R curve were listed in Table 2.6. Orifice radii determined for the average clinical targets were rounded to the nearest tool dimensions available for fabrication. The orifice radii for the modified design were 2.5 mm, 2.0 mm, 1.9 mm, 1.8 mm, and 1.5 mm.

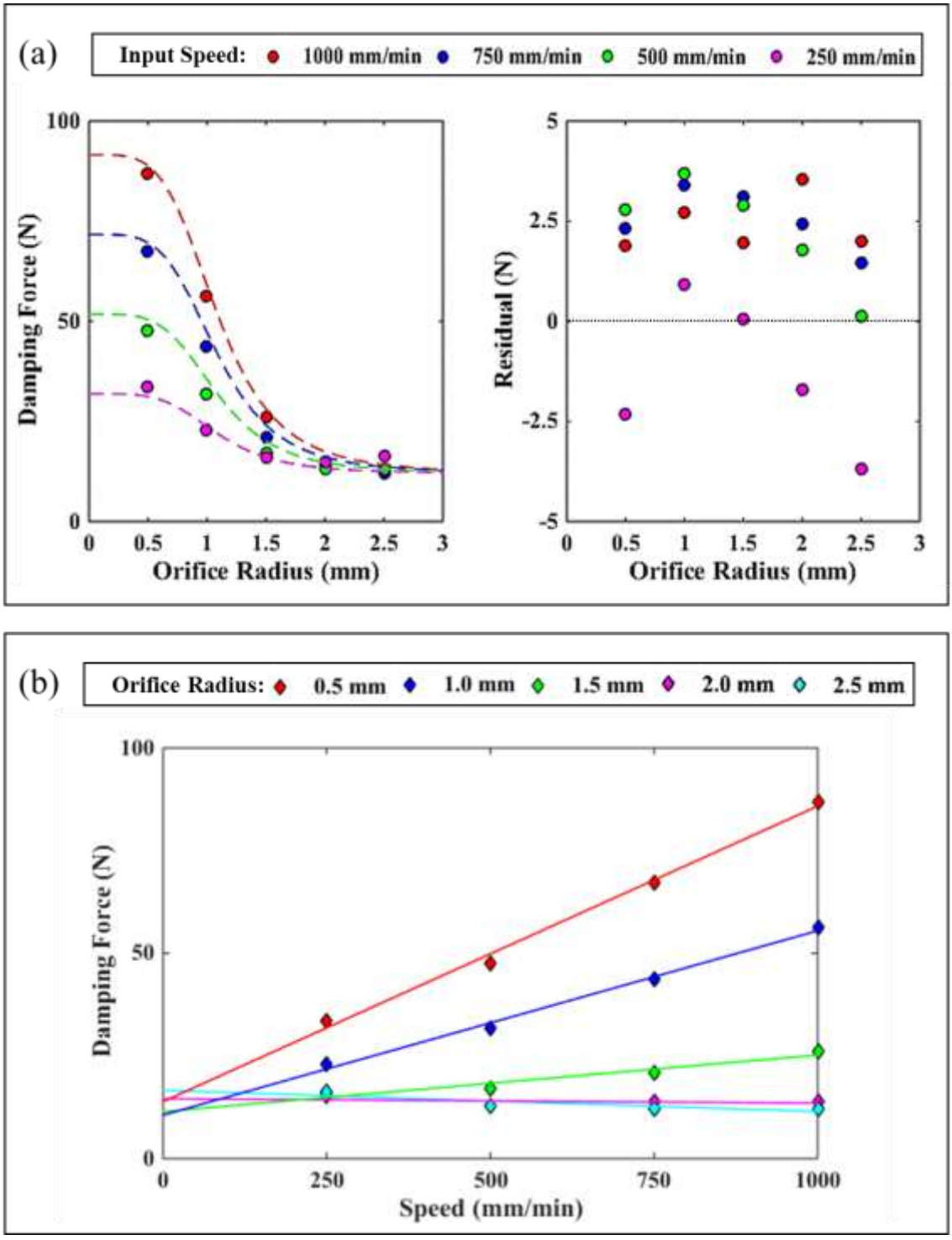

Figure 2.11: Results for the 100 mPa.s silicone oil. (a) Experimental results (circles) plotted against the analytical model Eq.(11) (dotted lines) in relation to orifice radii for different input speeds with the corresponding residual plot ($Residual = Analytical - Experimental$). The values of C_1, C_2, and C_3 are 0.65, 1.10, and 1.07, respectively. (b) Experimental results (diamonds) in relation to input speeds for different orifice radii with best-fit lines (solid lines).

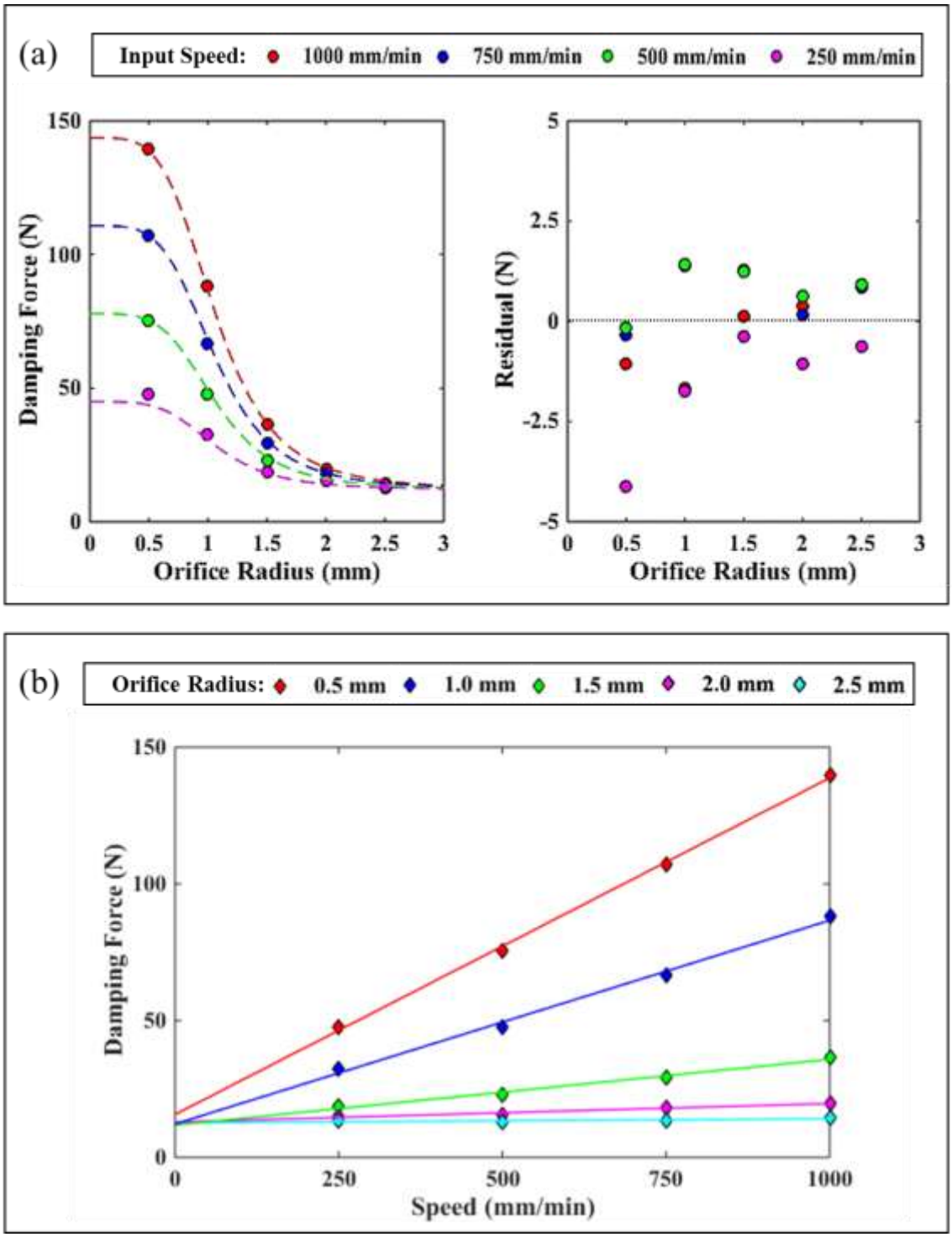

Figure 2.12: Results for the 150 mPa.s silicone oil. (a) Experimental results (circles) plotted against the analytical model Eq.(11) (dotted lines) in relation to orifice radii for different input speeds with the corresponding residual plot ($Residual = Analytical - Experimental$). The values of C_1, C_2, and C_3 are 0.65, 1.10, and 1.07, respectively. (b) Experimental results (diamonds) in relation to input speeds for different orifice radii with best-fit lines (solid lines).

Table 2.5: Linear and rotary viscosities for each orifice and silicone oil combination evaluated for the initial design (see Appendix B for conversion details).

Orifice Radius [mm]	Initial Design			
	100 mPa.s Silicone Oil		150 mPa.s Silicone Oil	
	Linear Viscosity B_L [N/(mm/min)]	Rotary Viscosity B_R [mN.m/(deg/s)]	Linear Viscosity B_L [N/(mm/min)]	Rotary Viscosity B_R [mN.m/(deg/s)]
2.5	-0.0011	-0.16	0.0015	0.22
2.0	-0.0051	-0.74	0.0058	0.84
1.5	0.0138	2.01	0.0240	3.49
1.0	0.0449	6.52	0.0744	10.80
0.5	0.0720	10.50	0.1230	17.90

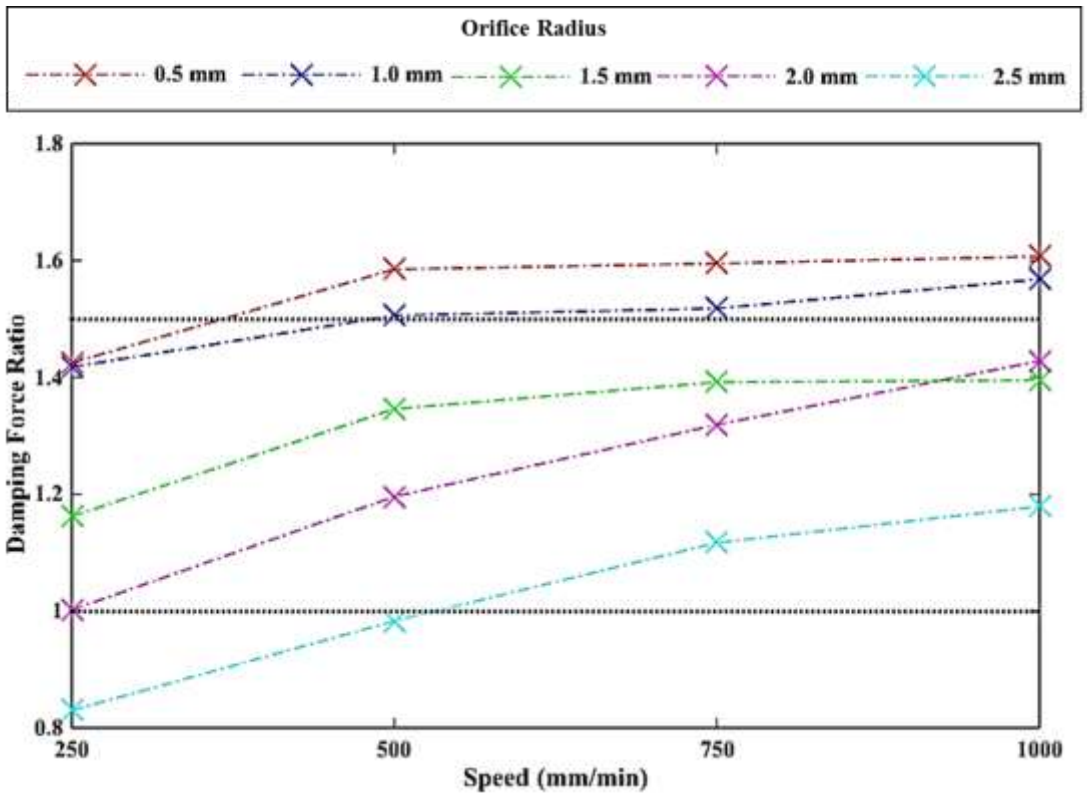

Figure 2.13: Ratio of experimental damping force with 150 mPa.s silicone oil to experimental damping force with 100 mPa.s silicone oil in relation to input speeds for different orifice radii.

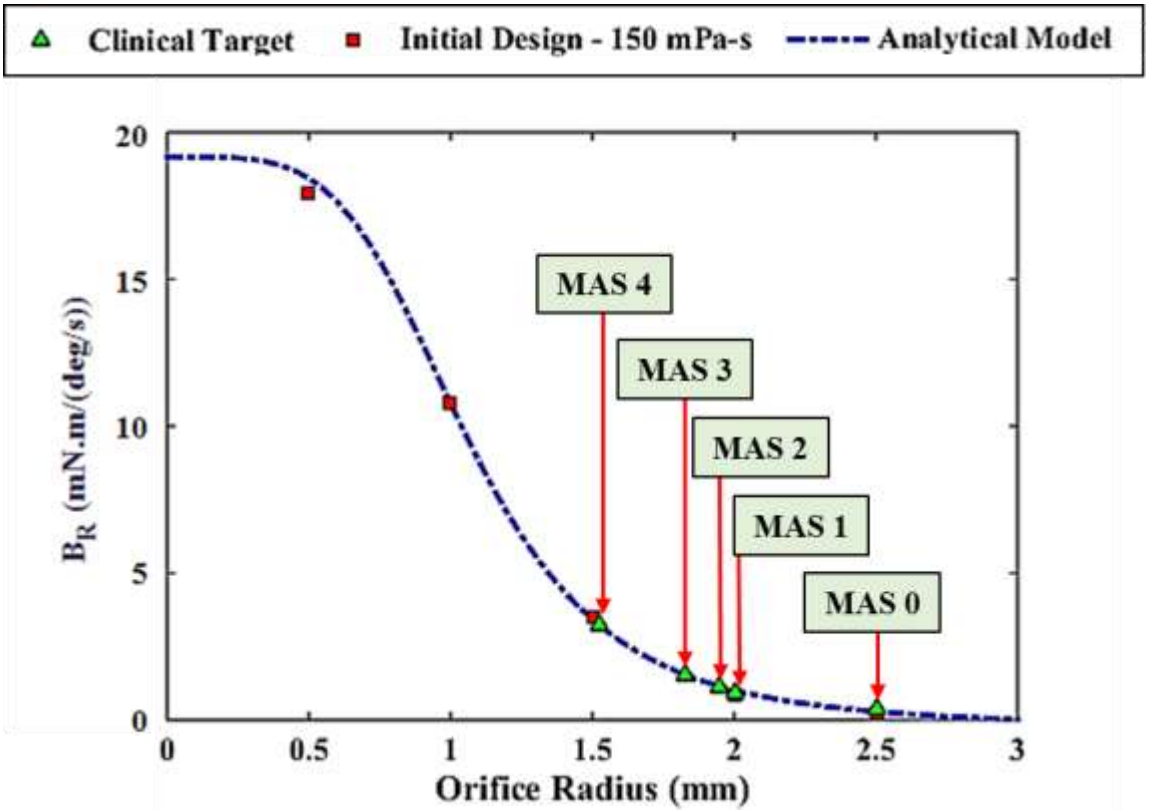

Figure 2.14: Experimental rotary viscosities (square) for the 150 mPa.s silicone oil plotted against the analytical model of rotary viscosity (dotted line) in relation to orifice diameters. Clinical targets (triangle) are displayed along the analytical curve.

Table 2.6: Numerical values of the clinical targets and the corresponding orifice radii shown in Figure 2.14. The approximated orifices were implemented in the modified design.

MAS	Clinical Target B_R [mN.m/(deg/s)]	Orifice Radius [mm]	Approximated Orifice Radius [mm]
0	0.38 ± 0.29	2.50	2.5
1	0.88 ± 0.43	2.05	2.0
2	0.99 ± 0.53	1.95	1.9
3	1.43 ± 0.59	1.83	1.8
4	3.04 ± 0.01	1.55	1.5
5	NA	NA	NA

2.3.2 RESULTS OF MODIFIED DAMPER DESIGN

Experimental results of the modified viscous damper design are displayed in Figure 2.15. The same general trends were observed for output damping force with respect to orifice geometry and input speed. The scaled analytical model determined from the initial design showed good agreeability with the modified design and the residual values were all within ± 2.0 N across all input speeds (Figure 2.15a). Linear viscosity B_L and rotary viscosity B_R for each orifice geometry were listed in Table 2.7. Experimental B_R values were 0.33 mN.m/(deg/s), 1.40 mN.m/(deg/s), 1.50 mN.m/(deg/s), 2.10 mN.m/(deg/s), and 3.60 mN.m/(deg/s) for orifice radii of 2.5 mm, 2.0 mm, 1.9 mm, 1.8 mm, and 1.5 mm, respectively.

In general, experimental results followed agreeably with the trend displayed in the target clinical behavior, despite deviating much from the average targets (Figure 2.16). The value of B_R for MAS 0 fell within the range of the clinical target, B_R for MAS 1 – 3 were approximately the same as the upper bound limit for the corresponding target, and B_R for MAS 4 was above the clinical range.

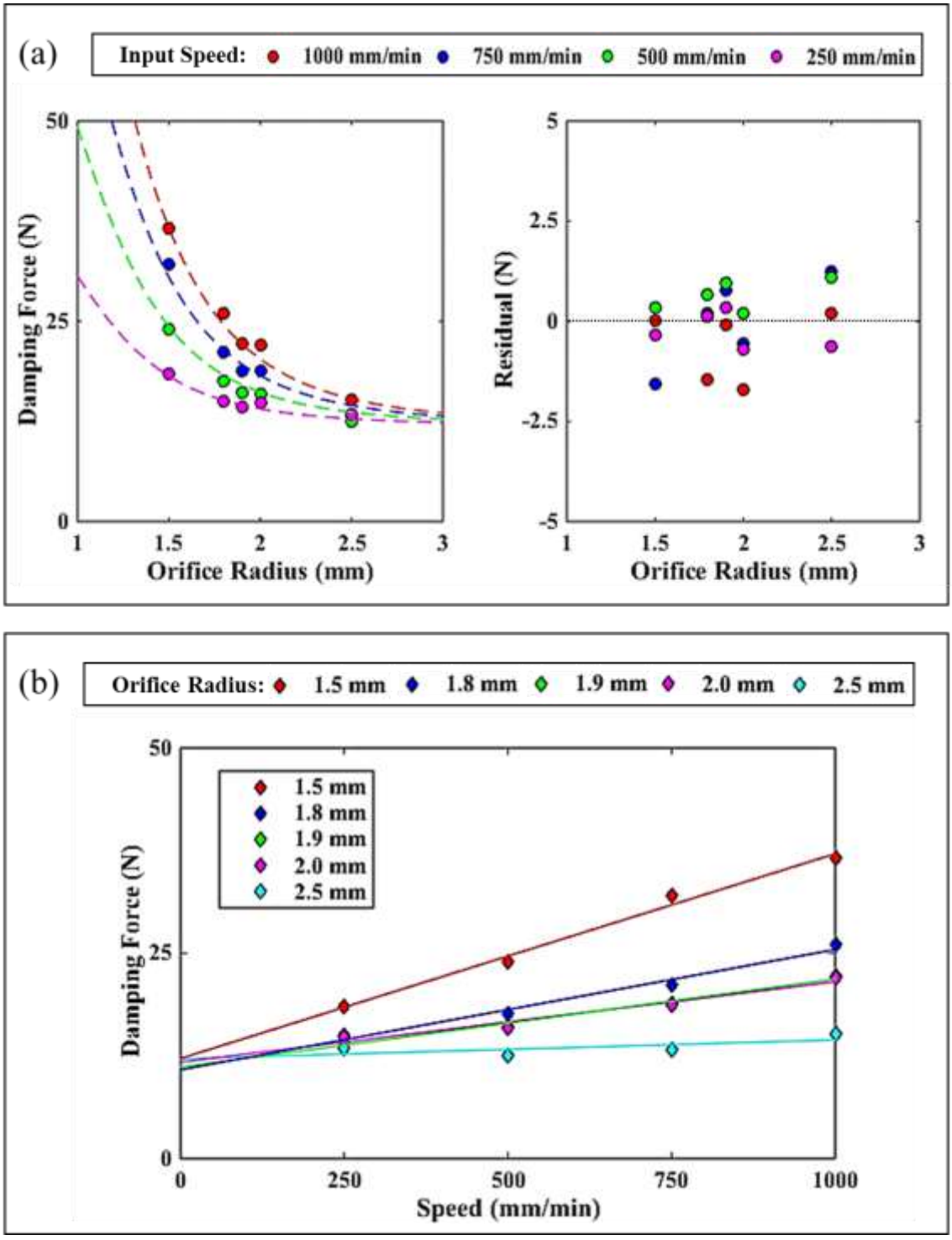

Figure 2.15: Results for the 150 mPa.s silicone oil with the modified design. (a) Experimental results (circles) plotted against the analytical model Eq.(11) (dotted lines) in relation to orifice diameters for different input speeds with the corresponding residual plot ($Residual = Analytical - Experimental$). The values of C_1, C_2, and C_3 are 0.65, 1.10, and 1.07 respectively. (b) Experimental results (diamonds) in relation to input speeds for different orifice diameters with best-fit lines (solid lines).

Table 2.7: Linear and rotary viscosities for each orifice evaluated for the modified design with the corresponding MAS scores and clinical target viscosity.

MAS	Approximated Orifice Radius [mm]	Modified Design		Clinical Target B_R [mN.m/(deg/s)]
		Linear Viscosity B_L [N/(mm/min)]	Rotary Viscosity B_R [mN.m/(deg/s)]	
0	2.5	0.0023	0.33	0.38 ± 0.29
1	2.0	0.0098	1.40	0.88 ± 0.43
2	1.9	0.0107	1.50	0.99 ± 0.53
3	1.8	0.0146	2.10	1.43 ± 0.59
4	1.5	0.0249	3.60	3.04 ± 0.01
5	NA	NA	NA	NA

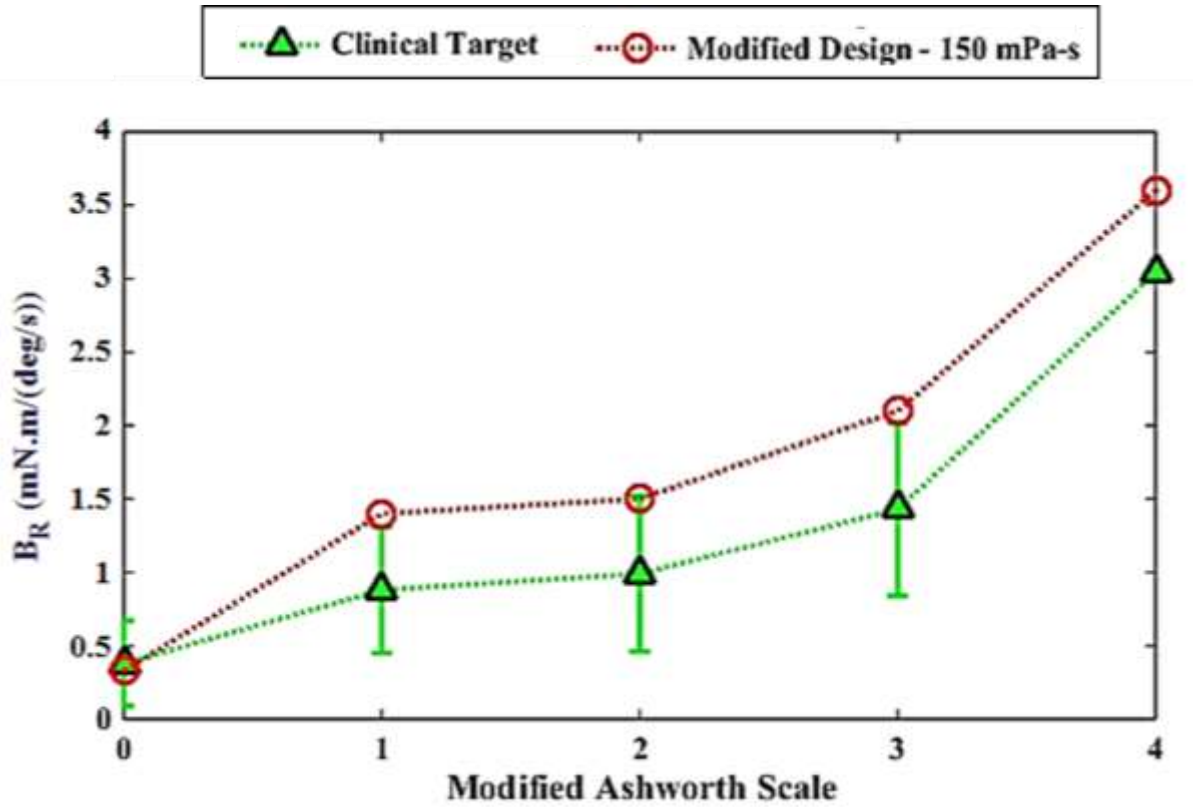

Figure 2.16: Experimental rotary viscosities of the modified design plotted against the clinical targets (average and standard deviation) in relation to MAS score.

2.3.3 RESULTS OF FULLY ASSEMBLED SIMULATOR

Preliminary results obtained from evaluating the overall performance of the hydraulic-based simulator are displayed in Figure 2.17 and Figure 2.18. The measured behavior of the simulator corresponded to the general geometry and speed-dependent trends observed from evaluating the passive damper designs (Figure 2.3). As the orifice radius decreased (increasing MAS score), the output torque of the simulator increased (Figure 2.17 and Table 2.8), and for increasing input stretch speed, a proportional increase in the output torque was observed (Figure 2.18). Maximum output torque always occurred at the mid-range of motion (approximately 40 °) due to the linkage design chosen for this mechanism.

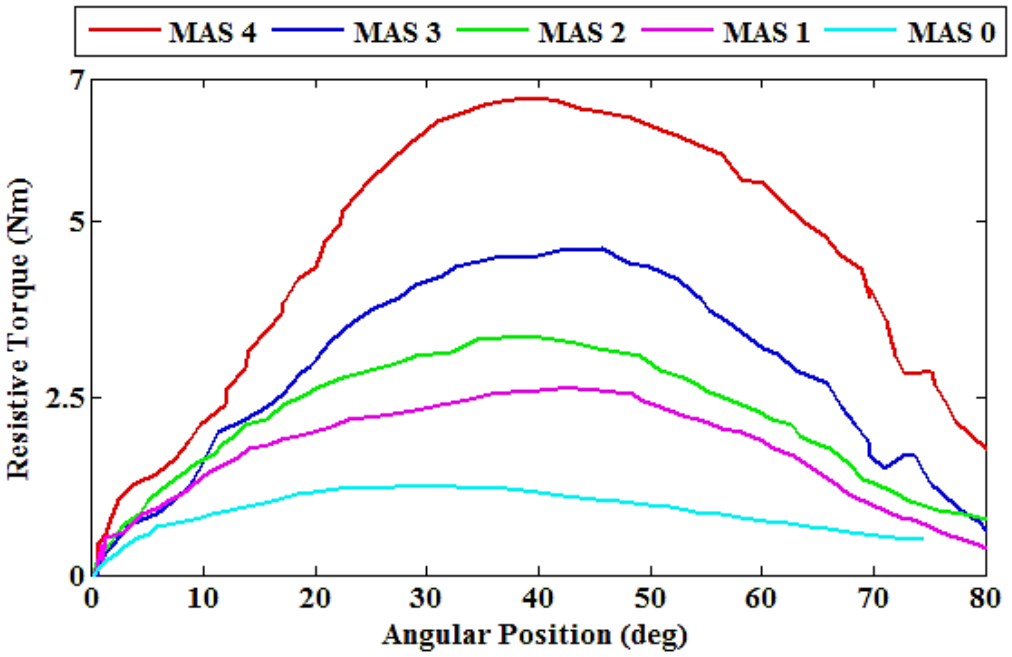

Figure 2.17: Experimentally measured response of the fully-integrated simulator; resistive torque versus relative angular position between upper arm and forearm for MAS 0 – 4 at high input stretch speed (> 150 deg/s).

Table 2.8: Average angular speed and peak torque values obtained from preliminary evaluation of the simulator prototype (Figure 2.17) for each MAS score.

MAS Score	Avg. Angular Speed [deg/s]	Peak Torque [Nm]
0	200	1.25
1	170	2.60
2	190	3.32
3	185	4.56
4	160	6.68

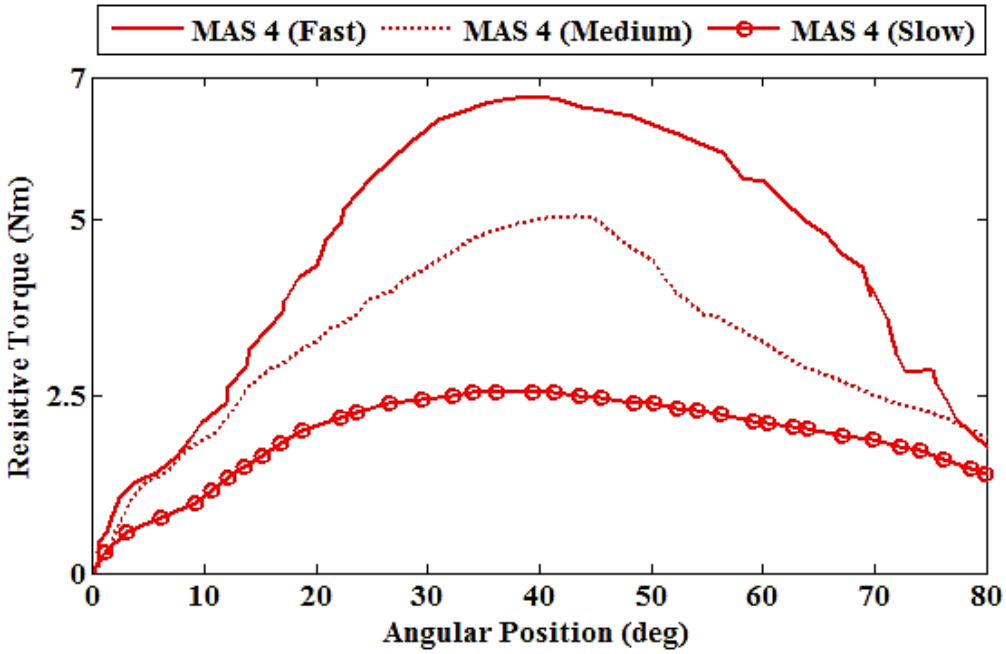

Figure 2.18: Experimental results of resistive torque in relation to relative angular position for MAS 4 at high input ($\dot{\theta}$ = 160 deg/s), medium ($\dot{\theta}$ = 130 deg/s), and slow ($\dot{\theta}$ = 50 deg/s) input stretch speeds.

2.4 DISCUSSION

The goal of this project was to design a portable, low-cost forearm simulator for replicating different levels of spasticity in the elbow joint during a passive flexion stretch test. A purely mechanical approach was pursued during the development process to eliminate the need

for any high-cost components associated with a typical electromechanical design. The resulting forearm simulator could replicate five distinct speed-dependent spasticity behaviors representing MAS 0 – 4 without need for a computational scheme (i.e. no active control). This simulator was a standalone product that could be used in any environment (does not require any additional device attachment such as electrical power).

The speed-dependent characteristics of the simulator were driven by a novel hydraulic-based system embedded within the device. Through an iterative design process that involved analytical modelling and experimental prototyping, a passive damper using viscous fluid in combination with creative flow channel configurations was developed. Operating solely on the principal of viscous pressure-driven flow, this custom-fabricated damper was able to generate a wide range of resistive feedbacks in response to different input speeds. Preliminary results obtained from evaluating the passive viscous damper and fully assembled simulator suggested the possibility of using this novel design to mimic spasticity (Figures 2.16-18).

An analytical model (Eq.(11)) that characterized the fluid behavior inside the viscous damper was developed as a tool to make deterministic design decisions. Scaling factors C_1, C_2, and C_3 added to the analytical model were determined through experimentation and were found to be 0.65, 1.10, and 1.07, respectively, for both fluids. All correction factors were order one, suggesting minimal deviation of geometric specifications. In the ideal situation, these scaling factors should all be 1.0. The values of C_2 and C_3 were both within 10% of 1.0. However, the value of C_1 was 35% lower than 1.0. This larger discrepancy was likely due to the sensitivity of the model to geometric parameters of the design, in particular small gap dimensions. For instance, increasing the gap width b from the original value of 0.3 mm to 0.31 mm would change C_1 from 0.65 to 0.73, while C_2 and C_3 would be held constant.

As input speed increased, the output damping force generally increased linearly, except for the 2.5 mm and 2.0 mm orifice radii with the 100 mPa.s silicone oil (Table 2.5). Friction force dominated for these particular orifice-fluid combinations, and the negative viscosity values indicated that friction (due to piston sealing) was decreasing with speed.

The scaled analytical model had good agreeability with experimental results (Figures 2.11, 2.12, 2.15). Orifice geometries for the modified damper design were chosen based on the scaled model to replicate spasticity behaviors corresponding to MAS 0 – 4. Quantitative data adapted from literature were used as design targets to tune the simulator (Table 2.2). The large discrepancy between the average clinical target viscosities and the experimental results (Figure 2.16) could come from multiple sources. It may be due to the inexact sizing of the orifice geometry during design modification, since orifice radii were rounded to match the available tool size for fabrication. The actual orifice radii implemented in the new design were smaller than the exact values; therefore the resulting rotary viscosities were higher than the targets. Moreover, friction due to piston sealing may have been larger in the modified design, hence a greater overall resistive force was measured.

Evaluation of the simulator prototype was performed while holding the upper arm fixed at an angle of approximately 30 – 45 deg. Due to the linkage geometries, the output response of the simulator would vary slightly depending on upper arm orientation (component of damping force perpendicular to the forearm). Analytical results were calculated assuming that the upper arm was fixed at 45 deg which is the typical angle that a clinician would hold the patient's upper arm at during clinical assessment.

Preliminary evaluation of the fully assembled hydraulic-based simulator confirmed the feasibility of using a purely mechanical system to achieve spasticity simulation; however, there

is much to be done before this prototype could be used in actual clinical training. The viscous damper used in the simulator was very sensitive to geometric variation; therefore a precise fabrication method is required to properly tune the output behaviors. Also, due to the lack of quantitative data, many features of spasticity remain unknown to healthcare clinicians and researchers. In order to create a training simulator that can truly represent varying degrees of spasticity, proper measurement methods and a good database of quantitative data are necessary to establish design targets for the development process. When the simulator is properly tuned, a panel of clinical experts should be invited to provide feedback on the design and to ensure that the device is comparable to actual patients.

2.5 CONCLUSION

A passive, hydraulic-based forearm simulator for elbow flexion spasticity replication was proposed and developed through this project. Unlike any existing designs, this simulator does not rely on a computational (active control) scheme to generate different levels of spasticity behaviors. The implementation of a novel passive viscous damper enabled the device to generate distinctive force feedback in response to different input speeds. Preliminary results obtained from evaluating the viscous damper and the fully assembled simulator suggested the possibility of using this design in replicating spasticity. However, better quantitative data and a precise fabrication method are required to properly tune the simulator behaviors to the desired clinical targets. The hydraulic-based simulator presents an entirely different approach to replicate spasticity in the elbow joint. With more development and evaluation, it is possible to expand the framework of the current prototype to replicate other types of behaviors in various human joints.

2.6 LIST OF REFERENCES

[1] G. Sheean, "The pathophysiology of spasticity," *Eur J Neurol,* vol. 9 Suppl 1, pp. 3-9, 53-61, May 2002.

[2] A. D. Pandyan, M. Gregoric, M. P. Barnes, D. Wood, F. Van Wijck, J. Burridge, H. Hermens, and G. R. Johnson, "Spasticity: clinical perceptions, neurological realities and meaningful measurement," *Disabil Rehabil,* vol. 27, pp. 2-6, Jan 7-21 2005.

[3] D. Burke, "Spasticity as an adaptation to pyramidal tract injury," *Adv Neurol,* vol. 47, pp. 401-423, 1988.

[4] M. P. Barnes and G. R. Johnson, *Upper motor neurone syndrome and spasticity: clinical management and neurophysiology*: Cambridge University Press, 2008.

[5] M. P. Barnes, "An overview of the clinical management of spasticity," in *Upper motor neurone syndrome and spasticity: clinical management and neurophysiology*, M. P. Barnes and G. R. Johnson, Eds., ed Cambridge, United Kingdom: Cambridge University Press, 2001, pp. 1-11.

[6] American Association of Neurological Surgeons. (2006). *Spasticity* [Web]. Available: http://www.aans.org/Patient%20Information/Conditions%20and%20Treatments/Spasticity.aspx [Accessed: Jul. 2, 2016]

[7] R. L. Lieber, S. Steinman, I. A. Barash, and H. Chambers, "Structural and functional changes in spastic skeletal muscle," *Muscle Nerve,* vol. 29, pp. 615-627, May 2004.

[8] B. G. Vickrey, R. D. Hays, R. Harooni, L. W. Myers, and G. W. Ellison, "A health-related quality of life measure for multiple sclerosis," *Qual Life Res,* vol. 4, pp. 187-206, Jun 1995.

[9] A. Schrag, M. Jahanshahi, and N. Quinn, "What contributes to quality of life in patients with Parkinson's disease?," *J Neurol Neurosurg Psychiatry,* vol. 69, pp. 308-312, 2000.

[10] H. M. Lee, Y. Z. Huang, J. J. Chen, and I. S. Hwang, "Quantitative analysis of the velocity related pathophysiology of spasticity and rigidity in the elbow flexors," *J Neurol Neurosurg Psychiatry*, vol. 72, pp. 621-629, May 2002.

[11] R. W. Bohannon and M. B. Smith, "Interrater reliability of a modified Ashworth scale of muscle spasticity," *Phys Ther*, vol. 67, pp. 206-207, Feb 1987.

[12] R. N. Boyd, S. A. Barwood, C. E. Baillieu, and H. K. Graham, "Validity of a clinical measure of spasticity in children with cerebral palsy in a randomized clinical trial," *Dev Med Child Neurol*, vol. 40, p. 7, 1998.

[13] W. K. Yam and M. S. Leung, "Interrater reliability of Modified Ashworth Scale and Modified Tardieu Scale in children with spastic cerebral palsy," *J Child Neurol*, vol. 21, pp. 1031-1035, Dec 2006.

[14] A. Siderowf, M. McDermott, K. Kieburtz, K. Blindauer, S. Plumb, I. Shoulson, and G. Parkinson Study, "Test-retest reliability of the unified Parkinson's disease rating scale in patients with early Parkinson's disease: results from a multicenter clinical trial," *Mov Disord*, vol. 17, pp. 758-763, Jul 2002.

[15] M. Richards, K. Marder, L. Cote, and R. Mayeux, "Interrater reliability of the Unified Parkinson's Disease Rating Scale motor examination," *Mov Disord*, vol. 9, pp. 89-91, Jan 1994.

[16] L. V. Metman, B. Myre, N. Verwey, S. Hassin-Baer, J. Arzbaecher, D. Sierens, and R. Bakay, "Test-retest reliability of UPDRS-III, dyskinesia scales, and timed motor tests in patients with advanced Parkinson's disease: an argument against multiple baseline assessments," *Mov Disord*, vol. 19, pp. 1079-1084, Sep 2004.

[17] J. Mehrholz, K. Wagner, D. Meissner, K. Grundmann, C. Zange, R. Koch, and M. Pohl, "Reliability of the Modified Tardieu Scale and the Modified Ashworth Scale in adult patients with severe brain injury: a comparison study," *Clin Rehabil,* vol. 19, pp. 751-759, Oct 2005.

[18] J. Mehrholz, Y. Major, D. Meissner, S. Sandi-Gahun, R. Koch, and M. Pohl, "The influence of contractures and variation in measurement stretching velocity on the reliability of the Modified Ashworth Scale in patients with severe brain injury," *Clin Rehabil,* vol. 19, pp. 63-72, Jan 2005.

[19] T. Kaya, A. G. Karatepe, R. Gunaydin, A. Koc, and U. Altundal Ercan, "Inter-rater reliability of the Modified Ashworth Scale and modified Modified Ashworth Scale in assessing poststroke elbow flexor spasticity," *Int J Rehabil Res,* vol. 34, pp. 59-64, Mar 2011.

[20] J. F. M. Fleuren, G. E. Voerman, C. V. Erren-Wolters, G. J. Snoek, J. S. Rietman, H. J. Hermens, and A. V. Nene, "Stop using the Ashworth Scale for the assessment of spasticity," *J Neurol Neurosurg Psychiatry,* vol. 81, pp. 46-52, Jan 10 2010.

[21] A. H. Al-Elq, "Simulation-based medical teaching and learning," *J Family Community Med,* vol. 17, pp. 35-40, Jan 2010.

[22] J. L. Lane, S. Slavin, and A. Ziv, "Simulation in medical education: A review," *S&G,* vol. 32, pp. 297-314, 2001.

[23] Y. Takhashi, T. Komeda, H. Koyama, S. Yamamoto, T. Arimatsu, Y. Kawakami, K. Inoue, and Y. Ito, "Development of an upper limb patient simulator for physical therapy exercise," in *IEEE 12th International Conference on Rehabilitation Robotics*, 2011, pp. 1-4

[24] H.-S. Park, Q. Peng, and L.-Q. Zhang, "Causality-based portable control system design for tele-assessment of elbow joint spasticity," in *IEEE 9th International Conference on Rehabilitation Robotics*, 2005, pp. 303-306

[25] H. S. Park, J. Kim, and D. L. Damiano, "Development of a Haptic Elbow Spasticity Simulator (HESS) for improving accuracy and reliability of clinical assessment of spasticity," *IEEE Trans Neural Syst Rehabil Eng,* vol. 20, pp. 361-370, May 2012.

[26] T. Mouri, H. Kawasaki, Y. Nishimoto, T. Aoki, and Y. Ishigure, "Development of robot hand for therapist education/training on rehabilitation," in *IEEE/RSJ International Conference on Intelligent Robots and Systems*, 2007, pp. 2295-2300

[27] M. Heinrich, C. Mattson, M. Ramuta, J. Stock, J. Liang, M. Morris, S. Tippett, E. Hsiao-Wecksler, and J. Henderson, "Pneumatic Elbow Simulator of Spasticity and Rigidity for Training of Healthcare Clinicians," in *2nd Fluid Power Innovation & Research Conference* Chicago, IL, 2015.

[28] T. Kikuchi, K. Oda, and J. Furusho, "Leg-Robot for Demonstration of Spastic Movements of Brain-Injured Patients with Compact Magnetorheological Fluid Clutch," *Adv Robotics,* vol. 24, pp. 671-686, 2010.

[29] D. I. Grow, M. Wu, M. J. Locastro, S. K. Arora, A. J. Bastian, and A. M. Okamura, "Haptic simulation of elbow joint spasticity," in *IEEE Symposium on Haptic Interfaces for Virtual Environment and Teleoperator Systems*, 2008, pp. 475-476

[30] T. Fujisawa, M. Takagi, Y. Takahashi, K. Inoue, T. Terada, Y. Kawakami, and T. Komeda, "Basic research on the upper limb patient simulator," in *IEEE 10th International Conference on Rehabilitation Robotics*, 2007, pp. 48-51

[31] Y. N. Wu, H. S. Park, Y. Ren, D. Gaebler-Spira, J. J. Chen, and L. Q. Zhang, "Measurement of elbow spasticity in stroke patients using a manual spasticity evaluator," in *28th Annual International Conference of the IEEE Engineering in Medicine and Biology Society* 2006, pp. 3974-3977

[32] Y. N. Wu, Y. Ren, A. Goldsmith, D. Gaebler, S. Q. Liu, and L. Q. Zhang, "Characterization of spasticity in cerebral palsy: dependence of catch angle on velocity," *Dev Med Child Neurol,* vol. 52, pp. 563-569, Jun 2010.

[33] H. M. Lee, J. J. Chen, M. S. Ju, C. C. Lin, and P. P. Poon, "Validation of portable muscle tone measurement device for quantifying velocity-dependent properties in elbow spasticity," *J Electromyogr Kinesiol,* vol. 14, pp. 577-589, Oct 2004.

[34] J. J. Chen, Y. N. Wu, S. C. Huang, H. M. Lee, and Y. L. Wang, "The use of a portable muscle tone measurement device to measure the effects of botulinum toxin type a on elbow flexor spasticity," *Arch Phys Med Rehab,* vol. 86, pp. 1655-1660, Aug 2005.

[35] V. M. Zatsiorsky, V. N. Seluyanov, and L. G. Chugunova, "Methods of determining mass-inertial characteristics of human body segments," in *Contemporary problems of biomechanics*. vol. 272, ed Moscow, Russia: Mir Publishers 1990.

[36] G. Haskell and D. Lee, "Fluid viscous damping as an alternative to base isolation," *ASME Publications Pvp,* vol. 330, pp. 35-40 1996.

[37] D. Lee and D. P. Taylor, "Viscous damper development and future trends," *Struct Des Tall Buil,* vol. 10, pp. 311-320, Mar 2001.

[38] H. S. Badeer and C. E. Synolakis, "The Bernoulli-Poiseuille Equation," *Physics Teacher,* vol. 27, pp. 598-601, 1989.

[39] N. Kate and T. Jadhav, "Mathematical modelling of an automobile damper," *Int J Engg Research*, vol. 2, pp. 467-471, 2013.

[40] M.S. Tallbot and J. Starkey, “An experimentally validated physical model of a high performance mono-tube damper”, *SAE Motorsports Engineering Conference and Exhibition*, 2002.

[41] H. H. Moretto, M. Schulze, and G. Wagner, "Silicones," in *Ullmann's Encyclopedia of Industrial Chemistry* ed Hoboken, NJ: John Wiley and Sons, 1993.

3 CONCLUSION

3.1 REVIEW OF FINDINGS

This thesis presents the design approach of a purely mechanical, hydraulic-based simulator that has the potential to replicate different types of abnormal muscle behaviors in human limb joints. In order to validate the feasibility of this novel design concept, a prototype of the simulator for spasticity replication in the elbow joint was constructed.

The fluid-based simulator utilized a custom-fabricated passive viscous damper to replicate different degrees of spasticity behavior in the elbow joint. An analytical model for fluid behavior was developed to relate the output force of the damper in relation to the associated geometric parameters and input speed. A series of experiments were executed using the viscous damper in order to characterize and validate its performance. Validation results were used to calibrate the analytical model to predict performance of future designs. Using the adjusted analytical model, orifice geometries and viscous fluid combinations were chosen to represent varying degrees of spasticity on the Modified Ashworth Scale (MAS).

Preliminary evaluation of the fully assembled spasticity simulator confirmed that the device was capable of generating a wide range of speed-dependent responses during operation. The simulator behavior is mainly influenced by the rate in which fluid passes from the compression chamber to the rebound chamber of the viscous damper as the piston strokes. This volumetric flow rate (and thus speed dependency) was controlled by two factors: orifice geometry and input piston speed. In this case, orifice geometry was a design factor that was manipulated to adjust the speed sensitivity of the design.

The intended goal of this initial prototype was to replicate spasticity in the elbow joint during flexion. The finished simulator was tuned to existing quantitative data (clinical targets [1, 2]) that describe the speed dependency of spasticity. In general, experimental results followed agreeably with the trend displayed in target clinical behavior, despite deviating much from the average targets (Table 2.7 and Figure 2.16 from Chapter 2). The overall performance of the simulator correlated with the typical torque versus displacement profile of spasticity (Figure 2.17 and Figure 2.18 from Chapter 2). Preliminary results suggest potential for the use of hydraulic-based simulators to replicate spasticity; however, more precise tuning and better quantification of the behavior are necessary to calibrate the device to match the corresponding clinical target.

3.2 LIMITATIONS AND FUTURE WORK

Although preliminary evaluation of the fully assembled hydraulic-based simulator confirmed the feasibility of using a non-electromechanical design to replicate spasticity, there is much to be done before this prototype could be used in actual clinical training. The viscous damper used in the simulator was very sensitive to geometric variation; therefore a precise fabrication method is required to properly tune the output behaviors. Also, due to the lack of quantitative data, many features of spasticity remain unknown to healthcare clinicians and researchers. In order to create a simulator that can truly represent varying degrees of spasticity, proper measurement method and a large database of quantitative data are necessary for the development process. When the simulator is properly tuned, a panel of clinical experts needs to be invited to provide feedback on the design and to ensure that the device is comparable to actual patients.

Having a large, high quality database of quantitative data would allow the simulator to create general behavior representing patients with the same clinical score. For this reason, a portable, lightweight device that can be incorporated into traditional clinical assessment of spasticity and other abnormal muscle behaviors is currently being developed by the author and her colleagues. Applied force, position, and velocity information will be collected from this portable device to fine-tune the simulator in future development. This quantitative database will also help clinicians to better understand and distinguish among different abnormal muscle behaviors and aid in the administration of more effective therapy to patients.

The use of a hydraulic damper enabled the simulator to replicate the slow, tonic muscle response; however, it lacked a tool to replicate the fast, phasic features. In the simulation of spasticity behavior, the passive viscous damper was able to replicate the speed-dependent tonic muscle behavior; however, it was unable to mimic the "catch-and-release" phenomenon in which the muscle tone spikes up and drops back down during mid-range of motion (Figure 3.1). To achieve a more realistic simulation, it may be beneficial to install an electric motor in parallel to the viscous damper to create a hybrid system such that the electric motor can be used to replicate the phasic features of spasticity.

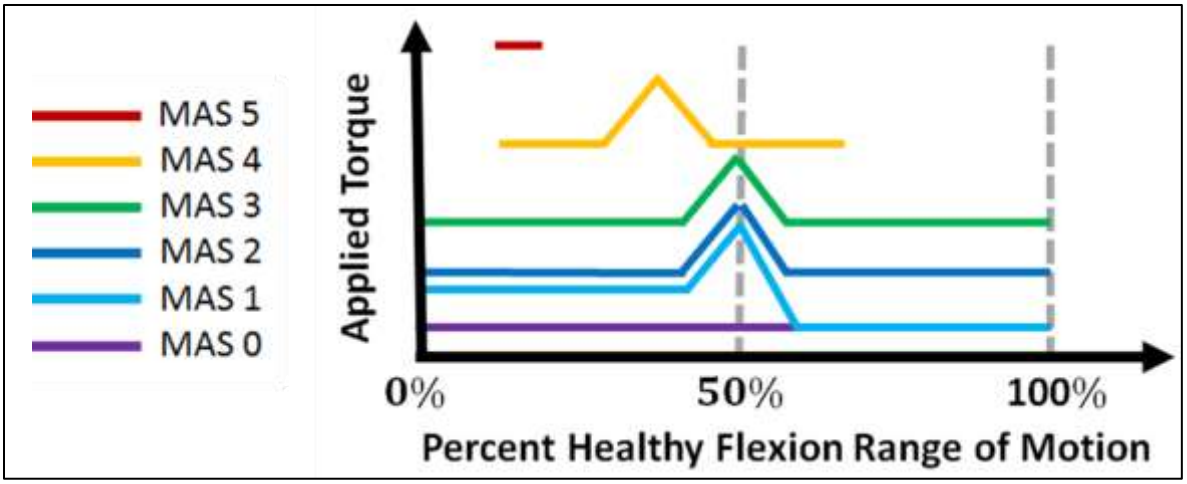

Figure 3.1: High level graphical interpretation of the Modified Ashworth Scale derived based on its qualitative description. The spike along each curve represents the "catch-and-release" phenomenon.

The current simulator used viscous Newtonian fluid, and this design can only replicate spasticity. However, the framework and method developed for the spasticity simulator can be further expanded to replicate the less speed sensitive rigidity behavior. Comprehensive characterization results of the passive viscous damper and preliminary evaluation of the full simulator assembly both confirmed that this novel design could generate a wide range of forces spanning across different speed sensitivities. Depending on the viscosity of the working fluid, there exists a range of orifice radii where the output force remains relatively constant in relation to different input speeds. When a less viscous fluid is chosen for operation, this design range widens up. However, the change in force amplitude due to orifice selection may not be distinctive enough to produce varying degrees of rigidity behavior; therefore the use of an additional fluid (or fluids) to replicate the remaining levels of severity may be necessary.

The use of viscous fluid poses many limitations in rigidity replication due to its inherent rate dependency. Viscous fluids are Newtonian fluids (constant viscosity) in which the stresses arising from its flow are linearly proportional to the strain rate (Figure 3.2) [3, 4]. This unique

characteristic of Newtonian fluid contributes to the linear relationship observed between output force and input speed during evaluation experiment of the passive viscous damper.

To effectively simulate rigidity, it is important to investigate alternative material options for use as the working fluid. Shear-thinning non-Newtonian fluid may be a viable candidate for this application. The viscosity of shear-thinning fluid decreases with increasing strain rate, leading to a non-linear profile of stresses (Figure 3.2) [3, 4]. Through controlling the properties of macromolecules suspended in the shear-thinning fluid [3], it is possible to balance the viscosity response and stress response of the fluid due to increasing strain rate, thus engineering a material such that it will have a constant output force across a wide range of input speeds.

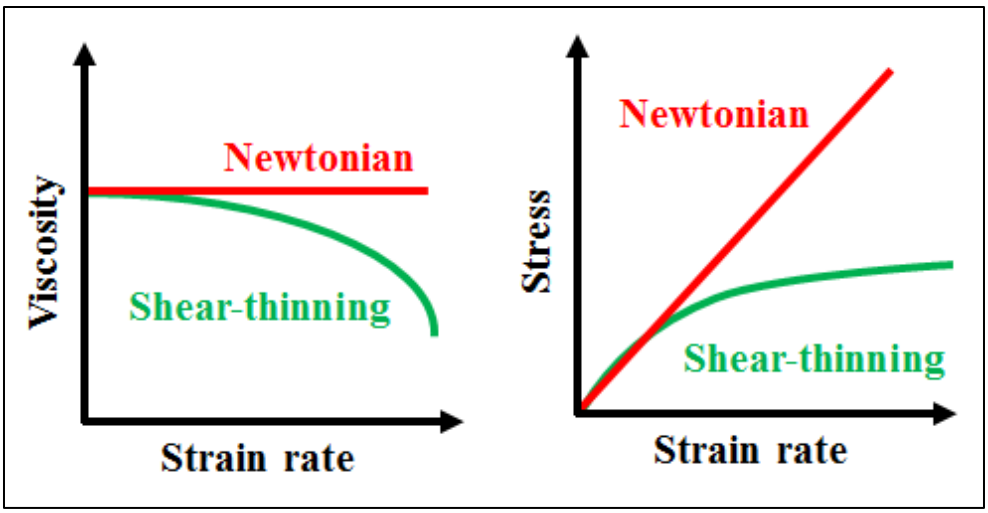

Figure 3.2: Viscosity and stress in relation to strain rate for Newtonian and shear-thinning fluids. Figure recreated from [4].

The passive hydraulic-based simulator presents an entirely different approach to replicate the altered biomechanical properties of human muscle. With more development and evaluation, it is possible to adapt the framework of the current prototype to replicate different types of abnormal muscle behaviors in various human joints. It was the intended goal of this project to

look into alternative design methods, apart from the traditional electromechanical approach, in order to guide future development of medical training simulation devices.

As an initial step to realize this goal, a forearm spasticity simulator utilizing a novel damper design was developed and evaluated. A purely mechanical approach was pursued during the development process to eliminate the need for any high-cost components associated with a typical electromechanical design. The resulting forearm simulator could replicate five distinct speed-dependent spasticity behaviors representing MAS 0 – 4 without need for a computational control scheme (i.e. no active control) and it is a standalone product (does not require any additional device attachment such as electrical power) that could be used in any environment.

3.3 LIST OF REFERENCES

[1] H. M. Lee, J. J. Chen, M. S. Ju, C. C. Lin, and P. P. Poon, "Validation of portable muscle tone measurement device for quantifying velocity-dependent properties in elbow spasticity," *J Electromyogr Kinesiol*, vol. 14, pp. 577-589, Oct 2004.

[2] J. J. Chen, Y. N. Wu, S. C. Huang, H. M. Lee, and Y. L. Wang, "The use of a portable muscle tone measurement device to measure the effects of botulinum toxin type a on elbow flexor spasticity," *Arch Phys Med Rehab*, vol. 86, pp. 1655-1660, Aug 2005.

[3] B.R. Bird, R.C. Armstrong, and O. Hassager. *Dynamics of Polyeric Liquids.* vol. 1, 2nd, ed Hoboken, NJ: John Wiley & Sons 1987.

[4] U. Brockel, W. Meier, and G. Wagner. *Product design and engineering: formulation of gels and pastes.* ed Hoboken, NJ: John Wiley & Sons 2013.

APPENDIX A: CLINICAL SCALES USED IN ASSESSMENT OF SPASTICITY AND RIGIDITY

Two clinical scales generally used in the assessment of spasticity are the Modified Ashworth Scale (MAS) and the Modified Tardieu Scale (MTS). As the name suggests, the MAS is a modified version of the Ashworth Scale (AS) and the MTS is a modified version of the Tardieu Scale (TS).

The AS (Table A.1) was originally developed by Ashworth in 1964 as a simple clinical classification to evaluate the effects of anti-spasticity drugs in patients with multiple sclerosis [1]. Since then, AS has gained widespread clinical acceptance as a measure of spasticity [2]. The MAS (Table A.2) was proposed by Bohannon and Smith in 1987 [3]. In this modified version, an additional grade of 1+ was added to the scale to enhance sensitivity and accommodate patients with rating on the lower end of the scale [2, 3]. Further, estimation of how soon and how much resistance was felt in the ROM at the affected limb was incorporated in the qualitative descriptions [2, 3]. The additional grade of 1+ proposed in the MAS is sometimes denoted as a grade of 2 with all the subsequent grades incremented by one (Table A.2, numbers in parenthesis).

Table A.1: Ashworth Scale for assessing spasticity, adapted from [1].

Score	Description
0	No increase in tone
1	Slight increase in tone giving a catch when the limb was moved in flexion or extension
2	More marked increase in tone but limb was easily flexed
3	Considerable increase in tone – passive movement difficult
4	Limb rigid in flexion or extension

Table A.2: Modified Ashworth Scale for assessing spasticity, adapted from [3].

Score	Description
0 (0)*	No increase in muscle tone
1 (1)	Slight increase in muscle tone, manifested by a catch and release or by minimal resistance at the end of the range of motion when the affected part(s) is moved in flexion or extension
1+ (2)	Slight increase in muscle tone, manifested by a catch, followed by minimal resistance throughout the reminder (less than half) of the range of motion
2 (3)	More marked increase in muscle tone through most of the range of motion, but affected part is easily moved
3 (4)	Considerable increase in muscle tone, passive movement difficult
4 (5)	Affected part is rigid in flexion or extension

* Numbers in parenthesis represents a variant of the Modified Ashworth Scale.

The TS (Table A.3) was developed by Held and Pierrot-Deseilligny in 1969 [4] based on the original work done by Tardieu on determining the reflex activity in the elbow flexors under slow and fast stretch speeds [5]. The TS has been suggested as a more suitable alternative to the AS for measuring spasticity since the scale evaluates the speed dependency of the behavior and differentiates it from contraction [6, 7]. The MTS (Table A.4) was proposed by Boyd and Graham in 1998 to standardize the stretch condition and limb alignment during passive stretch test and to expand the qualitative descriptions to include determination of catch angle and the occurrence of clonus during the ROM [8].

Table A.3: Tardieu Scale for assessing spasticity, adapted from [4].

Score	Description
0	No stretching
1	Only visible contraction
2	Simple jump felt during mobilization but that passes just as suddenly as it came
3	Lasting contraction or a few clonic tremors that go away after a few seconds
4	Contraction or clonus that does not cease, even after a few seconds

Table A.4: Modified Tardieu Scale for assessing spasticity, adapted from [8].

Score	Description
0	No resistance throughout passive movement
1	Slight resistance throughout, with no clear catch at a precise angle
2	Clear catch at a precise angle followed by release
3	Fatigable clonus (<10 secs) occurring at a precise angle
4	Un-fatigable clonus (>10 secs) occurring at a precise angle
5	Joint immobile

The Motor Section of the Unified Parkinson's Disease Rating System (UPDRS) (Table A.5) is generally used to assess rigidity. The UPDRS is made up of three distinct sections: (1) Mentation, Behavior, and Mood, (2) Activities of Daily Living, and (3) Motor [9]. This comprehensive rating system is often used to follow the longitudinal course of Parkinson's disease. The UPDRS was developed by a special committee (the UPDRS Development Committee) led by Fahn and Elton in 1987 [9].

Table A.5: Unified Parkinson's Disease Rating System for assessing rigidity, adapted from [9].

Score	Description
0	Rigidity absent
1	Rigidity slight or detectable only when activated by mirror or other movements
2	Rigidity mild to moderate
3	Rigidity marked, but full range of motion easily achieved
4	Rigidity severe; range of motion achieved with difficulty

LIST OF REFERENCES:

[1] B. Ashworth, "Preliminary Trial of Carisoprodol in Multiple Sclerosis," *Practitioner,* vol. 192, pp. 540-542, Apr 1964.

[2] D. L. Damiano, J. M. Quinlivan, B. F. Owen, P. Payne, K. C. Nelson, and M. F. Abel, "What does the Ashworth scale really measure and are instrumented measures more valid and precise?," *Dev Med Child Neurol,* vol. 44, pp. 112-118 2002.

[3] R. W. Bohannon and M. B. Smith, "Interrater reliability of a modified Ashworth scale of muscle spasticity," *Phys Ther,* vol. 67, pp. 206-207, Feb 1987.

[4] J. P. Held and E. Pierrot-Deseilligny, "Le bilan moteur central," in *Reeducation motrice des affections neurologiques.* , ed Paris, France: JB Bailliere et Fils, 1969, pp. 31-42.

[5] G. Tardieu, S. Shentoub, and R. Delarue, "A la recherche dune technique de mesure de la spasticite," *Revue Neurologique,* vol. 91, pp. 143-144, 1954.

[6] A. B. Haugh, A. D. Pandyan, and G. R. Johnson, "A systematic review of the Tardieu Scale for the measurement of spasticity," *Disabil Rehabil,* vol. 28, pp. 899-907, Aug 15 2006.

[7] W. Vattanasilp, L. Ada, and J. Crosbie, "Contribution of thixotropy, spasticity, and contracture to ankle stiffness after stroke," *J Neurol Neurosurg Psychiatry,* vol. 69, pp. 34-39, Jul 2000.

[8] R. N. Boyd, S. A. Barwood, C. E. Baillieu, and H. K. Graham, "Validity of a clinical measure of spasticity in children with cerebral palsy in a randomized clinical trial," *Dev Med Child Neurol,* vol. 40, p. 7, 1998.

[9] S. Fahn and R. Elton, *Recent Developments in Parkinson's Disease* vol. 2. Florham Park, NJ: Macmillan Health Care Information, 1987.

APPENDIX B: DATA CONVERSION TABLE

Since the author and colleagues are still in the process of developing a portable device to measure the muscle response during clinical evaluation of spasticity and other types of abnormal muscle behaviors, published data from literature that quantified the speed-dependent characteristics of spasticity were used in the simulator development process. Quantitative data summarized from studies [1, 2] done by Chen's group from the National Cheng Kung University in Taiwan were used as design parameters for tuning the initial simulator prototype.

To quantify the speed-dependent characteristics of spasticity, Chen's group proposed a viscosity measurement *B* to represent the sensitivity muscle torque in relation to passive stretch speed. Viscosity was defined as the ratio of speed-dependent torque [N.m] to input stretch frequency [Hz or cycles/s]. Quantification tests were performed under a sinusoidal stretch speed over a range of motion of 60 deg in both flexion and extension. The frequency value specifies the rate at which each test was repeated. A frequency value of 1 Hz indicates a full stretch test was done in one second with an approximated maximum speed of 188.4 deg/s over 60 deg (Figure B.1).

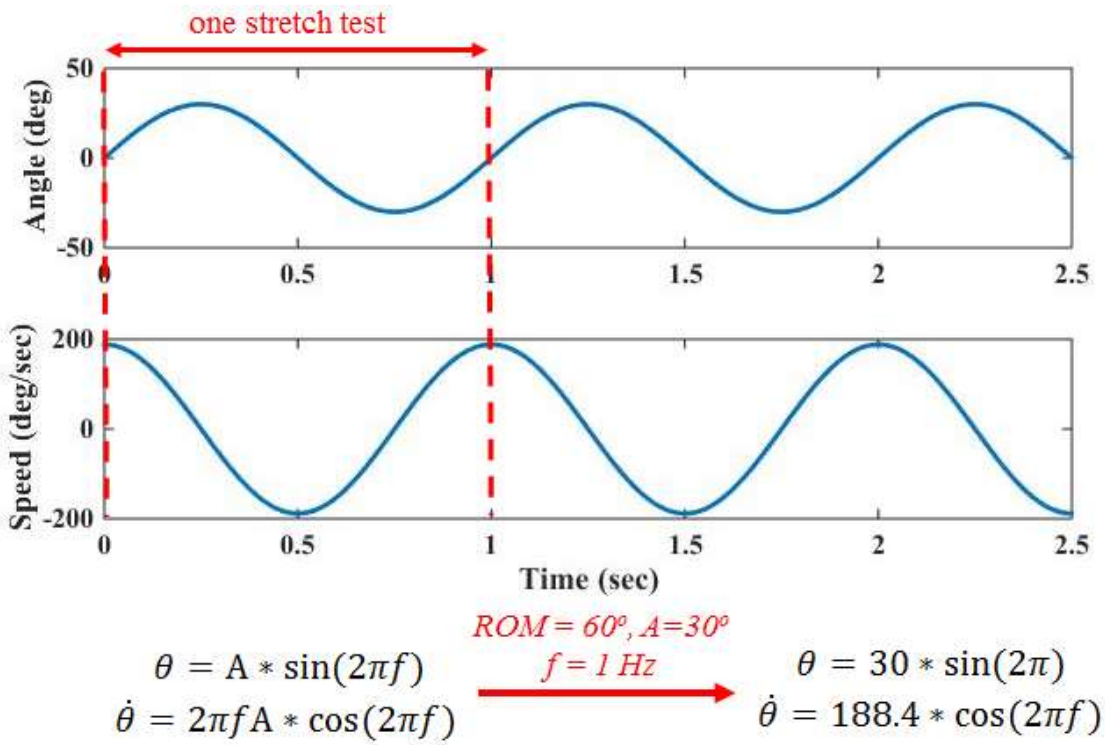

Figure B.1: Diagram explaining the displacement and speed profiles used by Chen's group.

In the first study [1], quantification test of elbow viscosity was performed on 30 subjects (15 normal and 15 spastic) over four stretch frequencies (1/3 Hz, 1/2 Hz, 1 Hz, and 3/2 Hz) and the corresponding results are shown in Table B.1. The average viscosity *B* for normal elbow joint was 0.045 ± 0.035 N.m/(cycles/s) and that for spastic elbow joint was 0.169 ± 0.121 N.m/(cycles/s).

Table B.1: Copy of Table 4 in [10]. *CVA* stands for cerebrovascular accidents, *BW* is the speed-dependent torque, and *B* is the average viscosity.

Table 4
Statistical comparison of parameters *BW* and *B* between normal and spastic elbow joints

Parameters	*BW*1/3	*BW*1/2	*BW*1	*BW*3/2	Averaged viscosity *B*	*P* value
Normal	0.043 ± 0.027	0.049 ± 0.029	0.069 ± 0.030	0.094 ± 0.038	0.045 ± 0.035	All $P < 0.001$
CVA	0.112 ± 0.066	0.148 ± 0.087	0.210 ± 0.133	0.288 ± 0.178	0.169 ± 0.121	

In the second study [2], the quantification test of elbow viscosity was performed on 10 spastic subjects over four stretch frequencies (1/3 Hz, 1/2 Hz, 1 Hz, and 3/2 Hz) before and after the intervention of an anti-spasticity drug. The condition of the patients was evaluated on the Modified Ashworth Scale (MAS) as part of the quantification test. The results for MAS rating (Table B.2) and elbow viscosity measurement *B* (Table B.3) for each patient before and after the drug intervention were correlated to create Table B.4. Average elbow viscosity and the corresponding standard deviation for MAS 1 – 4 were computed and included in the last row of Table B.4. Results for MAS 5 were not included since Chen et al. did not test patients at this level.

Table B.2: Copy of Table 2 in [2].

Table 2: Clinical Assessment of Spastic Elbow Flexor Before (Pre) and 2 Weeks After BTX-A Injection (Post) Using the MAS

	Subject									
MAS Score	A	B	C	D	E	F	G	H	I	J
Pre	1	2	3	1	4	4	3	3	3	3
Post	1	2	2	1	3	2	2	3	2	2

NOTE. Significant difference of the MAS was found using the Wilcoxon signed-rank sum test ($P<.05$).

Table B.3: Copy of Table 3 in [2].

Table 3: Quantification of Spasticity Using Viscosity Before (Pre) and After (Post) Injection

	Subject									
Viscosity	A	B	C	D	E	F	G	H	I	J
Pre	.078	.164	.364	.180	.366	.136	.170	.207	.292	.137
Post	.064	.101	.206	.098	.091	.007	.138	.091	.077	.128

NOTE. Significant difference was found using the Wilcoxon signed-rank sum test ($P<.05$).

Table B.4: Viscosity of elbow in relation to MAS scores. Mean ± standard deviation.

	MAS Score / # Counts	1	2	3	4
Viscosity [N.m/(cycles/s)]	1	0.078	0.164	0.091	0.364
	2	0.064	0.101	0.136	0.366
	3	0.18	0.206	0.17	NA
	4	0.098	0.007	0.207	NA
	5	NA	0.138	0.091	NA
	6	NA	0.077	0.292	NA
	7	NA	0.128	0.137	NA
	Average	0.105 ± 0.052	0.117 ± 0.064	0.161 ± 0.071	0.365 ± 0.001

The average viscosity *B* for normal elbow joint (or MAS 0) computed from the first study [1] and that for MAS 1 – 4 computed from the second study [2] were put together to create a summary table (Table B.5). Viscosity values presented in the summary table were used as design parameters in tuning the spasticity behavior of the passive hydraulic-based simulator.

Table B.5: Average (± standard deviation) viscosity of elbow muscles during passive stretch (for both flexion and extension) in relation to MAS score (derived from [1, 2]).

MAS Score	Viscosity – *B* [N.m/(cycles/s)]
0	0.045 ± 0.035
1	0.105 ± 0.052
2	0.117 ± 0.064
3	0.172 ± 0.071
4	0.365 ± 0.001
5	NA

In order to convert the data summarized from literature to tuning parameters for the simulator, the muscle behavior in relation to angular speed was needed. The original viscosity *B* was given in units of [N.m/(cycles/s)]. However, for the hydraulic simulator, it was necessary to convert these values to a rotary viscosity B_R with units of [mN.m/(deg/s)]. For an input frequency

of 1 Hz or 1 cycle/s, the maximum speed was 188.4 deg/s (Figure B.1). Since the stretch speed followed a sinusoidal profile, the average value over one stretch period was defined as 63.7% of its peak value, or 133.2 deg/s [12]. The viscosity B [N.m/(cycles/s)] was converted to rotary viscosity B_R [mN.m/(deg/s)] by using the following equation. The converted value for each corresponding viscosity is listed in Table B.6.

$$B_R = B * \frac{1\frac{cycles}{s}}{133.2\frac{deg}{s}} * \frac{1000\,mN}{1\,N} \rightarrow \left[\frac{N.m}{\frac{cycles}{s}}\right] * \frac{\left[\frac{cycles}{s}\right]}{\left[\frac{deg}{s}\right]} * \left[\frac{mN}{N}\right] = \left[\frac{mN.m}{\frac{deg}{s}}\right]$$

Table B.6: Average viscosity B and rotary viscosity B_R of the elbow in relation to MAS scores. Mean ± standard deviation.

MAS Score	Viscosity - B [N.m/(cycles/s)]	Rotary Viscosity – B_R [mN.m/(deg/s)]
0	0.045 ± 0.035	0.38 ± 0.29
1	0.105 ± 0.052	0.88 ± 0.43
2	0.117 ± 0.064	0.99 ± 0.53
3	0.172 ± 0.071	1.43 ± 0.59
4	0.365 ± 0.001	3.04 ± 0.01
5	NA	NA

In addition to converting the quantitative data from the literature into the appropriate units for the simulator, another conversion step was applied to the experimental data obtained from the evaluations of the passive viscous damper with the material testing device. The linear viscosity value B_L obtained from those evaluations was in units of [N/(mm/min)]. It was necessary to convert these values to correspond with rotary viscosity with units of [mN.m/(deg/s)] to compare the experimental results of the simulator prototype with desired viscosity behaviors corresponding to MAS scores 0 – 4 from the work of Chen and colleagues. First, a geometric relationship was used to convert the force value into torque value. The

effective moment arm R_{EFF} was measured to be 0.005 m (Figure 2.4 from Chapter 2). The next step was to convert linear speed to rotary speed. The stroke length *d* of the passive viscous device was 0.040 m and the range of motion *ROM* of the simulator was 82 deg. Linear speed and rotary speed were related through the following equation.

$$\frac{d}{v} = \frac{ROM}{\dot{\theta}} \rightarrow \dot{\theta} = \frac{ROM}{d/v}$$

For an input linear speed of 1.0 mm/min, the corresponding angular speed was approximately 0.0344 deg/s. The linear viscosity B_L [N/(mm/min)] was converted to rotary viscosity B_R [mN.m/(deg/s)] by using the following equation. The converted value for each corresponding experimental viscosity for the initial design is listed in Table B.7 and that for the modified design is listed in Table B.8.

$$B_R = B_L * R_{EFF} * \frac{1\,\frac{mm}{min}}{0.0344\,\frac{deg}{s}} * \frac{1000\,mN}{1\,N} \rightarrow \left[\frac{N}{\frac{mm}{min}}\right] * [m] * \frac{\left[\frac{mm}{min}\right]}{\left[\frac{deg}{s}\right]} * [\frac{mN}{N}] = [\frac{mN.m}{\frac{deg}{s}}]$$

Table B.7: Linear and rotary viscosities for each orifice radius and silicone oil combination evaluated for the initial design.

Orifice [mm]	Initial Design			
	100 mPa.s Silicone Oil		150 mPa.s Silicone Oil	
	Linear Viscosity [N/(mm/min)]	Rotary Viscosity [mN.m/(deg/s)]	Linear Viscosity [N/(mm/min)]	Rotary Viscosity [mN.m/(deg/s)]
2.5	-0.0011	-0.16	0.0015	0.22
2.0	-0.0051	-0.74	0.0058	0.84
1.5	0.0138	2.01	0.0240	3.49
1.0	0.0449	6.52	0.0744	10.80
0.5	0.0720	10.50	0.1230	17.90

Table B.8: Linear and rotary viscosities for each orifice radius evaluated for the modified design.

Orifice [mm]	Modified Design	
	Linear Viscosity [N/(mm/min)]	Rotary Viscosity [mN.m/(deg/s)]
2.5	0.0023	0.33
2.0	0.0098	1.40
1.9	0.0107	1.50
1.8	0.0146	2.10
1.5	0.0249	3.60

LIST OF REFERENCES:

[1] H. M. Lee, *et al.*, "Validation of portable muscle tone measurement device for quantifying velocity-dependent properties in elbow spasticity," *J Electromyogr Kinesiol*, vol. 14, pp. 577-89, Oct 2004.

[2] J. J. Chen, *et al.*, "The use of a portable muscle tone measurement device to measure the effects of botulinum toxin type a on elbow flexor spasticity," *Archives of Physical Medicine and Rehabilitation*, vol. 86, pp. 1655-1660, Aug 2005.

[3] Electronics Tutorials. (2016). *Average Voltage Tutorial* [Web]. Available: http://www.electronics-tutorials.ws/accircuits/average-voltage.html [Accessed: Jul. 2, 2016]

APPENDIX C: LINKAGE DESIGNS

Using the equation (Eq. (4) from Chapter 2) derived for the linkage mechanism, three distinct cam and path-constraint pairs were designed and fabricated (Figure C.1). But only one pair was implemented in the hydraulic-based spasticity simulator. The first linkage pair (Figure C.1a) was designed for rigidity replication with a linear output torque versus position profile. The second and third linkage pairs (Figure C.1b and Figure C.1c) were designed for spasticity replication with an output torque versus position profile where the maximum torque occurs at mid-range of motion. The second linkage pair was implemented and evaluated along with the hydraulic-based spasticity simulator.

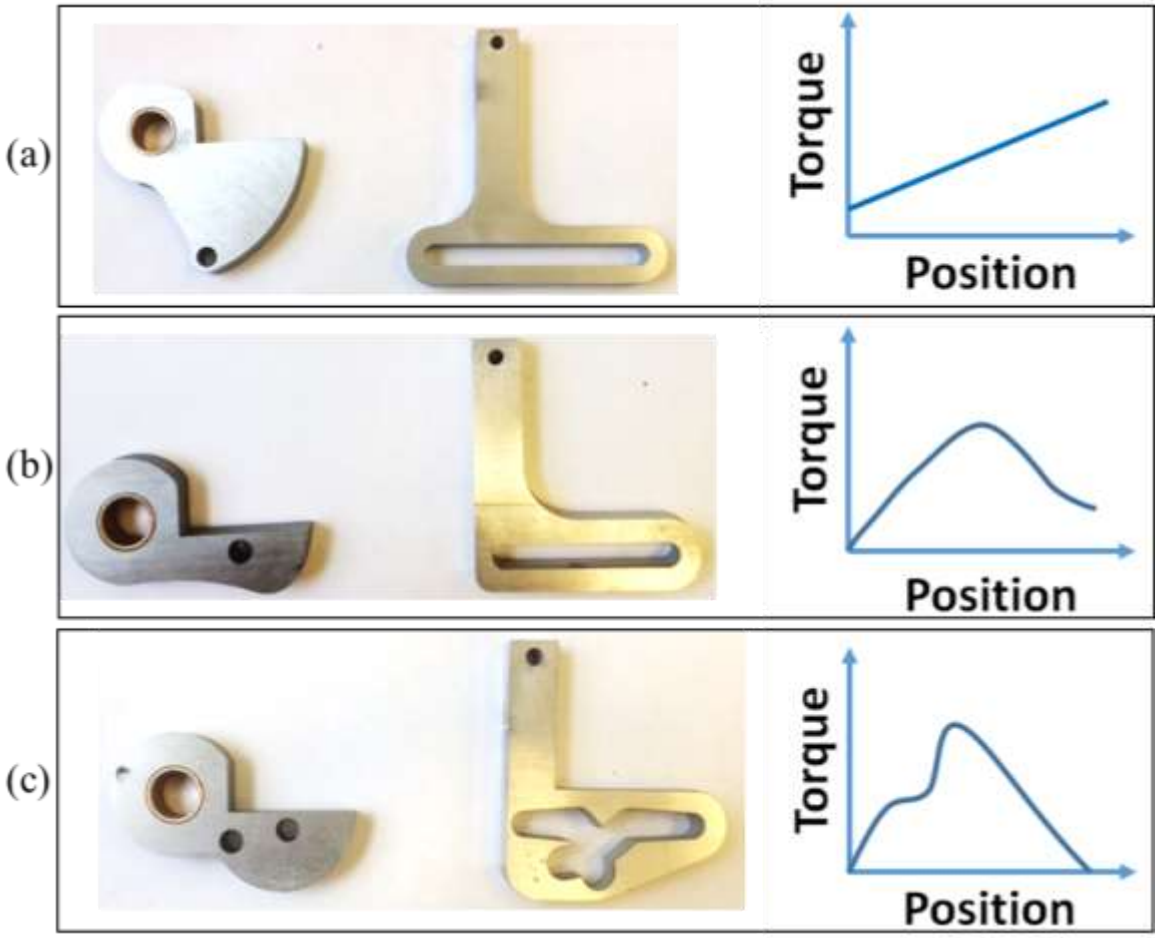

Figure C.1: Cam and path-constraint pairs for mimicking the output torque versus position profile of rigidity or spasticity.

APPENDIX D: REYNOLDS NUMBER CALCULATION

Analytical model for the fluid behavior was derived based on the assumption that flow inside the passive viscous damper would always be laminar. To ensure that this assumption would always hold true, calculations of the Reynolds number (ratio of inertial forces to viscous forces) [1] relating to the damper geometry and input speed were presented here.

$$Re = \frac{\rho v L}{\mu}$$

In the above equation, ρ was the fluid density, v was the input speed, L was the characteristics length, and μ was the fluid viscosity. Two options for input speed and characteristics length were available to approximate the Reynolds number. The first option was using the piston speed and piston diameter. The second option was using the flow speed through the orifice and orifice diameter.

The maximum input speed for the damper piston was calculated based on the simulator linkage geometries. Assuming a maximum input rotational speed of 300 deg/s, the corresponding linear speed for the viscous damper (v_p) was 0.15 m/s. The piston diameter ($2R_p$) was 0.05 m and the fluid density was approximately 1000 kg/m^3. The *Re* values for the 100 mPa.s and 150 mPa.s silicone oils were evaluated to be 75 and 50, respectively.

The speed of the fluid through any piston orifice pair (v_{po}) could be estimated through equating the volumetric flow rate.

$$2\pi R_{po}^2 v_{po} = \pi R_p^2 v_p \rightarrow v_{po} = \frac{1}{2}\left(\frac{R_p}{R_{po}}\right)^2 v_p$$

In the above equation, R_{po} was the piston orifice radius, v_{po} was the flow speed through the orifice, R_p was the piston radius, and v_p was the piston speed. R_p was 0.025 m and v_p was

0.15 m/s. The *Re* value for each orifice geometry and silicone oil combination was listed in Table D.1.

Table D.1: Reynolds number for each orifice geometry and silicone oil combination.

Orifice Radius [mm]	Flow Speed [m/s]	Reynolds Number	
		100 mPa.s	150 mPa.s
2.5	7.5	188	125
2.0	12	234	156
1.5	20	312	208
1.0	47	469	313
0.5	188	938	625

Either approach to calculate the Reynolds number associated with the viscous damper design showed that the values were always significantly less than 2300, indicating that the design was operating well within the laminar flow regime [1].

LIST OF REFERENCES:

[1] F.M. White and I. Cortfield, *Viscous fluid flow*, vol 3, ed. New York, NY: McGraw-Hill, 2006.

APPENDIX E: SUPPLEMENTARY IMAGES AND CAD RENDERINGS

MAS	Qualitative Description
0	No increase in muscle tone
1	Slight increase in muscle tone, manifested by a catch and release or by minimal resistance at the end of the range of motion
1+	Slight increase in muscle tone, manifested by a catch, followed by minimal resistance throughout the reminder (less than half) of the range of motion
2	More marked resistance in muscle tone through most of the range of motion, but affected part is easily moved
3	Considerable increase in muscle tone, passive movement difficult
4	Affected part is rigid in flexion or extension

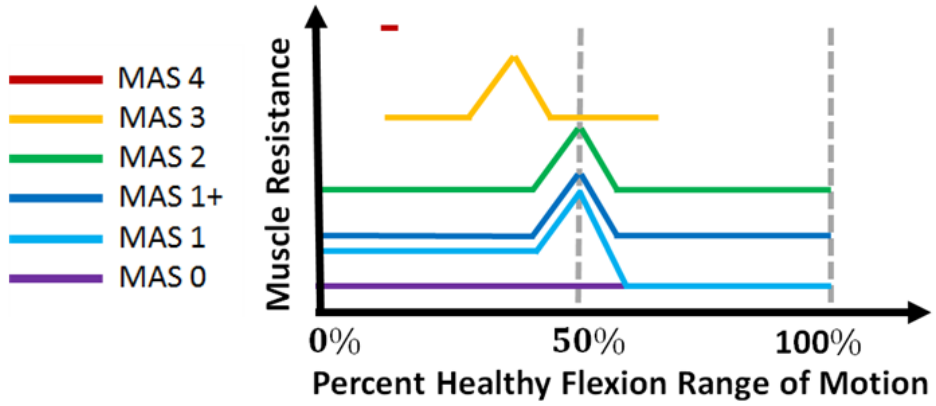

Figure E.1: Qualitative description and high level graphical interpretation of Modified Ashworth Scale describing degree of spasticity.

UPDRS	Qualitative Description
0	Rigidity absent
1	Rigidity slight or detectable only when activated by mirror or other movements
2	Rigidity mild to moderate
3	Rigidity marked, but full range of motion easily achieved
4	Rigidity severe; range of motion achieved with difficult

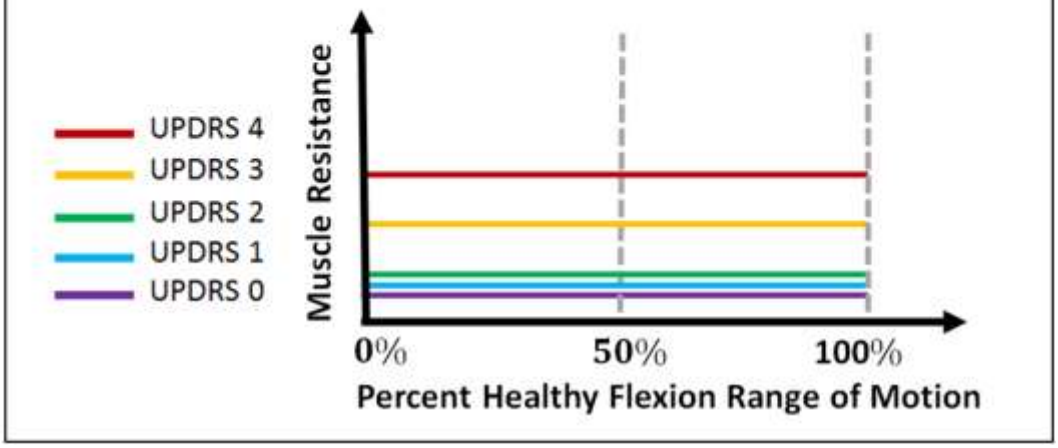

Figure E.2: Qualitative description and high level graphical interpretation of United Parkinson's Disease Rating System describing degree of rigidity.

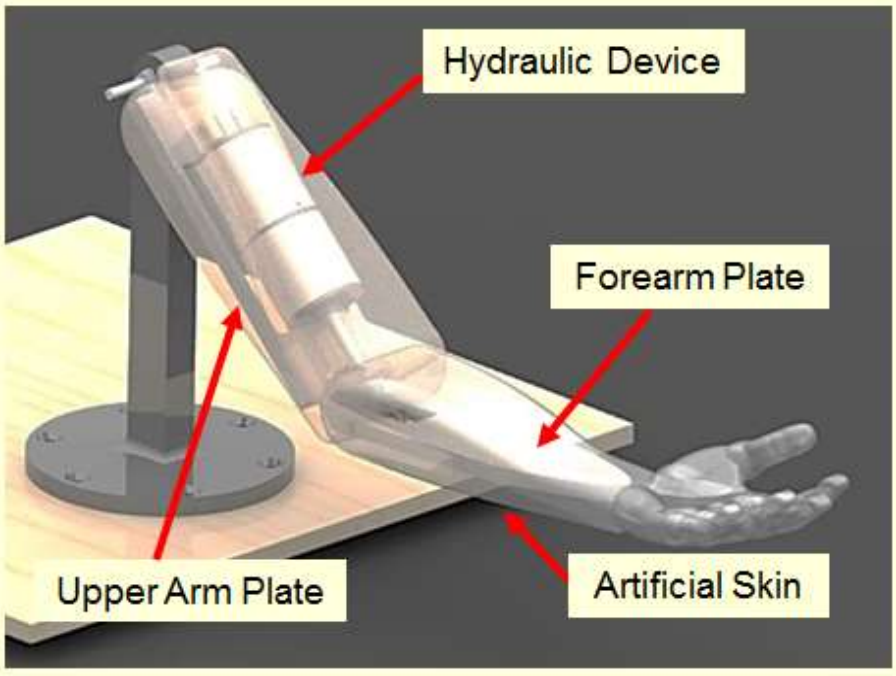

Figure E.3: Rendered image of the forearm simulator with an embedded hydraulic device.

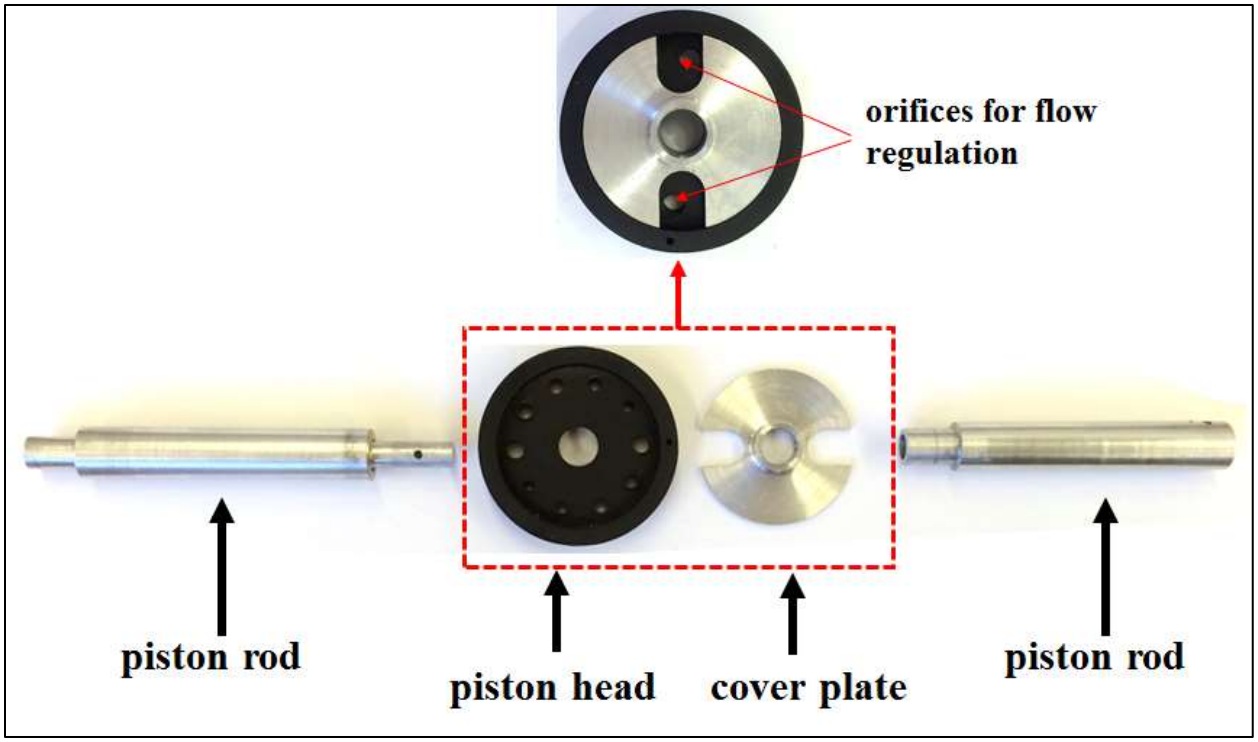

Figure E.4: Components of the 4-part piston inside the passive viscous damper.

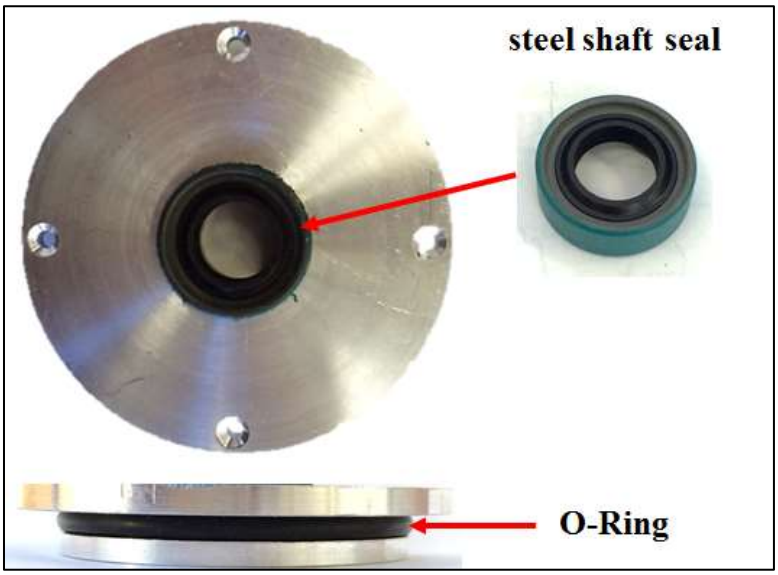

Figure E.5: Endcap of passive viscous damper.

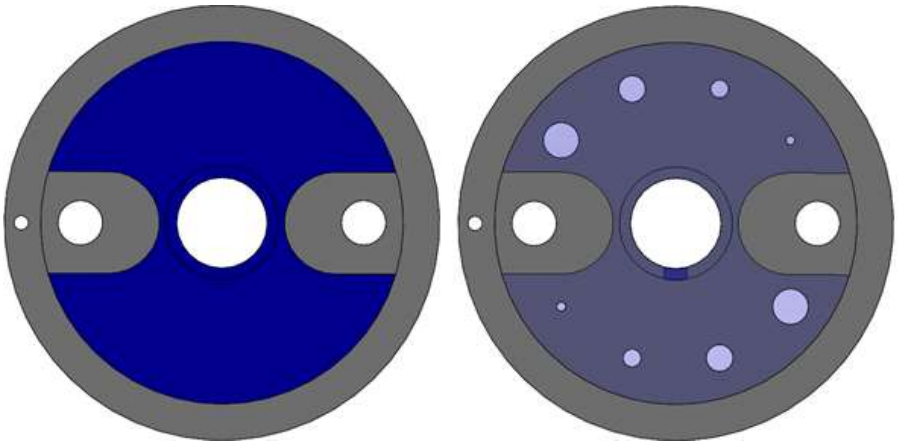

Initial Design Orifice Radius (mm)
2.5
2.0
1.5
1.0
0.5

Figure E.6: Initial design of the piston head with orifice radius sizes.

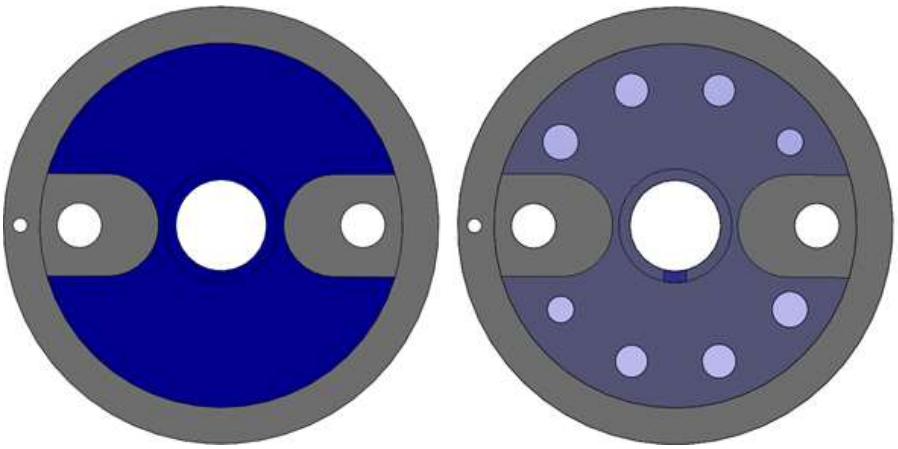

Modified Design Orifice Radius (mm)
2.5
2.0
1.9
1.8
1.5

Figure E.7: Modified design of the piston head with orifice radius sizes.

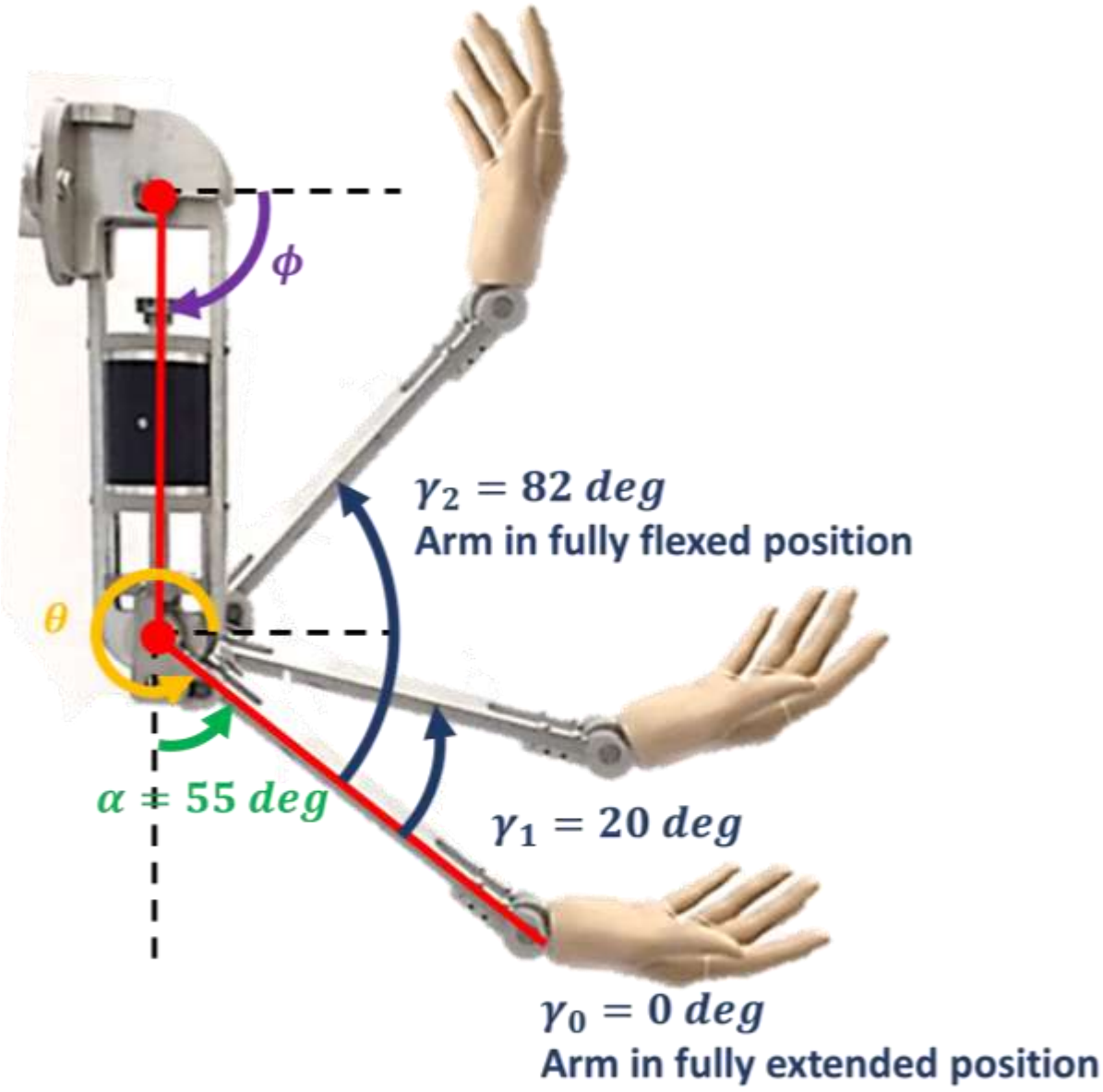

Figure E.8: Angle measurements associated with the spasticity simulator prototype.

APPENDIX F: EXPERIMENTAL RESULTS FOR VISCOUS DAMPER TESTING

Characterization experiments were performed on the initial and modified passive viscous damper designs. All experiments were done using a material testing system over constant speeds (Instron 5967; High Wycombe, UK). Force and displacement data were collected as outcomes of these evaluations. Force data collected from the moment when the damper piston touched the force plate until reaching a pre-defined displacement limit were analyzed. Average force and the corresponding standard deviation were computed over three independent trials (Table F.1).

Table F.1: Average damping force (± standard deviation) for each orifice radius, speed, and design combination. Values were calculated based on experimental data obtained from three independent trials.

	Orifice [mm]	Damping Force [N]			
		250 mm/min	500 mm/min	750 mm/min	1000 mm/min
Design #1 100 mPa.s	2.5	16.238 ± 1.445	12.969 ± 1.045	12.204 ± 0.917	12.203 ± 1.160
	2.0	15.094 ± 1.090	12.961 ± 0.963	13.692 ± 1.062	13.947 ± 0.832
	1.5	15.957 ± 0.913	17.158 ± 0.859	20.978 ± 1.002	26.170 ± 1.415
	1.0	22.833 ± 1.216	31.781 ± 1.268	43.812 ± 1.517	56.242 ± 2.071
	0.5	33.537 ± 1.803	47.650 ± 1.851	67.305 ± 3.068	86.953 ± 2.895
Design #1 150 mPa.s	2.5	13.474 ± 1.014	12.746 ± 0.842	13.626 ± 0.784	14.391 ± 0.751
	2.0	15.130 ± 0.998	15.501 ± 0.894	18.055 ± 1.147	19.920 ± 1.020
	1.5	18.540 ± 0.890	23.086 ± 0.680	29.201 ± 0.850	36.515 ± 1.010
	1.0	32.385 ± 1.630	47.866 ± 4.466	66.526 ± 1.612	88.203 ± 2.542
	0.5	47.797 ± 2.638	75.505 ± 5.045	107.344 ± 5.563	139.725 ± 8.606
Design #2 150 mPa.s	2.5	13.449 ± 1.076	12.546 ± 0.806	13.235 ± 0.694	15.130 ± 0.718
	2.0	14.775 ± 1.126	15.936 ± 1.192	18.766 ± 1.262	21.988 ± 1.446
	1.9	14.209 ± 1.686	16.113 ± 1.778	18.833 ± 2.131	22.237 ± 2.306
	1.8	15.022 ± 1.401	17.622 ± 1.037	21.221 ± 1.277	26.029 ± 1.395
	1.5	18.504 ± 0.719	23.980 ± 0.898	32.035 ± 0.928	36.593 ± 2.033